Single-cell imaging of cell cycle reveals that tissue-scale g1 lengthening involves cdc25b induced cell-to-cell heterogeneity in neural progenitor cells

Angie Molina[1], Frédéric Bonnet[1], Julie Pignolet[1], V. Lobjois[1], Sophie Bel-Vialar[1], Jacques Gautrais[2,*], Fabienne Pituello[1,*] and Eric Agius[1,*]

"Angie Molina" amolinad@unav.es
"Fréderic Bonnet" fbonnet@mdibl.org
„Julie Pignolet“ julie.pignolet@univ-tlse3.fr
"LOBJOIS Valérie" Valerie.LOBJOIS@univ-tlse3.fr
"Sophie vialar" sophie.vialar@univ-tlse3.fr
"Jacques GAUTRAIS" jacques.gautrais@univ-tlse3.fr
"Fabienne Pituello" fabienne.pituello@univ-tlse3.fr
"Eric Agius" eric.agius@univ-tlse3.fr

1: Unité de Biologie Moléculaire, Cellulaire et du Développement (MCD), Centre de Biologie Intégrative (CBI), Université de Toulouse, CNRS, Université Toulouse III – Paul Sabatier, Toulouse, France.

2: Centre de Recherches sur la Cognition Animale (CRCA), Centre de Biologie Intégrative (CBI), Université de Toulouse, CNRS, Université Toulouse III – Paul Sabatier, Toulouse, France.
*Co-corresponding authors

Corresponding authors: Eric AGIUS, Fabienne PITUELLO, Jacques GAUTRAIS Molecular, Cellular & Developmental biology unit (MCD) and Centre de Recherches sur la Cognition Animale (CRCA), Centre de Biologie Intégrative, Université de Toulouse, CNRS-UPS UMR 5077 ; 118 route de Narbonne, F-31062 Toulouse, France.
E-mail adresses : jacques.gautrais@univ-tlse3.fr, fabienne.pituello@univ-tlse3.fr, eric.agius@univ-tlse3.fr
Fax: (33)5 61 55 65 07, Phone: (33)5 61 55 67 39

Keywords: neural stem cells, neurogenesis, proliferation, differentiation, single cell imaging, cell cycle kinetics, G1 phase, retinoblastoma protein, CDC25 phosphatase, neural tube, vertebrate embryo

ABSTRACT

While lengthening of the cell cycle and G1 phase is a generic feature of tissue maturation during development, the underlying mechanism remains still poorly understood. Here we develop a time lapse imaging strategy to measure the four cell cycle phases in single neural progenitor cells in their endogenous environment. We show that neural progenitors are widely heterogeneous regarding the cell cycle length. This duration variability is distributed over all phases of the cell cycle, with the G1 phase being the one contributing the most. Within one cell cycle, each phase duration appears stochastic and independent except for a correlation between S and M phase duration. Lineage analysis indicates that the majority of daughter cells may have longer G1 phase than mother cells suggesting that at each cell cycle a mechanism lengthens the G1 phase. We identify that the CDC25B phosphatase known to regulate G2/M transition, indirectly increases the duration of the G1 phase partly through delaying restriction point crossing. We propose that CDC25B increases G1 phase range of heterogeneity revealing a novel mechanism of G1 lengthening associated with tissue development.

INTRODUCTION

Building a multicellular functional organ requires tight coordination between cell proliferation, cell fate specification and differentiation. In the developing nervous system, the spatio-temporal regulation of these processes is of key importance to construct functional neuronal circuits.

The cell cycle and components of the core cell cycle machinery have been shown to play a major role in the decision to proliferate or differentiate in embryonic stem cells, pluripotent stem cells and neural stem/progenitor cells (for a review see (Hardwick et al., 2015; Liu et al., 2019)). In numerous cell types including neural stem/progenitor cells, cell cycle and G1 phase lengthening is a general feature accompanying cell maturation and differentiation. During mammalian corticogenesis, where consecutive types of progenitors have been described, lengthening of the G1-phase is associated with the transition from neural-stem-like apical progenitors (AP)

to fate restricted basal progenitors (BP) and a shortening of the S phase with the transition from proliferative to neurogenic divisions (Arai et al., 2011). Reducing G1 phase length results in an inhibition of neurogenesis, while lengthening G1 duration promotes neurogenesis (Artegiani et al., 2011; Lange et al., 2009; Lim and Kaldis, 2012; Pilaz et al., 2009). In the developing spinal cord, different cell cycle kinetics are observed in discrete domains of neural progenitors (Molina and Pituello, 2017). Differentiation here progresses from ventral to dorsal with time. When the maximum differentiation rate is reached in the ventral domain, neural progenitor cells (NPCs) exhibit a long G1 phase and short S and G2 phases (Kicheva et al., 2014; Peco et al., 2012; Saade et al., 2013). In contrast, the dorsal domain mainly composed at the same age of proliferative NPCs, shows a short G1 phase accompanied by long S and G2 phases (Kicheva et al., 2014; Peco et al., 2012; Saade et al., 2013). Overexpressing D-type Cyclins in young neural tube increases the pool of proliferating progenitors and induces a transient reduction of neuron production (Cao et al., 2008; Lacomme et al., 2012; Lobjois et al., 2008), while more mature NPCs will differentiate regardless of Cyclin D overexpression and cell cycle exit (Lobjois et al., 2008). Shortening of the G2 phase associated with neurogenesis results from the upregulation in NPCs of a regulator of the G2/M transition, the CDC25B phosphatase. CDC25B promotes entry into mitosis by dephosphorylating its canonical substrates, the cyclin-dependent kinases (CDKs) complexes. Surprisingly for a positive regulator of the core cell cycle machinery, CDC25B has been shown to promote neurogenesis in mouse, chicken and Xenopus embryos (Gruber et al., 2011; Peco et al., 2012; Ueno et al., 2008). Gain and loss-of-function experiments performed in chicken neural tube show that CDC25B induces the conversion of proliferating NPCs into differentiating neurons by promoting neurogenic divisions (Bonnet et al., 2018). CDC25B acts using both CDK independent and dependent molecular mechanisms (Bonnet et al., 2018). A mathematical model has allowed us to hypothesize that CDC25B expression in neural progenitors progressively restricts the proliferative capacities of embryonic neural stem cells (Azaïs et al., 2019).

A weak point common to all these studies is that cell cycle analyses have been performed at the population level. Cell cycle and phases lengths were calculated from fixed tissues and correspond to estimated average length values considering the population of NPCs as homogeneous (Nowakowski et al., 1989). Whether this neural progenitor population is homogeneous or heterogeneous relative

to cell cycle kinetics is poorly documented. An indication that the population of NPCs is indeed heterogeneous comes from a study where the total cell cycle length (Tc) was determined from the length of time measured between two cell divisions using time-lapse imaging in chick embryo slice cultures (Wilcock et al., 2007). These single cell measurements reveal that the neural progenitor population displays marked range of heterogeneity regarding the Tc, which ranges from 9 hours to 28 hours. Moreover, previous data indicate that the cell cycle length of cells dividing to produce two progenitors was shorter than that producing one neuron and one progenitor (Wilcock et al., 2007). However, how this Tc heterogeneity translates into cell cycle kinetics and phases duration in single NPC remains enigmatic.

The goal of this study was to determine at the single cell level the features of NPCs cell cycle kinetics in their endogenous environment and the link with tissue maturation and differentiation. We set up a methodology based on the combination of the use of fluorescent cell cycle reporters together with high-resolution single-cell time-lapse imaging that allows tracking single NPCs within the developing neural tube over long periods to measure the duration of each phase of the cell cycle and to track the behavior of daughter cells after mitosis. We found that the lengths of the total cell cycle and of all phases, but M phase, are very heterogeneous. The duration of each phase can be described by a stochastic process without coupling between phase length within a cell cycle except for a potential correlation between M and S phases. The total cell cycle (Tc) length variation can be primarily explained by G1 range of heterogeneity. Our analysis indicated that the majority of daughter cells may have a longer G1 phase than their mother's suggesting that gradually at each cell cycle a mechanism lengthens the G1 phase. Finally, we showed that CDC25B increases cell-to-cell G1 length range of heterogeneity, thereby raising tissue-scale G1 length associated with tissue maturation and differentiation.

MATERIALS AND METHODS

Embryos

Fertile hens' eggs were incubated at 38°C in a humidified incubator to yield embryos appropriately staged (Hamburger and Hamilton, 1992).

DNA constructs and *in ovo* electroporation

In ovo electroporation experiments were performed using 1.5- to 2-day-old chicken as described previously (Peco et al., 2012). In the present study we used the Fluorescent Ubiquitination-based Cell Cycle Indicators (FUCCI; (Sakaue-Sawano et al., 2008)). FUCCI utilizes the cell cycle phase-dependent degradation of the replication licensing factor Cdt1 (FUCCI G1) that is degraded during S/G2/M and of Geminin (FUCCI S/G2/M) that is degraded during G1. Both are cloned in fusion with distinct fluorescent proteins. A protein constituted of Cdt1 in fusion with an orange fluorescent protein (mKo) serves as an indicator of the G1 phase, and a fusion protein of a Geminin with a green fluorescent protein allows visualizing the S, G2 and M phases. Rapid degradation of both fluorescent chimeric proteins, mediated by the ubiquitin proteasome system, allows to visually distinguish cells in G1 and S/G2/M phases of the cell cycle. To visualize cells through the G1 phase, we used the zebrafish FUCCI G1 marker mKO2-zCdt1 (Sugiyama et al., 2009) instead of the human Cdt1, which in chick NPCs, persists in all cell cycle phases, suggesting that it is not properly degraded (data not shown). To detect the four phases of the cell cycle we developed the mKO-zCdt1-pIRES-NLS-eGFP-L2-PCNA biosensor. In the pCAG plasmid, we inserted the Fucci G1 probe derived from zebrafish Cdt1 (Sugiyama et al., 2009) and downstream the IRES element, the NLS green fluorescently tagged proliferating cell nuclear antigen (PCNA, (Leonhardt et al., 2000). This FUCCI G1-PCNA vector is transfected at 0.5µg/µl by *in ovo* electroporation in the chicken neural tube to reproducibly obtain a high degree of mosaicism compatible with lineage tracing (Wilcock et al., 2007). The hCDC25B or hCDC25B$^{\Delta CDK}$ gain-of-function experiments were performed at 1.5µg/µl as in (Bonnet et al., 2018). The Fucci S/G2/M mAG-hGem (Sakaue-Sawano et al., 2008) and the Fucci G1 mKO2-zCdt1 (1/190) (Sugiyama et al., 2009) were used at 0.5 µg/µl.

Immunohistochemistry

Embryos or neural tube explants are fixed in 3.7% formaldehyde for 2 hours and sliced using a vibratome (Leica). Proteins were detected on 50 µm vibratome sections, as previously described (Peco et al., 2012). The antibodies used are: anti-Olig2 (Milipore), anti-Islet1/2, anti-HuC/D (molecular Probes) anti-MNR2 (Developmental Studies Hybridoma Bank), anti-GFP (Invitrogen), anti-γH2AX

(Novus), anti-active caspase 3 (Becton Dickinson Biosciences), anti phospho-Rb (Ser807/811) (Cell Signaling).

Determination of S-phase length (Ts) and total cell cycle length (Tc) were based on the relative numbers of cells that incorporated one or two thymidine analogs (Martynoga et al., 2005). For in ovo incorporation 10 µl of bromodeoxyuridine (BrdU Sigma, St Louis, MO, USA) (500 µM) were injected into embryos and followed after 90 minutes by EdU (500 µM, Invitrogen) incorporation. Embryos were fixed 30 minutes later. EdU was detected first (Click-iT EdU Alexa Fluor 647 Imaging Kit, Invitrogen), followed by BrdU detection using the G3G4 antibody that does not recognize EdU. For single BrdU incorporation, 10 µl of BrdU (500 µM) were injected into embryos, which were then reincubated for 30 minutes before fixation. BrdU immunodetection was performed on vibratome sections using anti-BrdU (mouse monoclonal, G3G4) as in (Lobjois et al., 2004). For EdU cumulative in ovo incorporation, 10 µl of EdU (500 µM, Invitrogen) were injected into E 2.5 embryos every 3 hours for up to 27 hours. Embryos were fixed and processed for vibratome sectioning and EdU detected according to manufacturer's instructions (Click-iT EdU Alexa Fluor 488 Imaging Kit, Invitrogen). Cell death was analyzed by immunofluorescence, using the anti-active caspase 3 antibody.

Flow cytometry analysis

1.5- to 2-day-old chicken embryos were electroporated with H2B-GFP or NLS-eGFP-L2-PCNA constructs. Neural tubes were dissected 24 h following electroporation, incubated at 37°C for 10 min in trypsin-EDTA to obtain a single-cell suspension, and fixed for 30 minutes in 4% formaldehyde. Cell suspensions were incubated for 30 min in 400 µl of propidium iodide (PI) (20µg/ml)/ RNAse (100µg/ml) cocktail (Sigma). PI and GFP fluorescence were acquired with a FACSCalibur cytometer (Cat#342975, Becton Dickinson), and DNA content analysis was performed using the FlowJo software.

Embryonic neural tube culture and Time-lapse Imaging

Electroporated E2 embryos were collected in PBS and 100 µm slices were obtained using a McIlwain tissue chopper (WPI), from the brachial region corresponding to somites 12 to 17 which generates the greatest number of motoneurons (Oppenheim et al., 1989). Sections were collected in 199 culture medium (GIBCO) and were

sorted out under a fluorescence microscope to control tissue integrity and the presence of isolated fluorescent cells along the dorso-ventral axis. Each slice was embedded into 10 µl of rat type I collagen (Roche Diagnosis; diluted at 80% with 1X MEM (GIBCO), 1X GlutaMax (GIBCO) and neutralizing bicarbonate (GIBCO)). 4 neural tube-containing collagen drops (5 µl) were distributed on a 35 mm glass-bottom culture dish (IBIDI) (procedure modified from (Das et al., 2012)). Collagen polymerization was performed at 38°C for 30 minutes and 1.5 ml of complete culture medium is added (Medium 199 (Gibco) supplemented with 1X GlutaMax (Gibco), 5% Fetal calf Serum (FCS, Fisher Scientific) and Gentamycin (Gibco, 40ug/mL)). The culture dish is placed in a humid atmosphere incubator with 5% CO2 for 12 hours before time lapse imaging. Alternatively, explants were cultured for 24 or 48 hours and then fixed in 3.7% formaldehyde (FA) and processed for immunostaining.

For time-lapse, images were acquired on an inverted microscope (Leica inverted DMI8) equipped with a heating enclosure (set up at 39°C) in an atmosphere containing 5% CO2, a spinning disk confocal head (CSU-X1-M1N, Yokogawa), a SCMOS camera and a 63X oil immersion objective (NA 1.4 -0.7). Attenuation of laser beam pulses were performed to reduced cell damage due to photo-toxicity (Boudreau et al., 2016). We recorded 40 µm thick z stacks (2 µm z-steps) at 5 min intervals for 48h.

Imaging, data analysis and statistics

IMARIS® and ImageJ softwares (Schneider et al., 2012) were used for image processing and data analysis. Statistical analyses were performed using GraphPad Prism and R softwares. Details for methods used in SI-Data are given in the relevant sections. The normality of the data sets was determined, analyses of variance performed. Values shown are mean ± standard error of the mean (s.e.m.). Significance was assessed by performing the Student-Mann-Whitney test. The significance values are: *P<0.05; **P<0.01; ***P<0.001. See also SI.

RESULTS

A single-cell time lapse imaging method to measure the four cell cycle phases length of NPCs within the neural tube

In order to determine cell cycle kinetics of individual spinal NPCs, we developed a combination of biosensors to detect unambiguously the four phases of

the cell cycle in living cells. We used FUCCI (Fluorescent Ubiquitination-based Cell Cycle Indicator), a set of fluorescent probes which enables visualization of cell cycle progression in living cells (Sakaue-Sawano et al., 2008) (see materials and Methods for details). To visualize cells through the G1 phase, we used the zebrafish FUCCI G1 marker mKO2-zCdt1 (Sugiyama et al., 2009). We verified its specificity in G1 by co-electroporating mKO2-zCdt1 with FUCCI S/G2/M and quantifying, 24 hours later, red, green and yellow cells corresponding to cells expressing respectively FUCCI G1, FUCCI S/G2/M or both (Fig. 1A). We quantified 43,7% and 41,4 % of cells expressing FUCCI G1 or FUCCI S/G2/M respectively and 14,9 % expressing both markers illustrating their transient overlap as already reported (Sakaue-Sawano et al., 2008). This result was comparable to previous quantifications performed by flow cytometry analysis (Benazeraf et al., 2006). To time more precisely the G1/S transition and to identify the S/G2 transition, we used the NLS-eGFP-L2-PCNA protein (Leonhardt et al., 2000). PCNA (Proliferating Cell Nuclear Antigen) is homogeneously distributed in the nucleus during G1 and G2 phase and, in early S phase, it is recruited at DNA replication sites which spread through the genome during the S-phase. Indeed, the NLS-eGFP-L2-PCNA reporter allowed to identify S phase onset by its punctuated distribution. A 30 minutes BrdU pulse confirmed that the punctuated distribution observed with NLS-eGFP-L2-PCNA corresponds to S phase cells (Fig. 1B). As shown by flow cytometry analysis, NLS-eGFP-L2-PCNA or H2B-GFP electroporation did not induce cell cycle disturbances (Fig. 1C). Moreover, the percentage +/- sem of cells positive for BrdU after a 30-minutes pulse are 41.44% +/- 0.043 after electroporation of the empty pCIG vector and 40.61% +/- 0.067 with the NLS-eGFP-L2-PCNA vector. This showed that, in our hands, the PCNA reporter expression does not affect the percentage of cells in S phase. These results confirmed that NLS-eGFP-L2-PCNA overexpression does not interfere with cell cycle timing, as previously reported in zebrafish neuroepithelia (Leung et al., 2011) or the mouse cortex (Fousse et al., 2019). To perform proper mosaic expression through *in ovo* electroporation into 2-day-old chick neural tube, we constructed a plasmid allowing the co-expression of mKO-zCdt1 and NLS-eGFP-L2-PCNA (FUCCI G1-PCNA vector, Fig. 1D).

To analyze cell cycle parameters, E2 embryonic neural tubes were electroporated with the FUCCI G1-PCNA vector and sliced after 6 hours of incubation. Thick slices of the brachial region of the embryos were placed in culture for 12 hours prior single-cell real time imaging experiments (Fig. 1E). This step of recovering is important to bypass the lengthening of the cell cycle and the delayed increase in the population of progenitors and neurons observed following slicing and culture (Suppl. Fig. 1). Time-lapse imaging was performed for 48 hours using a confocal microscope. It is important to stress that the use of 5% fetal calf serum in the culture medium and using spinning disk confocal microscopy associated with attenuation of laser beam pulses to reduce phototoxicity (Boudreau et al., 2016) are critical to perform cell cycle measurements. Visualization of the FUCCI G1 and PCNA reporters by time-lapse imaging revealed that the different transitions in the cell cycle could be discriminated using nuclear expression and distribution of both proteins (Fig. 1F). The G1 phase was characterized by the co-expression of mKO-FUCCI G1 and NLS-eGFP-L2-PCNA with a uniform distribution in the nucleus. S phase entry was detected by the appearance of the punctuated pattern of the NLS-eGFP-L2-PCNA associated with the gradual disappearance of the FUCCI-G1 reporter. In G2 phase, NLS-eGFP-L2-PCNA was evenly distributed inside the nucleus, and finally mitosis was detected by nuclear envelope breakdown accompanied by morphology changes of NPCs, which become rounded (Fig. 1F).

We have thus designed a long-term single-cell time-lapse imaging methodology to accurately measure the four cell cycle phases lengths in individual cycling neural progenitors in their endogenous environment, the neural tube.

Neural progenitor nuclei display INMs in phase with the cell cycle and three distinct behaviors after mitosis

Imaging following electroporation of the FUCCI G1 and PCNA reporters in E2 (HH12) stage embryos, showed cycling NPCs displaying G1 nuclei (orange) moving to the basal side, nuclei in S phase (green punctuated) located in the basal half of the ventricular zone and G2 nuclei (green) moving back to the apical side where mitosis occurs (Fig. 2A; Movie 1). These characteristic positions indicate that in neuroepithelia, the expression dynamics of the reporters is in accordance with the INM occurring in phase with the cell cycle progression (Fig. 2B) (Molina and Pituello, 2017). We also observed nuclei located on the basal side of the neural tube

expressing brighter orange fluorescence (Fig. 2A), probably due to the accumulation of FUCCI G1 in differentiating G0 neurons after cell cycle exit, as previously described (Sakaue-Sawano et al., 2008).

Nuclear tracking after mitosis reveals three different behaviors in daughter cells (Fig. 2C): both daughter cells re-enter S phase (nuclei switch from FUCCI G1 expression to PCNA-punctuated distribution), which clearly corresponds to the behavior of a NPC performing a proliferative division (PP) (P2 giving P2.1 and P2.2); only one daughter cell re-enters the cell cycle, while the nucleus of the other remains orange and migrates to the basal side (P3 giving P3.1 and N3.2); the two daughter cells nuclei remain orange and migrate to the basal side (P1 giving N1.1 and N1.2). These orange nuclei located at the basal side and displaying a G1 phase longer than 1000 min (16h40), were never observed re-entering S phase. We thus assumed that these NPCs correspond to cells primed to differentiate into neurons (Fig. 2A-Movie 1). To further characterize these cells, we performed HuC/D immunostaining after fixation of the sample at the end of the time lapse experiment (Fig. 2D). Over the 8 explants analyzed, we could identify 42 cells expressing the FUCCI-G1 reporter located at the basal side, of which 35 were positive for the HuC/D markers (arrows in Fig.2D). In addition, we could characterize long FUCCI G1 expression (more than 1000 min) for 4 cells located at the basal side of which 2 were positive for HuC/D staining. Over all, these data suggest that the FUCCI G1 expressing cells localized on the basal side of the explants and characterized by a long FUCCI G1 expression (>1000 min) are most probably differentiating neurons. The G1 lengths measured for these differentiating cells are excluded from our following analyses. Hence our strategy allows us to track the nuclei of NPCs along the cell cycle and to determine, following mitosis, whether the daughter cells re-enter the cell cycle or not.

Cell cycle kinetics are highly heterogeneous in the population of NPCs

Using the methodology described previously, we measured G1, S, G2, M phases and cell cycle (Tc) duration of individual NPCs within the neural tube of embryos electroporated at E2 (HH12) to ensure that we analyzed young proliferative progenitors (Fig.3A). The mean durations measured using time lapse for the total cell cycle (Tc) is 14h01 (n=33), 5h09 for the G1 phase (n=50), 1h17 (n=54) for the G2 phase and 31 min (n=50) for the M phase (Table 1). These data are in agreement with those determined from fixed embryos at equivalent developmental stages (Tc :

10h and 16h, G1 : 4h30 and 7h, G2 : 1h18 min and 2h and mitosis : 30 minutes) (Kicheva et al., 2014; Le Dreau et al., 2014; Peco et al., 2012; Saade et al., 2013; Wilcock et al., 2007). The S phase length measured using time lapse (7h18 ± 23 min) presents an average value higher than reported in fixed tissues (3h42 min and 5h54 min). To test whether this increase in S phase length was due to photoxicity induced by time lapse imaging, we analyzed expression of γH2AX, a marker for double-strand breaks induced by DNA damage (Suppl. Fig. 2). No increase in γH2AX immunostaining was observed after time lapse imaging suggesting that S phase lengthening does not primarily result from DNA damage. Thus, except for the S phase, which was slightly increased in our conditions, the mean duration determined from time-lapse experiments are consistent with those reported for fixed tissues at equivalent developmental stage.

At the single cell level, our analyses showed a high degree of heterogeneity regarding Tc duration, as it ranges from 9h55 min (595 min) to 24h45 min (1485 min) (Table 1; Fig. 3A) which is in accordance with previous time lapse measurements reporting a total cell cycle length between 9 hours and 28 hours (see FigS2 in Wilcock et al., 2007). We verified whether NPCs performing very long cell cycle are also present in the neural tube of embryos developing in ovo. We performed cumulative EdU experiments with EdU incorporation every 3 hours for up to 27 hours (Suppl. Fig.3). After 27 hours of cumulative EdU incorporation an average of 5% -/+0.5% of NPCs nuclei EdU negative were detected (Suppl. Fig. 4B) indicative of NPCs displaying very long cell cycle or being quiescent. The use of the FUCCI G1 and PCNA reporters allowed us to determine how this heterogeneity was translated at the level of the different cell cycle phases (Table 1; Fig. 3A). G1 phase durations were comprised between 2h20 (140 min) and 16h20 (980 min). S phase durations spanned from 2h10 (130 min) to 15h45 (945 min), the G2 phase from 35 min to 2h55 (175 min), and mitosis from 20 min to 55 min. Since data are durations before exiting the phase, we characterized the corresponding distributions using survival analysis (Fig. 3B-E). Each phase can be characterized by a minimal duration (D_{min}) and a mean exit time (τ) corresponding to the average duration spent in the phase after that minimal duration (Table 1, SI-Data section 1.2). Mean exit time reflects the slope of the survival function after minimal duration. The gentler the slope, the larger the mean exit time, the more heterogeneous the distribution. At the opposite, a very homogeneous population would display durations close to the minimal duration and a

vanishing mean exit time. Hence, the mean exit time is a meaningful readout of the phase duration heterogeneity. The shapes of the survival curves and their mean exit times indicate that all the phases are heterogeneous (Table 1, Fig. 3B-D, SI-Data section 1.3). To exclude the possibility that this heterogeneity reflects the variation of cell cycle kinetics of NPCs depending upon their position along the dorso-ventral axis of the neural tube (see introduction), we determined whether the range of heterogeneity observed for the G1 phase was linked with the position of the NPCs along the dorso-ventral axis. Most of the cells for which we analyzed the G1 phase, were located in the dorsal half of the spinal cord (Suppl. Fig. 4A). In that domain, the range of heterogeneity was not dependent on the spatial localization of the NPCs. Notably, the range of heterogeneity was also independent of the time elapsed since the beginning of the recording (Suppl. Fig. 4B).

To identify the quantitative relationships between phases, we performed further analyses using the subset of 33 cells for which a complete cell cycle was monitored (Fig. 3F, Table 1, SI-Data section 2). In this sample, NPCs spent 37% of the cell cycle in G1, 52% in S phase, 9% in G2 and 4% in mitosis, in accordance with previous data obtained on fixed samples (Saade et al., 2013). Variation partitioning analysis showed that 58 % of Tc variation is due to G1 range of heterogeneity alone (Fig. 3F, SI-Data section 2.2). We then tested correlations within each pair of phases (SI-Data section 2.3), and found no patterns, except for an unexpected significant positive correlation between S and M durations (Fig. 3G, SI-Data section 2.3). No correlation was identified between G1 length and S/G2/M lengths (P>>0.05, SI-Data section 2.3.1), suggesting that phases durations are independent from each other within the same cell cycle.

To further test the likelihood of the hypothesis of full independence among phases durations, we examined how it would correctly predict the observed distribution of Tc. To build this prediction analytically, the survival curves of exit times for each phase in the subset have been approximated by a simple exponential decay (red line in Suppl Fig. 5, SI-Data section 2.5.1), which would correspond to a model in which cell cycle phase exit is a stochastic process driven by a constant probability per unit time to exit after minimal duration. Under such a hypothesis, for each phase, duration can be described by a stochastic exit process D defined as

$$D \sim D_{min} + E$$

where

$$E \sim Exp(\tau)$$

is an exponentially distributed variable with mean time τ.

Under this hypothesis, the complete cell cycle duration would then obey a stochastic process Dc simply defined as:

$$D_c = D_{G1} + D_S + D_{G2} + D_M$$

that is, the total duration would just result from the sum of four independent exit processes as defined above, each with its corresponding parameters for minimal duration and mean time before phase exit (see SI-Data section 2.4.1 for the analytical expression for Dc distribution under this hypothesis). We found that the predicted survival function for Dc under this hypothesis (brown curve in Fig. 3H) is actually well compatible with the observed one (black line in Fig. 3H) suggesting that the phases are independent. This is confirmed using Monte Carlo permutation, a random sampling technique (red line in Fig. 3H, SI-Data section 2.4.2 and 2.6). The experimental distribution appears well compatible with random mixing of phases durations (p=0.84, two-samples KS goodness of fit test). The model shows that the phase length of the four phases can be considered as independent. To challenge phase duration uncoupling, we illustrate the opposite hypothesis where Tc length would result from the dataset reordered so that the lengths of G1 and S/G2/M phases are fully anti-correlated (blue line in Fig. 3H, SI-Data section 2.4.3). In this case, the range of heterogeneity of Tc is greatly reduced compared to the experimental one, and not compatible with the experimental distribution (p=0.0048, two-samples KS goodness of fit test).

Together these data show that the spinal NPCs population is highly heterogeneous regarding the distribution of cycling time. Duration of each phase seems largely stochastic and independent within one cell cycle, suggesting the absence of coupling between phases duration. The phase mostly responsible for Tc variation is the G1 phase.

CDC25B activity increases the range of heterogeneity in G1 phase duration

As mentioned above, single-cell analysis reveals a high degree of heterogeneity in G1 phase length. One hypothesis is that a mechanism intrinsic to the cell cycle induces a lengthening of the G1 phase in individual proliferative NPCs. Recently, we showed that CDC25B is involved in NPCs maturation (Bonnet et al., 2018; Peco et al., 2012). We then tested the impact of a gain of function of the CDC25B phosphatase on cell cycle kinetics using our time lapse strategy. We used a vector that reproduces the iterated cell cycle regulated expression of CDC25B during S and G2 phases (Bonnet et al., 2018; Korner et al., 2001). As observed in control condition, cell cycle kinetics is also highly heterogeneous after CDC25B gain-of-function (Fig. 4A and Table 1). As expected from its role in G2/M transition (Bonnet et al., 2018; Peco et al., 2012), CDC25B gain-of-function induced a significant 12.7% decrease of the mean G2 phase length ($p = 0.029$, Fig. 4C and Table 1). The mean Tc length increase of 32.8% ($p=0.004$ when compared to control; Table 1) results from a slight increase in the mean lengths of S and M phase (12.4% and 5.5% respectively) and from a drastic 59.9% increase in the mean G1 phase length ($p<0.0001$ when compared to control; Fig.4C, Table 1). Survival curves and the corresponding frequency distribution histograms representation were then compared to analyze the dispersion of the data in various conditions (Fig. 4 D-H). The 4h16 min (256 min) increase observed in mean Tc length induced by CDC25B is associated with a rise of the exit time (from 247 to 503 min) without modification of the minimal duration (583 min vs 586 min, Table 1). This clearly defines that CDC25B increases the dispersion of the dataset. The pace at which CDC25B expressing cells exit the cell cycle is about three times slower (hazard ratio of 0.35) than that of control cells (red curve compared to black curve in Fig. 4D, SI-Data section 3.1). Phase by phase comparison showed that CDC25B induces a significant increase in both G1 and S phase distribution compared to control (compare red and black curve in Fig. 4E-H). Variation partitioning revealed that about 50% of Tc variation are explained by G1 heterogeneity alone and 20% by S phase alone (Suppl. Fig. 6A, SI-Data section 2.2). Minimal durations do not appear altered, but rather exit times are affected, with a mean lengthening of 2h45 (165 min) and 1h02 (62 min) and 0.41 and 0.65 hazard ratios for G1 and S phases, respectively (SI-Data section 3.2 and 3.3). No significant effect was found on the G2 or M phase survival distributions (Fig. 4F-H, Table 1, SI-Data section 3.4 and 3.5). We note that mean G2 length shortening appears to be

associated with a shorter minimal duration, with no effect upon its heterogeneity (shape of the curve in Fig. 4F, Table 1). Correlation analysis between phase lengths showed that phases are uncoupled (SI-Data section 2.3.2). Monte Carlo permutations of the data set (10^4 samples) suggest that the distribution of Tc is compatible with independent cell cycle phase durations (compare red and black curve in Suppl. Fig. 6B and SI-Data section 2.6.2**)**. Notwithstanding no heritable correlation between mother cells G2 phase length and the daughter cells G1 phase length could be detected (Suppl. Fig. 6C, D).

All these results show that in a context where each cell cycle phase duration is stochastic and independent, CDC25B enhances the range of heterogeneity in G1 phase duration leading to a lengthening of G1 and Tc mean values at the population level.

CDC25B gain-of-function in G2-phase delays the passage through the restriction point in NPCs.

We previously showed that part of CDC25B function in neurogenesis does not require interaction with its canonical substrate CDK1 (Bonnet et al., 2018). We then tested whether it is the case for the effects on G1 phase length. Electroporation of CDC25B$^{\Delta CDK}$ unable to interact with CDK induced 4 cells with a G1>1000 minutes (open circles in Fig. 4B) in line with its neurogenic effect. In our experiments, CDC25B$^{\Delta CDK}$ was not able to significantly change cell cycle phases length and dispersion compared to control conditions (Fig. 4B-H; Table 1, SI-Data section 3). Thus, the G1 phase modification induced by CDC25B is dependent on its interaction with CDK indicating that it might be related to its function in the cell cycle.

The next question was then to determine whether CDC25B acts directly in G1. As mentioned above, to misexpress CDC25B we used the mouse cell cycle dependent CDC25B cis regulatory element (ccRE) that reproduces the cell cycle regulated transcription of CDC25B (Bonnet et al., 2018; Korner et al., 2001). To determine precisely the timing of expression of the ectopic CDC25B protein during the cell cycle, we electroporated an eGFP-CDC25B expressing vector in NPCs. We showed that the eGFP-CDC25B fusion protein is detected in only 6.6+/-0.8% of the electroporated population identified using pCS2:H2B-RFP (Suppl. Fig. 7 B, D). To determine whether some of the eGFP-CDC25B positive cells were in G1, we co-electroporated the eGFP-CDC25B expressing vector with the G1 phase marker

mKO-zFucci-G1. We did not detect co-expression of the eGFP-CDC25B fusion protein with the G1 phase marker (Suppl. Fig. 7 C, D) suggesting that the chimeric protein is not present during the G1 phase but rather in S/G2/M. The very limited periodic expression induced by the promoter and the intrinsic instability of CDC25B that is actively degraded at the end of mitosis probably precludes protein expression during the G1 phase. This data is in accordance with the absence of expression of the protein in G1 already described in synchronized cells in culture (Astuti et al. 2010). Thus, CDC25B expressed in S/G2/M would increase indirectly G1 phase length in NPCs.

One critical event during the G1 phase is the passage through the restriction point from which cells are committed to enter S phase. The passage through the restriction point depends on the phosphorylation of the retinoblastoma protein (Rb) that is used as a marker for cell cycle commitment. Recent studies have shown in epithelial cell lines that in some cells Rb becomes dephosphorylated as they exit mitosis and these cells can stay in this state for variable durations before re-entering the cell cycle, whereas other cells exit mitosis with a hyperphosphorylated Rb and are immediately committed to the next cell cycle (Gookin et al., 2017; Spencer et al., 2013). Moreover, it is suggested that the timing of restriction point crossing in G1 depends on the signaling history of the mother cell in the previous cell cycle and particularly on accumulation of regulators in the G2-phase (Min et al., 2020; Moser et al., 2018; Naetar et al., 2014). Considering that CDC25B is expressed in G2, this data led us to hypothesize that the G1 lengthening induced by CDC25B in proliferative NPCs could be the consequence of a delay of the restriction point passage. Immunostaining for phospho-Rb (S807/811) is classically used to analyze crossing of the restriction point (Moser et al., 2018; Spencer et al., 2013). Our goal was then to identify NPCs displaying Rb dephosphorylated in G1 (phospho-Rb negative cells) as a readout of the nuclei that are in the G1 pre restriction point phase. To restrict quantification to NPCs and avoid counting young neurons expected to be also phospho-Rb negative, we combined phospho-Rb staining and markers of young neurons (Tuj1/Tubb3 or HuC/D). We clearly identified phospho-Rb and Tuj1 or HuC/D negative cells in the ventricular zone (Fig.5 and not shown). We also verified that phospho-Rb/HuC/D negative cells were in G1 by using our FUCCI G1 and PCNA reporter (data not shown). We then quantified the percentage of phospho-Rb (S807/811) negative NPCs after CDC25B electroporation (Fig.5). To

restrict quantification to NPCs and avoid counting young neurons expected to be phospho-Rb negative, we combined phospho-Rb staining with a marker of young neurons (Tuj1/Tubb3). In dorsal spinal cord, 12.2%+/-0.8 of control electroporated cells where phospho-Rb/Tuj1 negative. This percentage raised to 19.9 %+/- 1.3% for CDC25B electroporated cells but was not affected by CDC25B$^{\Delta CDK}$ electroporation (10.9%+/-0.7%). This data showing that CDC25B increases the proportion of NPCs displaying dephosphorylated Rb in G1 suggest that it could thereby delay the passage through the restriction point and lengthen the G1 phase.

G1 phase lengthening occurs within NPC lineage

We then wanted to determine whether there was a link between the mode of division of NPCs and the length of the G1 phase. Three modes of division are observed in the developing spinal cord: proliferative where a progenitor gives rise to two progenitors (PP) and neurogenic where a progenitor gives rise to one progenitor and one neuron (PN) or to two neurons (NN). In our analysis, daughter cells are considered as proliferative progenitors (P) when, after mitosis, they entry into S-phase (display the punctuated distribution of the PCNA reporter). A cell which stops cycling (FUCCI G1 expression longer than 1000 min) is considered as a committed neuron and referred as N. We have characterized 32, 27 and 48 divisions of progenitors in Control, CDC25B and CDC25B$^{\Delta CDK}$ conditions, respectively (Table 2). In these dividing cells, 14 out of 20 G1 phase length of the mother cell performing PP divisions are below four hours (240 min) (Suppl. Fig. 8A). Noteworthy, 6 out of 20 cells performing PP division can still be observed with G1 phase length above five hours (300 min, Suppl. Fig. 8A) suggesting that a long G1 phase does not preclude proliferative division. G1 phase length heterogeneity is also observed for the few neurogenic divisions we were able to analyze (green points in Suppl. Fig. 8A). In these conditions, no clear correlation was observed between S phase duration and the mode of division (Suppl. Fig. 8B). However, the small amount of data is only indicative and does not allow to draw a clear answer.

We then took advantage of our single-cell tracking method to decipher how cell cycle dynamics evolves with time within a cell lineage. One example is given in Fig. 6A and an explicative scheme given in Fig.6B. We characterized the entire cell cycle of a mother cell and followed the cell cycle of the daughter cells. Cell by cell lineage analyses revealed that mother cells (MC) and daughter cells (DC) displayed

differential behavior in terms of G1 phase length. In control conditions, 12 out of 16 DC presented a longer G1 phase than their MC. To strengthen these data, given the difficulty of carrying out cell lineages, we performed the same type of analysis in the CDC25B$^{\Delta CDK}$ gain-of-function experiments since there is no modification of the cell cycle phases compared to control and in the CDC25B condition (Fig 4C). In the CDC25B$^{\Delta CDK}$ condition, 25 out of 33 DC exhibited a longer G1 phase (Fig. 6C). The average G1 phase length increased from 257+/-28 min to 309+/- 38 min and from 249+/-28 to 315+/-29 min in control and CDC25B$^{\Delta CDK}$ conditions, respectively. Among these DC, few exhibit FUCCI G1 expression longer than 1000 min corresponding to cell committed to neuronal differentiation (1 and 3 cells in control and CDC25B$^{\Delta CDK}$ condition, respectively; Fig 6C). To further analyze the evolution of G1 phase length, we plotted mother and daughter cell G1 phase lengths (Fig. 6D). Dots are mostly found above the bisector between the axes (dotted line), suggesting that DC G1 length is most often longer than its MC G1 length. We tested the hypothesis that the probability of finding a DC G1 length longer than its MC is greater than 0.5 using binomial tests. We obtained the following 95% CI and p-values: Control [0.52; 1.00], p=0.04, CDC25B : [0.19 ; 1.00], p=0.5 (NS, sample too small) and CDC25B$^{\Delta CDK}$ [0.60;1.00], p=0.0023 reinforcing the hypothesis that DC might display more often longer G1 phase that their MC. Interestingly, this effect does not appear to depend upon the MC G1 length.

Discussion

In this paper we detailed a live imaging strategy allowing us to follow the behavior of single NPCs over 48 hours in their endogenous environment. We show that the cell cycle duration and, more interestingly, the length of each phase is very heterogeneous and with no apparent links between phase lengths within one cell cycle or between mother cells G2 phase and daughter cells G1 phase. Though, we find that G1 phase length increases with cell generations and is the one which contributes mainly to the total cell cycle lengthening. We eventually show that expression of the G2/M regulator CDC25B enhances the percentage of non-phosphorylated Rb nuclei and G1 length range of heterogeneity in NPCs contributing to neural tissue maturation (Fig. 7).

The lengthening of the cell cycle results from enhanced range of heterogeneity

We show that the total cell cycle length exhibits a high degree of heterogeneity, ranging from 9h55 min to 24h45 min without apparent patterns or coupling between the phase length except a link between the S and M phase. Such a heterogeneity of the total cell cycle length has already been observed using time lapse imaging in neural stem/progenitor cells including spinal NPCs (Wilcock et al., 2007), mice neural stem cells in culture (Roccio et al., 2013), or human nervous system primary tissues and organoids (Subramanian et al., 2017). We show here that total cell cycle range of heterogeneity is the result of cumulative heterogeneity observed for each phase of the cell cycle, the phase that contributes the most to the total cell cycle variability being the G1 phase. In our analysis, we observe a correlation between the M and S phase. To our knowledge no link has been made between M and S phase duration but one between duration of M and the total cell cycle length has been observed in the work by Araujo and colleague (2016). They show that a modification of the cdk1-cyclinB1 positive feedback loop couples variability in cell-cycle length to duration of mitosis (Araujo et al., 2016).

Usually, analyses of cell cycle parameters were performed on fixed tissues, considering that neural stem cells are a homogenous population of asynchronous proliferating cells. Using this approximation, these analyses showed that as developmental time progresses, the proliferation rate of neural progenitors decreases and their cell cycle lengthens (Kicheva et al., 2014; Kicheva and Briscoe, 2015; Molina and Pituello, 2017). This evolution of the cell cycle length most often associated with differentiation was also observed in various stem cell types (Dalton, 2015; Julian et al., 2016). If the population of NPCs was homogeneous, an increase of the mean cell cycle duration with time would correspond to an increase of the cell cycle duration in each individual NPCs. Instead, we observed that the population of NPCs is heterogeneous in term of cell cycle length, and in this case the increase in the mean cell cycle duration occurring with time correlates with an increase in range of heterogeneity. To test possible relationships between the four phase lengths, we developed a mathematical model in which Tc length results of the sum of cell cycle phase duration stochastic and independent of each other. The experimental and theoretical Tc survival curves display a very similar pattern, suggesting that indeed cell cycle phase durations are stochastic and independent. It does not mean that the phases are independent, as cell divisions should not occur unless DNA is properly

replicated for example, but that their length is independent. One hypothesis is that permitting such stochastic variations at the single cell level is cost efficient for the population, which does not need to strictly control the cell cycle kinetics of each single cell and thereby is probably more robust. To our knowledge it is the first time this is observed for progenitors within their endogenous environment. These results are reminiscent of experimental data and modeling obtained using various cell lines in culture. In NIH3T3 cell cultures, lengthening one phase does not imply lengthening other phases, suggesting that durations of cell cycle phases can be regarded as independent (Mura et al., 2019). This is also observed for three independent human cell lines, where the cell cycle corresponds to a series of uncoupled memoryless phases (Chao et al., 2019).

A novel mechanism to generate the CDC25B-dependent increase of G1 and cell cycle length heterogeneity.

Time lapse analysis showed that even if all cell cycle phase lengths are heterogeneous the S and the G1 phases contribute the most to the total cell cycle range of heterogeneity, and that the G1 phase is the most affected one upon development. G1 phase heterogeneity has already been observed in neuroepithelial cells in culture (Roccio et al., 2013), in human embryonic stem cells in culture (Jang et al., 2019), and in mouse epidermal stem cell in vivo (Xie and Skotheim, 2020). Here we identified a new actor that triggers cell-to-cell G1 phase heterogeneity in NPCs, the CDC25B phosphatase. Electroporation in chick neural tube leads to mosaic expression. We therefore considered whether G1 heterogeneity could be caused by the method we used. If cells expressing a different amount of plasmid have different responses depending on the dose received, the variation observed should be similar in all phases. To address this, we used the exit time (τ) in Table 1 as a read out of the heterogeneity range. Comparison of the exit time in control versus CDC25B conditions shows an increase of 18% in Mitosis, 19% in S phase, 36% in G2 phase and 97% in G1 phase. Moreover, we did not detect the presence of the ectopic protein in G1. This strongly suggests that the increase in G1 heterogeneity range cannot be solely linked to the mosaic expression induced by electroporation but that it is mainly caused by the activity of CDC25B.

We have shown that the expression of CDC25B in NPCs correlates spatially and temporally with neurogenesis (Agius et al., 2015; Bonnet et al., 2018; Peco et al., 2012). Gain and loss-of-function experiments, revealed that CDC25B promotes neurogenic divisions (Bonnet et al., 2018; Peco et al., 2012) and, acts as a maturating factor reducing the proliferative capacities of the NPCs (Azaïs et al., 2019; Bonnet et al., 2018). Both CDK-dependent and CDK-independent activities of CDC25B are required for its full neurogenic activity. Here, we show that CDC25B induces a lengthening of the G1 phase duration in a CDK dependent manner. The effect on G1 is probably indirect since we did not detect the GFP-CDC25B fusion protein in G1. CDC25B gain-of-function induces a CDK dependent-increase of the percentage of NPCs with unphosphorylated retinoblastoma protein. This result suggests that CDC25B could, certainly indirectly, have an impact on the timing of restriction point crossing in NPCs. Indeed, one of the major mechanisms controlling the progression in the G1-phase is the restriction point that divides the G1 phase into two parts, G1 that lasts from mitosis to the restriction point and the G1 period after passage through the restriction point and the entry into S-phase. Spencer and coll. working on epithelial cells in culture have shown that, restriction point crossing might occurs after mitosis exit either directly or after a variable time spent in G1 (Gookin et al., 2017; Spencer et al., 2013). Interestingly, the same authors showed that the timing of restriction point crossing during G1 is associated to level of Cyclin D protein synthesis occurring in G2 (Min et al., 2020). CDC25B is shortening the G2 phase and therefore could hinder the synthesis of Cyclin D thereby delaying the restriction point crossing by reducing the level of Rb phosphorylation in daughter cells after mitosis. It is tempting to propose that NPCs which do not express CDC25B display longer G2 phases and cross the restriction point early after they exit mitosis, whereas, those expressing CDC25B exhibit shorter G2 phases and have a variable restriction point crossing time. CDC25B control of restriction point crossing could therefore contribute, at least partly, to G1 phase length heterogeneity. Deciphering this hypothesis in our model system is challenging and will require further investigations, including single cell measurement of the time spent in G1 prior restriction point crossing.

In CDC25B gain-of-function experiments, the total cell cycle duration was increased at least partly as a consequence of G1 phase lengthening. In our recent theoretical studies (Azaïs et al., 2019), we proposed that CDC25B expression in neural progenitors progressively restricts proliferative capacities of the cell. We

propose that CDC25B reiteration at each cell cycle will indirectly increase G1 phase range of heterogeneity, lengthening cell cycle duration associated with differentiation and participating to tissue maturation (Fig.7). Such a mechanism is likely to be applicable to other developing organs or tissues as well as to stem cells including human stem cells.

Acknowledgement

We want to thank Bernard Ducommun, Alice Davy and Xavier Morin for critical review of the manuscript and Caroline Monod for improving the English. We thank the CBI Toulouse Regional Imaging platform (TRI) for technical support. We acknowledge the Developmental Studies Hybridoma Bank, created by the NICHD of the NIH and maintained at The University of Iowa, Department of Biology, Iowa City, IA 52242, for supplying monoclonal antibodies. Work in FP's laboratory is supported by the Centre National de la Recherche Scientifique, Université P. Sabatier, Ministère de L'Enseignement Supérieur et de la Recherche (MESR) et Agence Nationale de la Recherche (ANR-19-CE16-0006-01). Angie Molina was a recipient of IDEX UNITI and Fondation ARC. Fréderic Bonnet was recipient of MESR studentships. The funding entities had no role in study design, data collection and analysis, decision to publish, or preparation of the manuscript.

Author Contributions

A.M., F.B., J.P, V.L, F.P., J.G. and E.A. conceived experiments. A.M., F.B., J.P. and E.A. performed experiments. A.M., F.B., V.L., F.P., J.G. and E.A wrote the manuscript. F.P., J.G., V.L. S.B.V. and E.A secured funding. S.B.V. provided expertise and feedback.

Declaration of interests

The authors declare no competing interests.

Bibliography

Agius, E., Bel-Vialar, S., Bonnet, F. and Pituello, F. (2015). Cell cycle and cell fate in the developing nervous system: the role of CDC25B phosphatase. *Cell Tissue Res* **359**, 201-213.

Arai, Y., Pulvers, J. N., Haffner, C., Schilling, B., Nusslein, I., Calegari, F. and Huttner, W. B. (2011). Neural stem and progenitor cells shorten S-phase on commitment to neuron production. *Nat Commun* **2**, 154.

Artegiani, B., Lindemann, D. and Calegari, F. (2011). Overexpression of cdk4 and cyclinD1 triggers greater expansion of neural stem cells in the adult mouse brain. *J Exp Med* **208**, 937-948.

Azaïs, M., Agius, E., Blanco, S., Molina, A., Pituello, F., Tregan, J. M., Vallet, A. and Gautrais, J. (2019). Timing the spinal cord development with neural progenitor cells losing their proliferative capacity: a theoretical analysis. *Neural Dev* **14**, 7.

Bajar, B. T., Lam, A. J., Badiee, R. K., Oh, Y. H., Chu, J., Zhou, X. X., Kim, N., Kim, B. B., Chung, M., Yablonovitch, A. L., et al. (2016). Fluorescent indicators for simultaneous reporting of all four cell cycle phases. *Nat Methods* **13**, 993-996.

Benazeraf, B., Chen, Q., Peco, E., Lobjois, V., Medevielle, F., Ducommun, B. and Pituello, F. (2006). Identification of an unexpected link between the Shh pathway and a G2/M regulator, the phosphatase CDC25B. *Dev Biol* **294**, 133-147.

Bonnet, F., Molina, A., Roussat, M., Azais, M., Vialar, S., Gautrais, J., Pituello, F. and Agius, E. (2018). Neurogenic decisions require a cell cycle independent function of the CDC25B phosphatase. *Elife* **7**.

Boudreau, C., Wee, T. L., Duh, Y. R., Couto, M. P., Ardakani, K. H. and Brown, C. M. (2016). Excitation Light Dose Engineering to Reduce Photo-bleaching and Photo-toxicity. *Sci Rep* **6**, 30892.

Cao, X., Pfaff, S. L. and Gage, F. H. (2008). YAP regulates neural progenitor cell number via the TEA domain transcription factor. *Genes Dev* **22**, 3320-3334.

Chao, H. X., Fakhreddin, R. I., Shimerov, H. K., Kedziora, K. M., Kumar, R. J., Perez, J., Limas, J. C., Grant, G. D., Cook, J. G., Gupta, G. P., et al. (2019). Evidence that the human cell cycle is a series of uncoupled, memoryless phases. *Mol Syst Biol* **15**, e8604.

Dalton, S. (2015). Linking the Cell Cycle to Cell Fate Decisions. *Trends Cell Biol* **25**, 592-600.

Das, R. M., Wilcock, A. C., Swedlow, J. R. and Storey, K. G. (2012). High-resolution live imaging of cell behavior in the developing neuroepithelium. *J Vis Exp*.

Fawal, M. A., Jungas, T., Kischel, A., Audouard, C., Iacovoni, J. S. and Davy, A. (2018). Cross Talk between One-Carbon Metabolism, Eph Signaling, and Histone Methylation Promotes Neural Stem Cell Differentiation. *Cell Rep* **23**, 2864-2873.e2867.

Fousse, J., Gautier, E., Patti, D. and Dehay, C. (2019). Developmental changes in interkinetic nuclear migration dynamics with respect to cell-cycle progression in the mouse cerebral cortex ventricular zone. *J Comp Neurol* **527**, 1545-1557.

Gookin, S., Min, M., Phadke, H., Chung, M., Moser, J., Miller, I., Carter, D. and Spencer, S. L. (2017). A map of protein dynamics during cell-cycle progression and cell-cycle exit. *PLoS Biol* **15**, e2003268.

Gruber, R., Zhou, Z., Sukchev, M., Joerss, T., Frappart, P. O. and Wang, Z. Q. (2011). MCPH1 regulates the neuroprogenitor division mode by coupling the centrosomal cycle with mitotic entry through the Chk1-Cdc25 pathway. *Nat Cell Biol* **13**, 1325-1334.

Hamburger, V. and Hamilton, H. L. (1992). A series of normal stages in the development of the chick embryo. 1951. *Dev Dyn* **195**, 231-272.

Hardwick, L. J., Ali, F. R., Azzarelli, R. and Philpott, A. (2015). Cell cycle regulation of proliferation versus differentiation in the central nervous system. *Cell Tissue Res* **359**, 187-200.

Icha, J., Weber, M., Waters, J. C. and Norden, C. (2017). Phototoxicity in live fluorescence microscopy, and how to avoid it. *Bioessays* **39**.

Jang, J., Han, D., Golkaram, M., Audouard, M., Liu, G., Bridges, D., Hellander, S., Chialastri, A., Dey, S. S., Petzold, L. R., et al. (2019). Control over single-cell distribution of G1 lengths by WNT governs pluripotency. *PLoS Biol* **17**, e3000453.

Julian, L. M., Carpenedo, R. L., Rothberg, J. L. and Stanford, W. L. (2016). Formula G1: Cell cycle in the driver's seat of stem cell fate determination. *Bioessays* **38**, 325-332.

Kicheva, A., Bollenbach, T., Ribeiro, A., Valle, H. P., Lovell-Badge, R., Episkopou, V. and Briscoe, J. (2014). Coordination of progenitor specification and growth in mouse and chick spinal cord. *Science* **345**, 1254927.

Kicheva, A. and Briscoe, J. (2015). Developmental Pattern Formation in Phases. *Trends Cell Biol* **25**, 579-591.

Knobloch, M. and Jessberger, S. (2017). Metabolism and neurogenesis. *Curr Opin Neurobiol* **42**, 45-52.

Korner, K., Jerome, V., Schmidt, T. and Muller, R. (2001). Cell cycle regulation of the murine cdc25B promoter: essential role for nuclear factor-Y and a proximal repressor element. *J Biol Chem* **276**, 9662-9669.

Kosodo, Y., Suetsugu, T., Suda, M., Mimori-Kiyosue, Y., Toida, K., Baba, S. A., Kimura, A. and Matsuzaki, F. (2011). Regulation of interkinetic nuclear migration by cell cycle-coupled active and passive mechanisms in the developing brain. *EMBO J* **30**, 1690-1704.

Kumagai, A. and Dunphy, W. G. (1991). The cdc25 protein controls tyrosine dephosphorylation of the cdc2 protein in a cell-free system. *Cell* **64**, 903-914.

Lacomme, M., Liaubet, L., Pituello, F. and Bel-Vialar, S. (2012). NEUROG2 drives cell cycle exit of neuronal precursors by specifically repressing a subset of cyclins acting at the G1 and S phases of the cell cycle. *Mol Cell Biol*.

Laguesse, S., Peyre, E. and Nguyen, L. (2015). Progenitor genealogy in the developing cerebral cortex. *Cell Tissue Res* **359**, 17-32.

Lange, C., Huttner, W. B. and Calegari, F. (2009). Cdk4/cyclinD1 overexpression in neural stem cells shortens G1, delays neurogenesis, and promotes the generation and expansion of basal progenitors. *Cell Stem Cell* **5**, 320-331.

Langman, J., Guerrant, R. L. and Freeman, B. G. (1966). Behavior of neuro-epithelial cells during closure of the neural tube. *J Comp Neurol* **127**, 399-411.

Le Dreau, G., Saade, M., Gutierrez-Vallejo, I. and Marti, E. (2014). The strength of SMAD1/5 activity determines the mode of stem cell division in the developing spinal cord. *J Cell Biol* **204**, 591-605.

Leonhardt, H., Rahn, H. P., Weinzierl, P., Sporbert, A., Cremer, T., Zink, D. and Cardoso, M. C. (2000). Dynamics of DNA replication factories in living cells. *J Cell Biol* **149**, 271-280.

Leung, L., Klopper, A. V., Grill, S. W., Harris, W. A. and Norden, C. (2011). Apical migration of nuclei during G2 is a prerequisite for all nuclear motion in zebrafish neuroepithelia. *Development* **138**, 5003-5013.

Lim, S. and Kaldis, P. (2012). Loss of Cdk2 and Cdk4 induces a switch from proliferation to differentiation in neural stem cells. *Stem Cells* **30**, 1509-1520.

Liu, L., Michowski, W., Kolodziejczyk, A. and Sicinski, P. (2019). The cell cycle in stem cell proliferation, pluripotency and differentiation. *Nat Cell Biol* **21**, 1060-1067.

Lobjois, V., Bel-Vialar, S., Trousse, F. and Pituello, F. (2008). Forcing neural progenitor cells to cycle is insufficient to alter cell-fate decision and timing of neuronal differentiation in the spinal cord. *Neural Dev* **3**, 4.

Lobjois, V., Benazeraf, B., Bertrand, N., Medevielle, F. and Pituello, F. (2004). Specific regulation of cyclins D1 and D2 by FGF and Shh signaling coordinates cell cycle progression, patterning, and differentiation during early steps of spinal cord development. *Dev Biol* **273**, 195-209.

Min, M., Rong, Y., Tian, C. and Spencer, S. L. (2020). Temporal integration of mitogen history in mother cells controls proliferation of daughter cells. *Science* **368**, 1261-1265.

Molina, A. and Pituello, F. (2017). Playing with the cell cycle to build the spinal cord. *Dev Biol* **432**, 14-23.

Moser, J., Miller, I., Carter, D. and Spencer, S. L. (2018). Control of the Restriction Point by Rb and p21. *Proc Natl Acad Sci U S A* **115**, E8219-E8227.

Mura, M., Feillet, C., Bertolusso, R., Delaunay, F. and Kimmel, M. (2019). Mathematical modelling reveals unexpected inheritance and variability patterns of cell cycle parameters in mammalian cells. *PLoS Comput Biol* **15**, e1007054.

Naetar, N., Soundarapandian, V., Litovchick, L., Goguen, K. L., Sablina, A. A., Bowman-Colin, C., Sicinski, P., Hahn, W. C., DeCaprio, J. A. and Livingston, D. M. (2014). PP2A-mediated regulation of Ras signaling in G2 is essential for stable quiescence and normal G1 length. *Mol Cell* **54**, 932-945.

Nowakowski, R. S., Lewin, S. B. and Miller, M. W. (1989). Bromodeoxyuridine immunohistochemical determination of the lengths of the cell cycle and the DNA-synthetic phase for an anatomically defined population. *J Neurocytol* **18**, 311-318.

Oppenheim, R. W., Cole, T. and Prevette, D. (1989). Early regional variations in motoneuron numbers arise by differential proliferation in the chick embryo spinal cord. *Dev Biol* **133**, 468-474.

Peco, E., Escude, T., Agius, E., Sabado, V., Medevielle, F., Ducommun, B. and Pituello, F. (2012). The CDC25B phosphatase shortens the G2 phase of neural progenitors and promotes efficient neuron production. *Development* **139**, 1095-1104.

Pilaz, L. J., Patti, D., Marcy, G., Ollier, E., Pfister, S., Douglas, R. J., Betizeau, M., Gautier, E., Cortay, V., Doerflinger, N., et al. (2009). Forced G1-phase reduction alters mode of division, neuron number, and laminar phenotype in the cerebral cortex. *Proc Natl Acad Sci U S A* **106**, 21924-21929.

Pituello, F., Yamada, G. and Gruss, P. (1995). Activin A inhibits Pax-6 expression and perturbs cell differentiation in the developing spinal cord in vitro. *Proc Natl Acad Sci U S A* **92**, 6952-6956.

Roccio, M., Schmitter, D., Knobloch, M., Okawa, Y., Sage, D. and Lutolf, M. P. (2013). Predicting stem cell fate changes by differential cell cycle progression patterns. *Development* **140**, 459-470.

Saade, M., Gutierrez-Vallejo, I., Le Dreau, G., Rabadan, M. A., Miguez, D. G., Buceta, J. and Marti, E. (2013). Sonic hedgehog signaling switches the mode of division in the developing nervous system. *Cell Rep* **4**, 492-503.

Sakaue-Sawano, A., Kurokawa, H., Morimura, T., Hanyu, A., Hama, H., Osawa, H., Kashiwagi, S., Fukami, K., Miyata, T., Miyoshi, H., et al. (2008). Visualizing spatiotemporal dynamics of multicellular cell-cycle progression. *Cell* **132**, 487-498.

Schneider, C. A., Rasband, W. S. and Eliceiri, K. W. (2012). NIH Image to ImageJ: 25 years of image analysis. *Nat Methods* **9**, 671-675.

Spencer, S. L., Cappell, S. D., Tsai, F. C., Overton, K. W., Wang, C. L. and Meyer, T. (2013). The proliferation-quiescence decision is controlled by a bifurcation in CDK2 activity at mitotic exit. *Cell* **155**, 369-383.

Subramanian, L., Bershteyn, M., Paredes, M. F. and Kriegstein, A. R. (2017). Dynamic behaviour of human neuroepithelial cells in the developing forebrain. *Nat Commun* **8**, 14167.

Sugiyama, M., Sakaue-Sawano, A., Iimura, T., Fukami, K., Kitaguchi, T., Kawakami, K., Okamoto, H., Higashijima, S. and Miyawaki, A. (2009). Illuminating cell-cycle progression in the developing zebrafish embryo. *Proc Natl Acad Sci U S A* **106**, 20812-20817.

Ueno, H., Nakajo, N., Watanabe, M., Isoda, M. and Sagata, N. (2008). FoxM1-driven cell division is required for neuronal differentiation in early Xenopus embryos. *Development* **135**, 2023-2030.

Wilcock, A. C., Swedlow, J. R. and Storey, K. G. (2007). Mitotic spindle orientation distinguishes stem cell and terminal modes of neuron production in the early spinal cord. *Development* **134**, 1943-1954.

Xie, S. and Skotheim, J. M. (2020). A G1 Sizer Coordinates Growth and Division in the Mouse Epidermis. *Curr Biol* **30**, 916-924.e912.

Figures and Tables

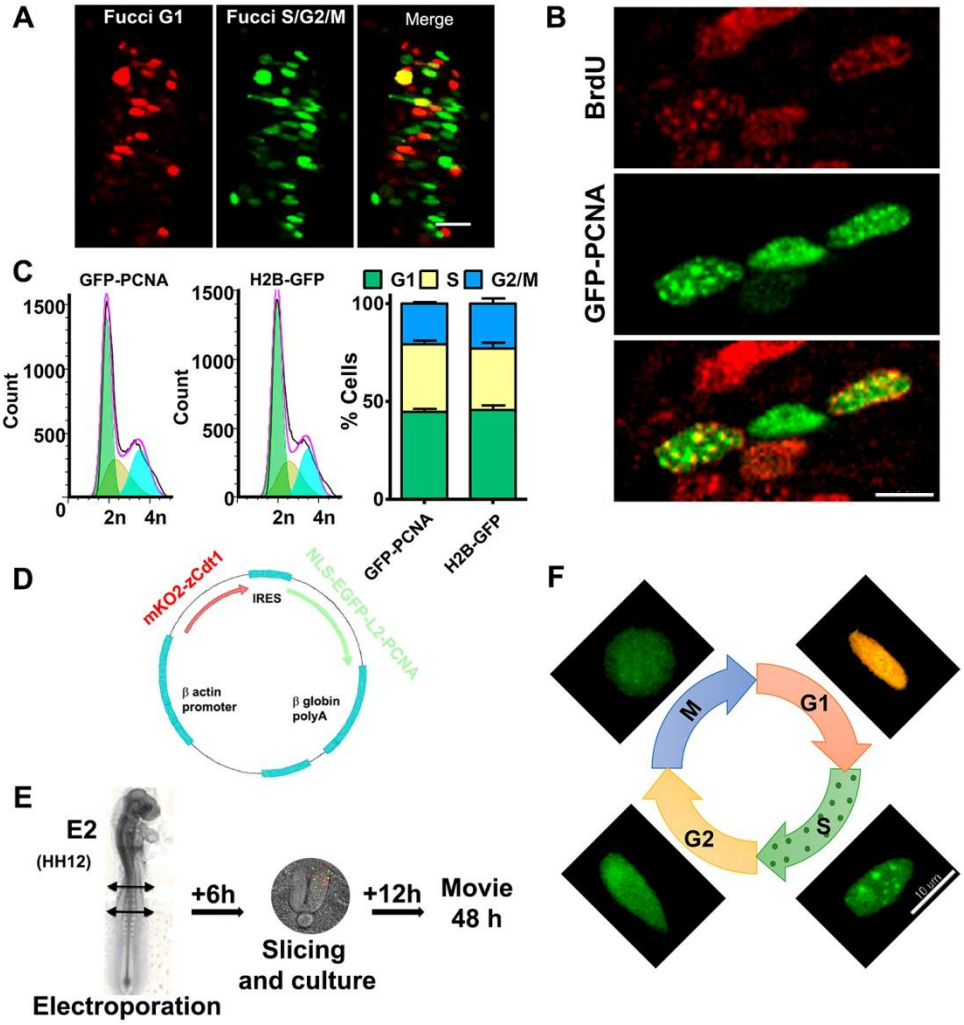

Figure 1. FUCCI-G1-PCNA biosensor marks the four cell cycle phases in chick neuroepithelium. **A)** Cross-sections of chick neural tube expressing FUCCI G1 (red) and FUCCI S/G2/M (green) vectors. **B)** Representative sections of chick embryonic spinal cord expressing GFP-PCNA (green) and stained after BrdU incorporation (red) to identify S-phase cells. **C)** Flow cytometry profiles of DNA content for GFP-PCNA or H2B-GFP electroporated NPCs (left panels). The diagram (right panel) corresponds to the deduced percentage of cells in G1 (44.7 ± 1.4% compared to 45.7 ± 2.4%), S (34.5 ± 1.9% compared to 31.4 ± 2.9%) and G2/M phases (20.8 ± 0.7% compared to 22.9 ± 2.6%) after GFP-PCNA or H2B-GFP electroporation respectively. **D)** Schematic representation of the mKO-zCdt1-pIRES-NLS-EGFP-L2-PCNA reporter. **E)** Scheme of the experimental protocol for time-lapse imaging. **F)**

Representative images of chick NPC nuclei through the cell cycle after electroporation of FUCCI G1-PCNA vector. The four phases are identified by differential expression and distribution of FUCCI- G1 (red) and GFP-PCNA (green) proteins. Scale bar : 10 µm.

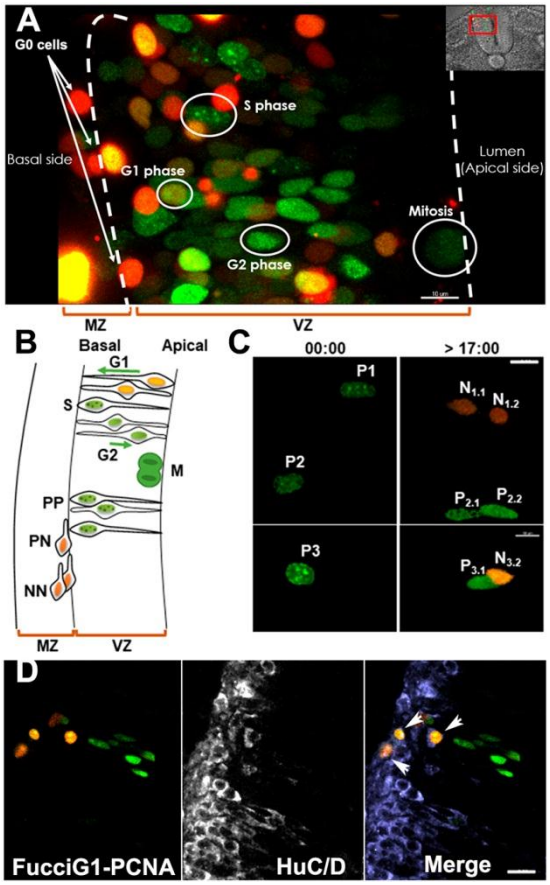

Figure 2. Time lapse observation of NPCs displaying three types of cell division after mitosis. A) Still picture of a time lapse video showing the expression of the FUCCI G1-PCNA reporter in the nucleus of NPCs that allows identification of the four cell cycle phases and the corresponding position within the neuroepithelium. **B)** Schematic representation of the interkinetic nuclear movement (INM) and of the three modes of division (PP, PN and NN) occurring in the neural tube. MZ, mantle zone. VZ, ventricular zone. **C)** Still images of a E2.25 culture time lapse movie showing the three modes of division observed in the spinal cord from progenitors P1 (NN), P2 (PP), P3 (PN). Scale bars : 10 µm. **D)** Images of an explant, immunostained for HuC/D, after a time lapse video of 48 hours. The FUCCI G1 expressing cells (orange) located at the basal side (arrows) are HuC/D positive. Scale bar: 20 µm

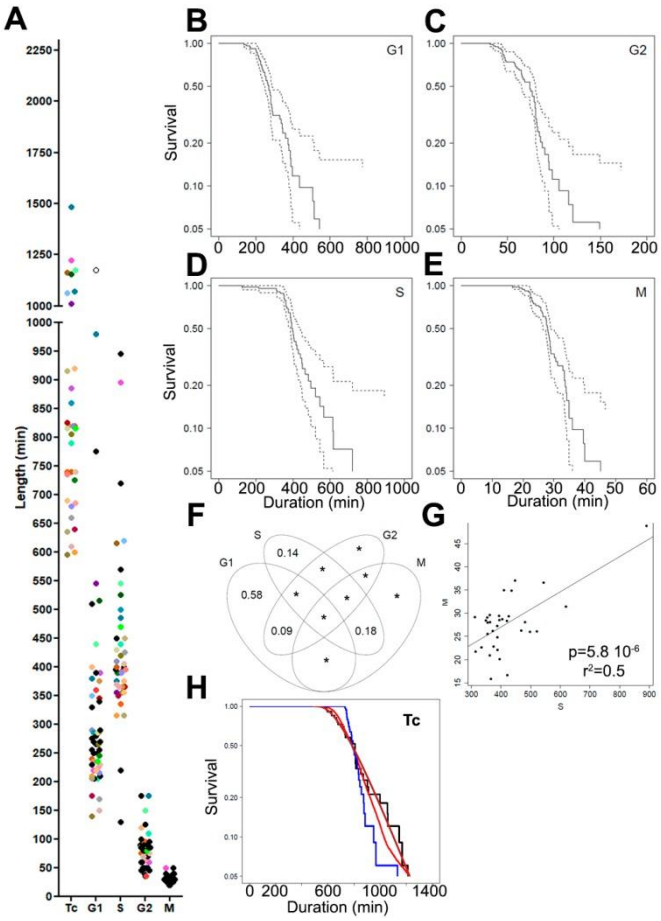

Figure 3. Neural progenitor cell population is highly heterogeneous regarding the cell cycle. A: Scatter dot-plot representing distributed lengths of total (Tc) and cell cycle phases for E2.25 embryonic spinal cord cells observed in live imaging (see numbers in Table1). Each colored dot in the Tc column can be found in the cell cycle phase columns and corresponds to the same tracked nucleus. The empty dot corresponds to a cell with a G1 length of 1175 min (19h35min) that does not start S phase. **B-E:** Survival curves to quantify absolute dispersion of G1 phase (**B**), G2 phase (**C**), S phase (**D**), and mitosis (**E**). Black line corresponds to Kaplan-Meier estimates of survival and dashed lines to confidence intervals. **F:** Variation partitioning showing how much variation of the Tc is attributed to each phase. Stars (*) represent values below 0.05. **G:** Correlation analysis between S and M phases. **H**: Tc Survival curve. Black line corresponds to Kaplan-Meier estimate from data. Brown line corresponds to expected survival assuming a random sampling of cell cycle phase duration (see SI-section). Red line corresponds to survival curve obtained in Monte Carlo permutation of phase durations from the data set. Blue curve corresponds to the case with G1 and S/G2/M phase lengths fully anti-correlated (see SI-section).

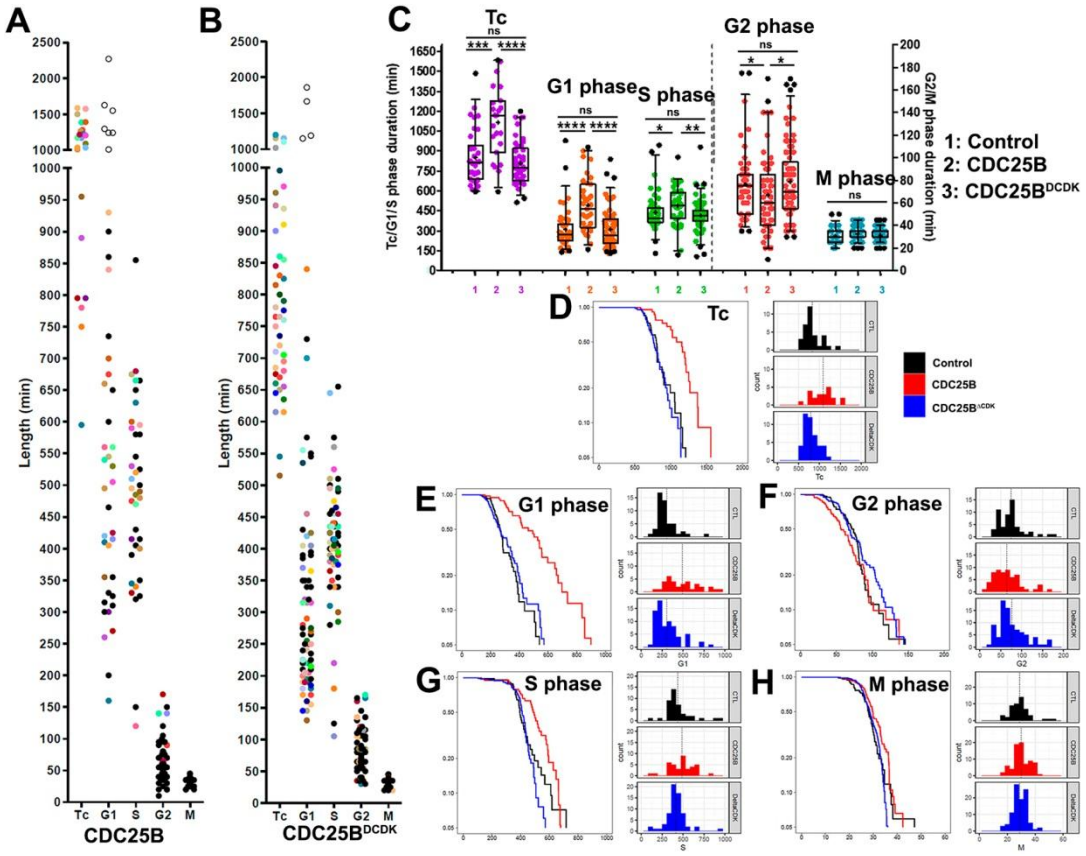

Figure 4. CDC25B gain-of-function increases G1 phase length heterogeneity. **A-B:** Scatter dot-plot representing distributed lengths of total (Tc) and cell cycle phases measured in live imaging E2.25 cultures for cells electroporated with CDC25B (**A)** or CDC25B$^{\Delta CDK}$ (**B).** Each colored dot in the Tc column can be found in the cell cycle phase columns and corresponds to the same tracked nucleus. Empty dots represent cells with a G1 length longer than 1000 minutes (16h40min). **C:** Box and whiskers plots (5-95 percentile) illustrating the comparison of total (Tc) and cell cycle phase lengths for Control, CDC25B, CDC25B$^{\Delta CDK}$ gain-of-function. The top and the bottom of each box indicate upper and lower quartiles, respectively; the horizontal line represents the median and the cross indicates the mean value. **D-H**: Survival curves and histogram representation comparing Control (black), CDC25B (red), and CDC25B$^{\Delta CDK}$ (blue) conditions for the Tc (**D**), G1 **(E**), G2 **(F**), S **(G**), and M (**H**), phases. The vertical dotted line in histograms reports the average of the distribution.

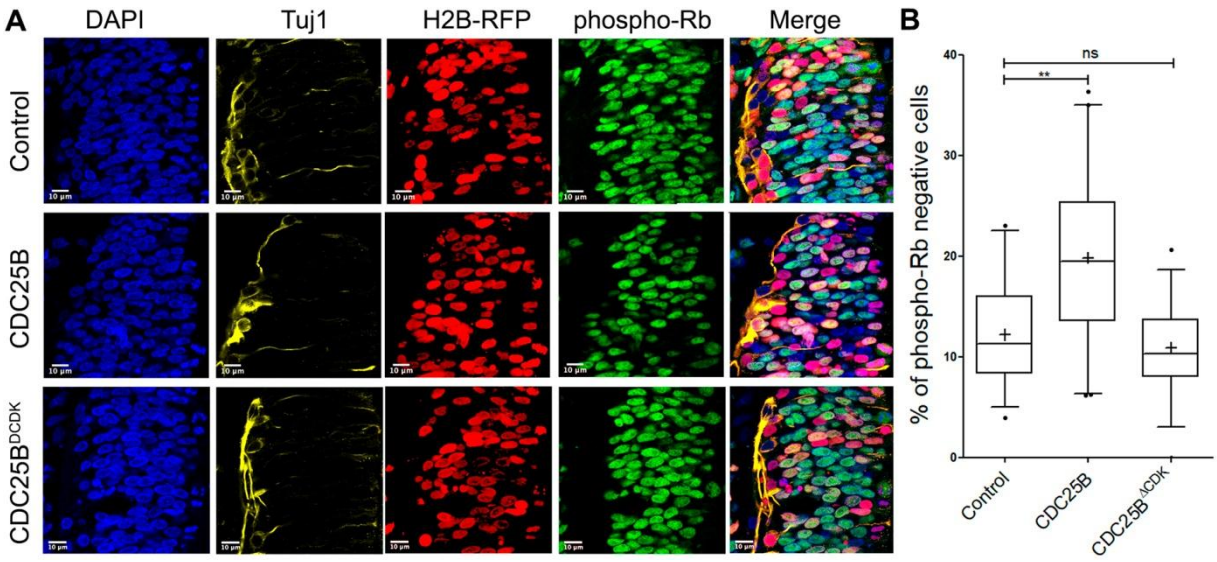

Figure 5. CDC25B but not CDC25B$^{\Delta CDK}$ gain-of-function reduces the percentage of phosphorylated retinoblastoma protein. A: Representative cross-sections of HH17 chick spinal cord, 24 hours after co-electroporating pCS::H2B-RFP and a control, CDC25B or CDC25B$^{\Delta CDK}$ vector. Sections are stained with a DNA marker (DAPI), a neuronal marker (Tuj1) and the phospho-Rb (S807/811) marker. **B:** Box and whiskers plots (5-95 percentile) illustrating the comparison of the proportion of phospho-Rb negative cells in the electroporated population. The cross represents the mean. **p<=0,001, ns: non-significant. Data are from three independent experiments.

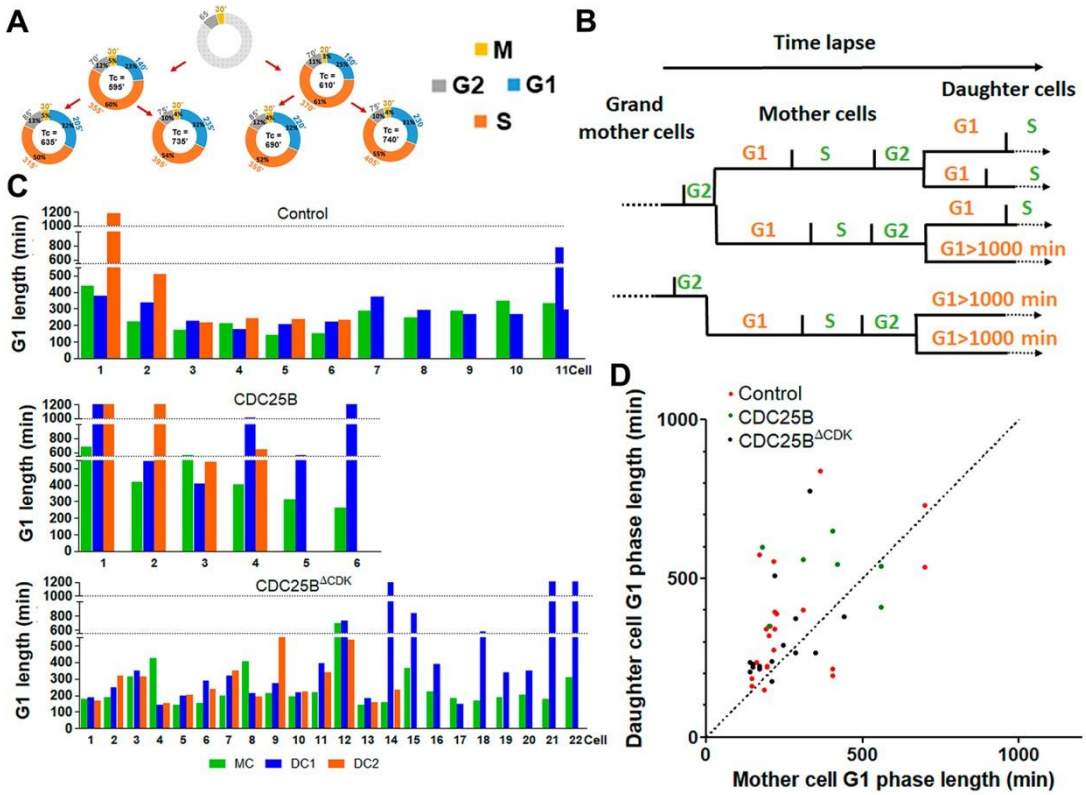

Figure 6. G1 phase tends to lengthen in daughter cells. A: Schematic representation of nuclei tracking over two generations of proliferating NPCs. Cell cycle total (Tc) and phase lengths are calculated from time-lapse images. Proportion of each phase in the whole cell cycle according to Tc is represented inside the circles. Light grey represents undetermined values. **B:** Schematic representation of lineage tracking over two generations of proliferating NPCs. The entire cell cycle of mother and daughter cells is observed and the cell cycle of the daughter cells allows to differentiate cells reentering the cycle from those stopping in G1 (G1>1000 min). **C:** Bar diagrams illustrating G1 phase length of mother (MC, green) and daughter (DC, blue and orange) NPC in Control (top) CDC25B (middle) or CDC25B$^{\Delta CDK}$ (bottom) conditions. **D:** From data represented in C, only pairs of mother cell (MC), and daughter cell (DC) where DC G1 length is <1000 minutes were kept. Each DC G1 length is reported in ordinates at abscissa of the corresponding MC G1 phase length. In 12 out of 16 for Control (red), 5 out of 7 in CDC25B (green) and 25 out of 33 for CDC25B $^{\Delta CDK}$ (black) DC G1 length is longer than its MC G1 length.

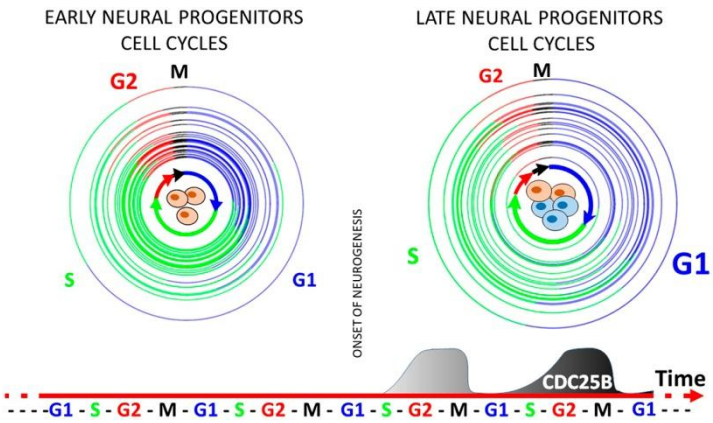

Figure 7. schematic representation of the evolution of neural progenitor cell cycle kinetics. Each cell cycle is represented by a colored line. In early stages, the population of neural progenitors display heterogeneous cell cycles. At the onset of neurogenesis, the cyclic expression of CDC25B leads to an increase in G1 phase length heterogeneity.

Table 1 Column statistics of the cell cycle parameters

		Tc (min)	G1 (min)	S (min)	G2 (min)	M (min)
Control	Mean	841	309	439	77	31
	Median	815	268	395	75	30
	Minimum	595	140	130	35	20
	Maximum	1485	980	945	175	55
	Minimal duration (Dm)	595	140	130	35	20
	Exit time (τ)	246	169	309	42	11
	Std. Deviation	205	148	149	30	7
	Number of values	33	50	41	54	50
Complete Cycles	Mean	841	307	423	80	30
	Median	815	265	395	80	30
	Minimum	595	140	315	35	20
	Maximum	1485	980	895	175	50
	Minimal duration (Dm)	584	139	311	33	20
	Exit time (τ)	247	166	110	45	12
	Std. Deviation	205	156	108	29	6
	Number of values	33	33	33	33	33
CDC25B	Mean	1099	494	488	67	33
	Median	1170	465	493	60	30
	Minimum	595	160	120	10	20
	Maximum	1585	930	855	170	45
	Minimal duration (Dm)	595	160	120	10	20
	Exit time (τ)	505	334	368	57	13
	Std. Deviation	266	202	147	34	6
	Number of values	23	35	38	61	76
CDC25B $^{\Delta CDK}$	Mean	809	310	416	79	31
	Median	775	265	415	70	30
	Minimum	515	130	105	30	20
	Maximum	1200	840	930	170	45
	Minimal duration (Dm)	509	130	105	30	20
	Exit time (τ)	294	180	311	49	11
	Std. Deviation	170	144	116	33	5
	Number of values	45	71	66	86	98

Table 2: Percentage of the modes of division observed during time lapse under various conditions.

Mode of division	Control (32)	CDC25B (27)	CDC25B$^{\Delta CDK}$ (48)
PP	59,4%	40,7%	58,3%
PN	3,1%	14,8%	2,1%
NN	3,1%	14,8%	8,3%
P?	34,4%	25,9%	25,0%
N?	0%	3,7%	6,3%

P? and N? correspond to cells for which only one daughter cell could be identified

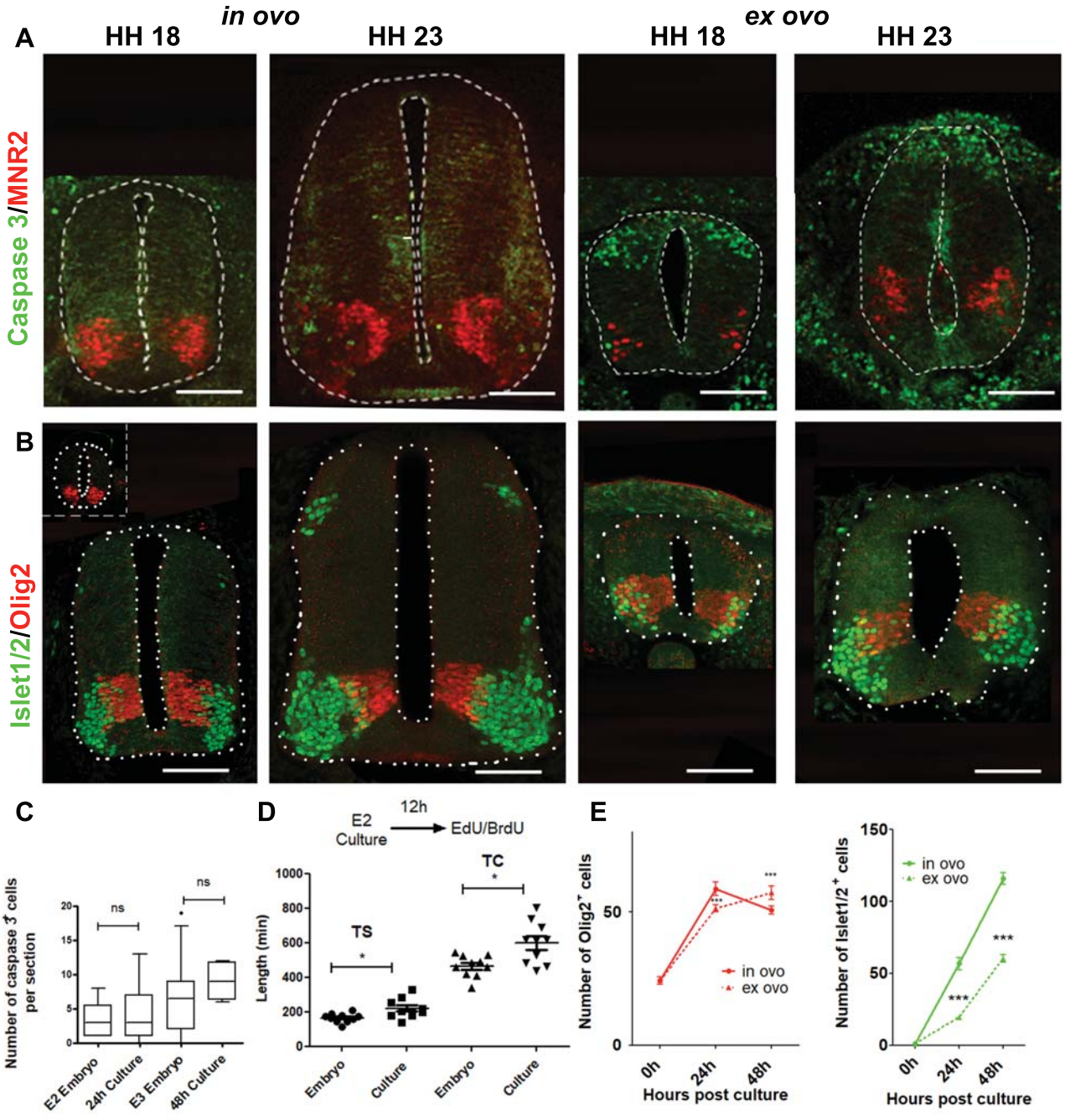

Fig. S1. Characterization of *ex vivo* culture of chick embryonic neural tube explants. A, B: Cross-sections of E2.5 and E3.5 (stage HH18, HH23) chick embryo spinal cord (in ovo), and explants dissected at E1.5 and cultivated for 24 hours and 48h hours (ex ovo). Sections processed for anti-caspase3 (green) and anti-MNR2 (red) immunostaining (**A**) or anti-Olig2 (red) and anti-Islet1/2 (green) immunostaining (**B**). Inset in B, E1.5 (HH13) embryo section. **C:** Bar plots representing the number activated caspase 3 positive cells per optical section under various conditions. Means +/- sem of 3 different experiments with at least 4 embryos. **D:** Scatter dot plot representing S phase duration (Ts) and total cell cycle duration (Tc) calculated using Dual Pulse Labeling using EdU and BrdU incorporation paradigm in embryos and in cultures, revealing a transient lengthening of the cell cycle in progenitors at 12 hours after dissection that is recovered at 24 hours (not shown). **E:** Curves representing kinetics of the number of cells expressing Olig2 and Islet1/2 per section in the spinal cord (in ovo) or in explants (ex vivo) starting at E1.5 (t = 0h), 24 hours or 48 hours later. The increase in the population of progenitors and neurons in our culture conditions indicates that progenitors are performing both proliferative and neurogenic divisions. Data from three different experiments with at least four embryos for in ovo condition, and six sections from three embryos for the ex ovo condition. Scale bars represent 100 μm.

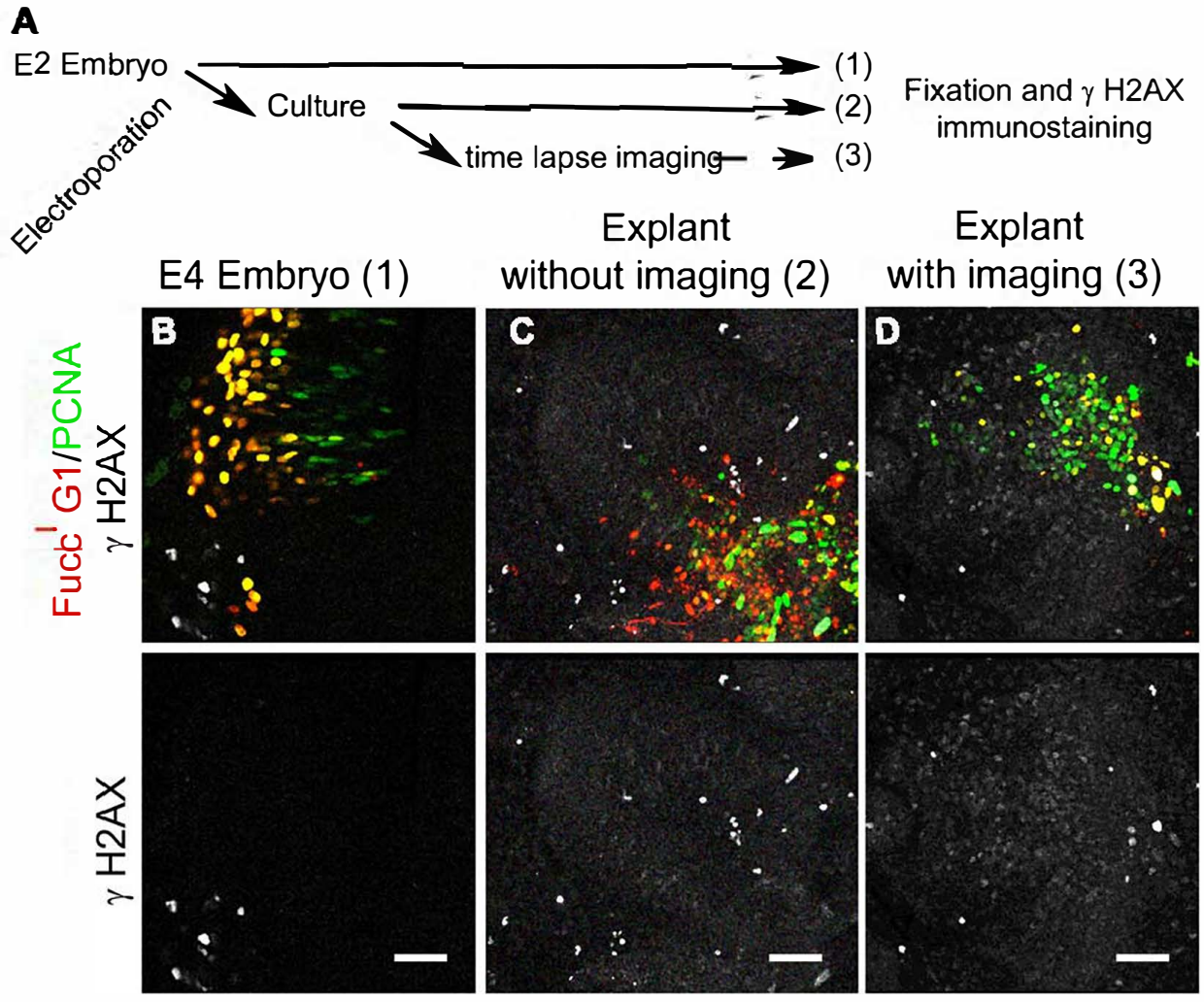

Fig. S2. γH2AX immunostaining after time lapse experiments. **A:** scheme of the protocol. **B:** Representative spinal cord section of an electroporated embryo with the FUCCI G1/PCNA plasmid and allowed to develop for 2.5 days. The γH2AX positive cells are apoptotic motoneurons. **C:** Spinal cord explant of an electroporated embryo with the FUCCI G1/PCNA plasmid and allowed to develop for 2.5 days in culture without imaging. **D:** Spinal cord explant of an electroporated embryo with the FUCCI G1/PCNA plasmid and imaged for 48 hours. Scale bars represent 50μm.

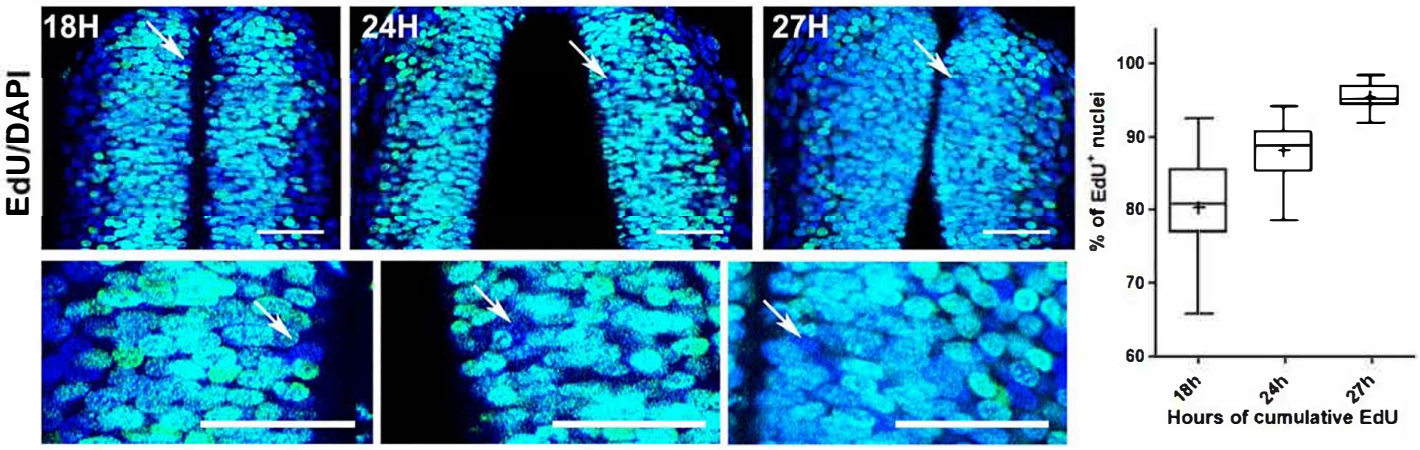

Fig. S3. Cumulative EdU experiment. **A:** E2.5 embryos received 10µl of 4µM EdU on the heart every 3 hours for 27 hours. Embryos were fixed at 6 hours, 12 hours, 18 hours, 24 hours and 27 hours, 30 min after the last EdU treatment. EdU (green) was revealed according to manufacturer's protocol (Invitrogen) and sections were counterstained using DAPI (blue). The figure shows spinal cord sections at 18, 24 or 27 hours. The arrows point to progenitor nuclei without EdU. Scale bars represent 50µm. **B:** Box and whiskers plots (5-95 percentile) illustrating the quantification of the percentage of EdU^+ nuclei in the dorsal spinal cord. At least 2 sections were counted on three embryos for each time points.

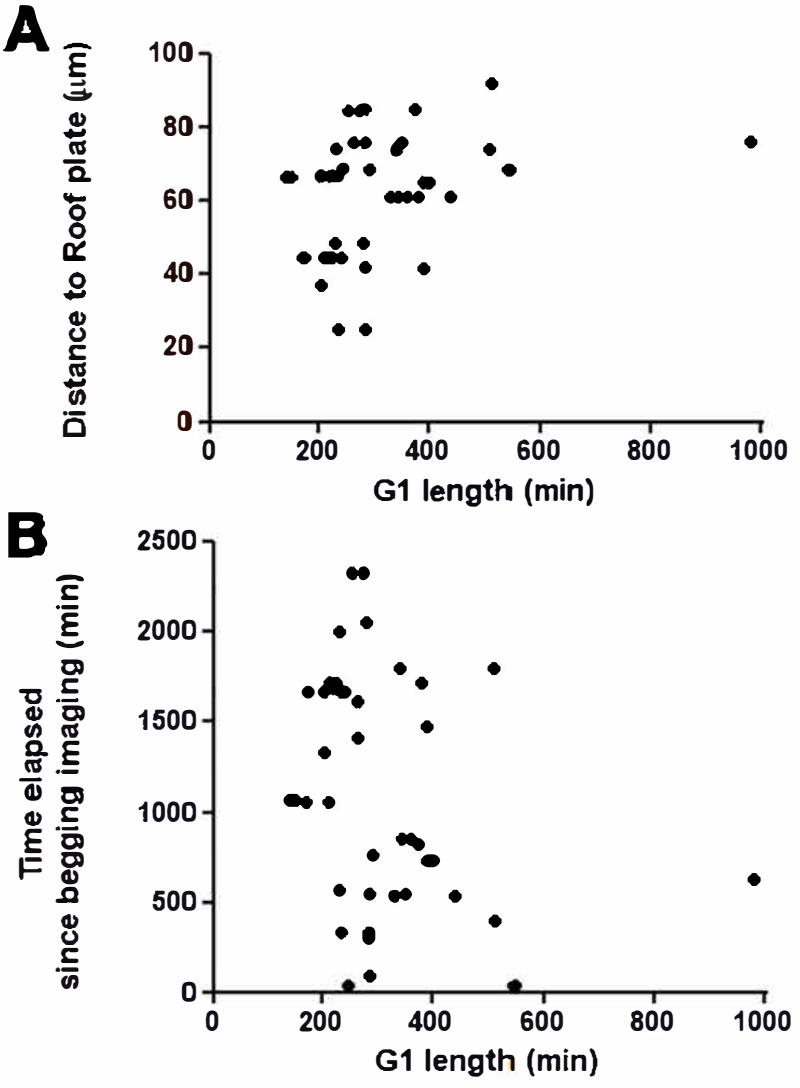

Fig. S4. The G1 phase length variation is independent of the clone position or of the time of analysis. A: Dot plot analysis of the G1 phase length plotted compared to the distance of the cell to the roof plate. **B:** Dot plot analysis of the G1 phase length plotted compared to the time elapsed since then beginning of the video.

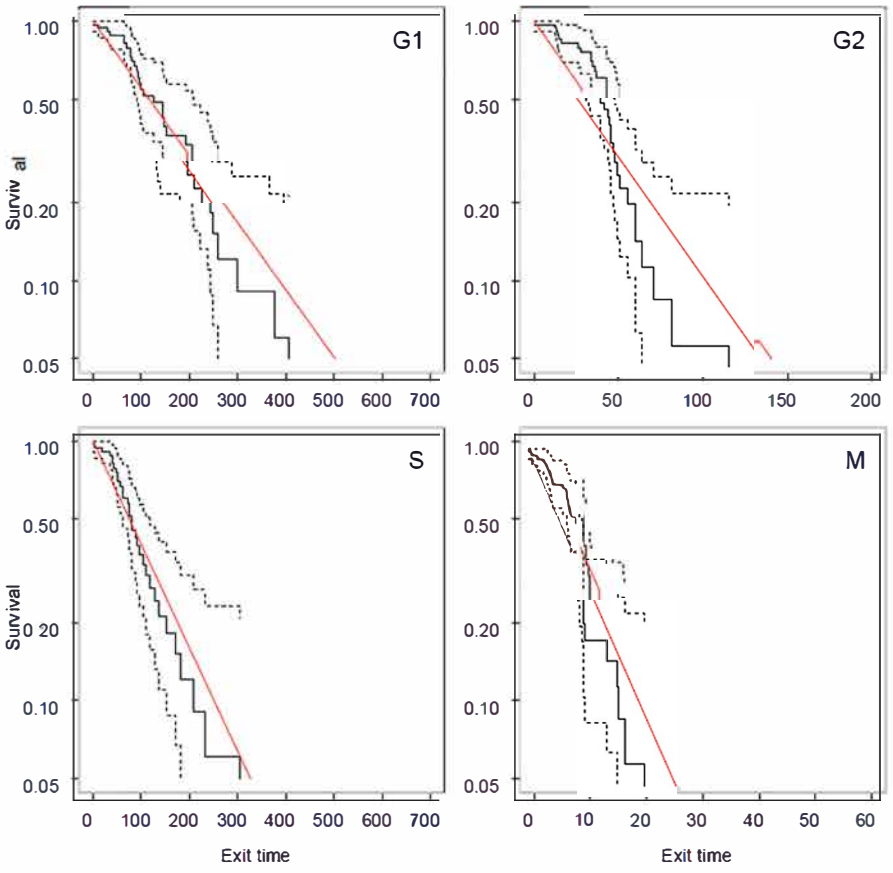

Fig. S5. **Survival curves for exit times for the four cell cycle phases**. Survival curves were obtained from the data subset of complete cell cycle tracked cells in control conditions. Exit times are obtained by subtracting minimal time from observed times. Black curves are Kaplan-Meier estimates of survival, with confidence interval. For this subset, survival curves appear to be about compatible with simple exponential decay (red curves), corresponding to a simple memoryless process.

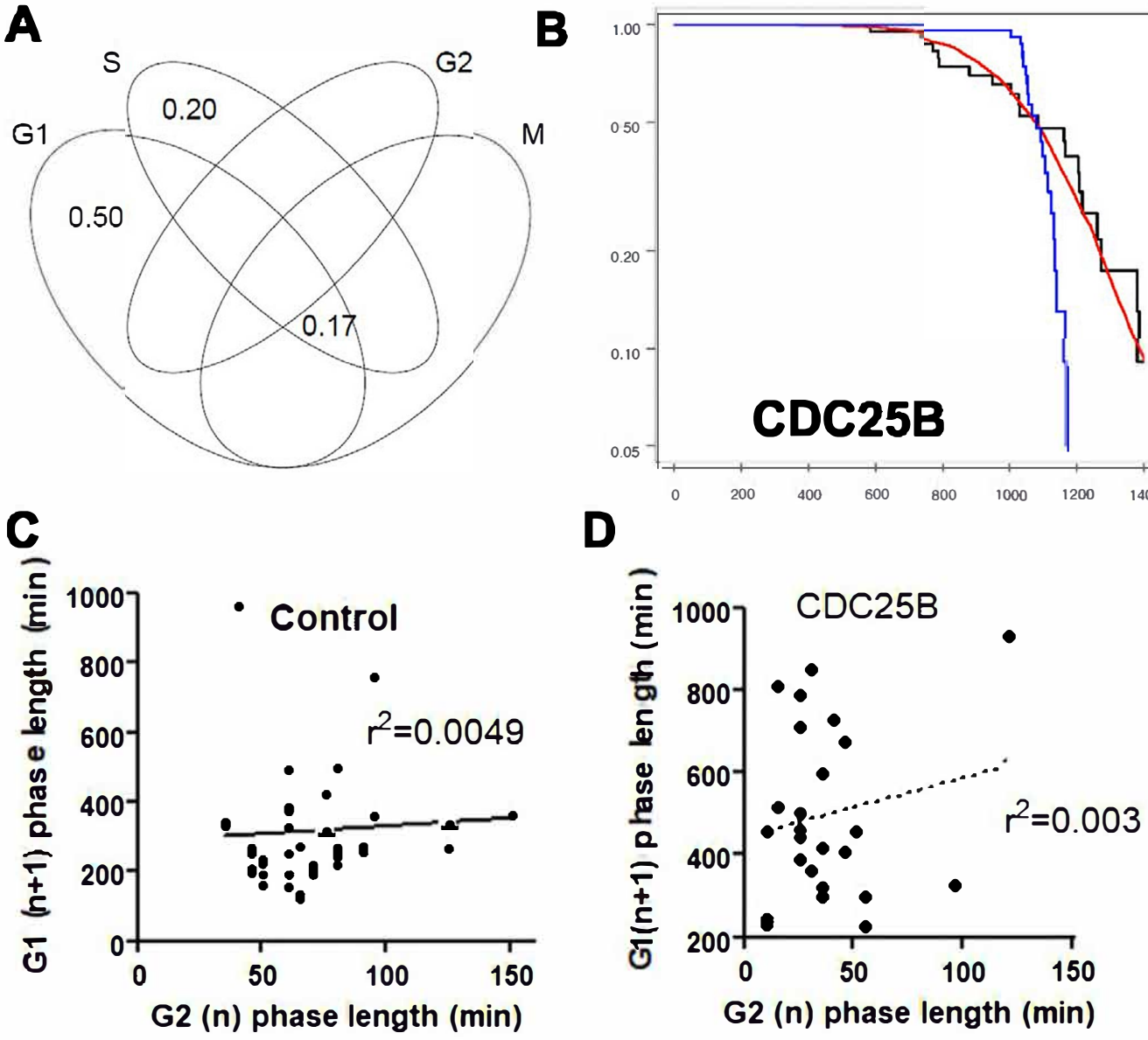

Fig. S6. CDC25B effects on cell cycle heterogeneity A: Variation partitioning (Venn Diagrams) in CDC25B gain of function showing how much variation is attributed to each phase. **B:** Survival curve of Tc phase length data in the CDC25B condition. Black line corresponds to Kaplan-Meier estimate from data. Red line corresponds to the survival curve obtained in Monte Carlo permutation of phase durations from the data set and the blue curve corresponds to the case with G1 and S/G2/M phases lengths fully anti-correlated (see SI-sect). **C, D:** Correlation analysis between G2 phase lengths of the mother cell and G1 phase lengths of the daughter cell in control (**C**) and CDC25B (**D**) conditions.

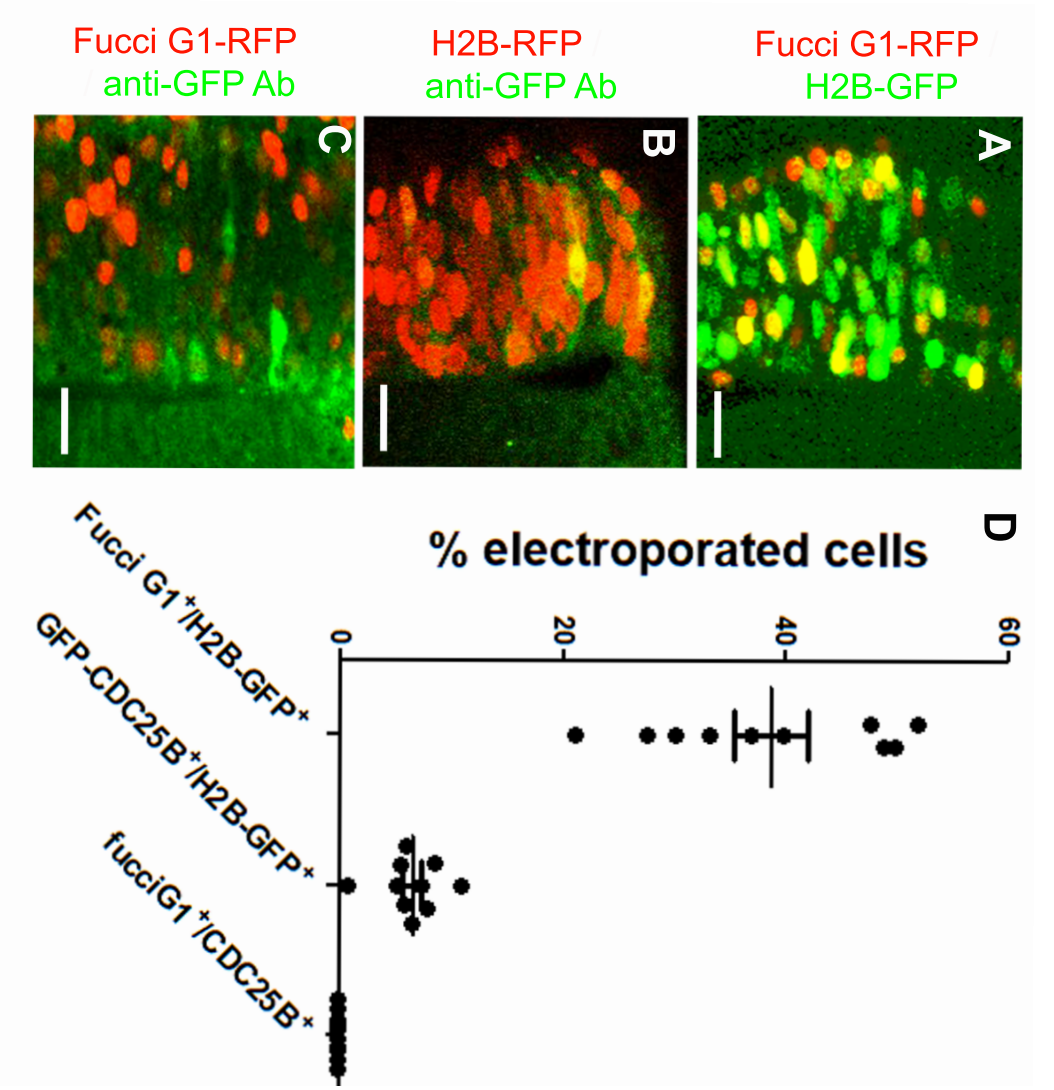

Fig. S7. CDC25B-GFP protein is not detected during the G1 phase. **A**: Co electroporation of pCS::H2B-GFP and mKO-zFucci-G1 to quantify the number of cells co-expressing the FUCCI G1-RFP and the H2B-GFP proteins (38.8+/-3.4%). **B**: immunodetection using an anti GFP antibody after co-electroporation of the ccRE::GFP-CDC25B (green) with pCS::H2B-RFP (red) to quantify the number of electroporated cells expressing CDC25B protein (6.6+/-0.8%). **C**: Immunodetection using an anti GFP antibody after co-electroporation of ccRE::GFP-CDC25B with mKO-zFucci-G1. CDC25B-GFP expressing cells are not expressing the G1 marker. **D:** The graph shows the percentage of co-electroporated cells in the indicated conditions. Dots correspond to sections from 3 embryos and 2 experiments. Mean+/- sem is shown for each condition.

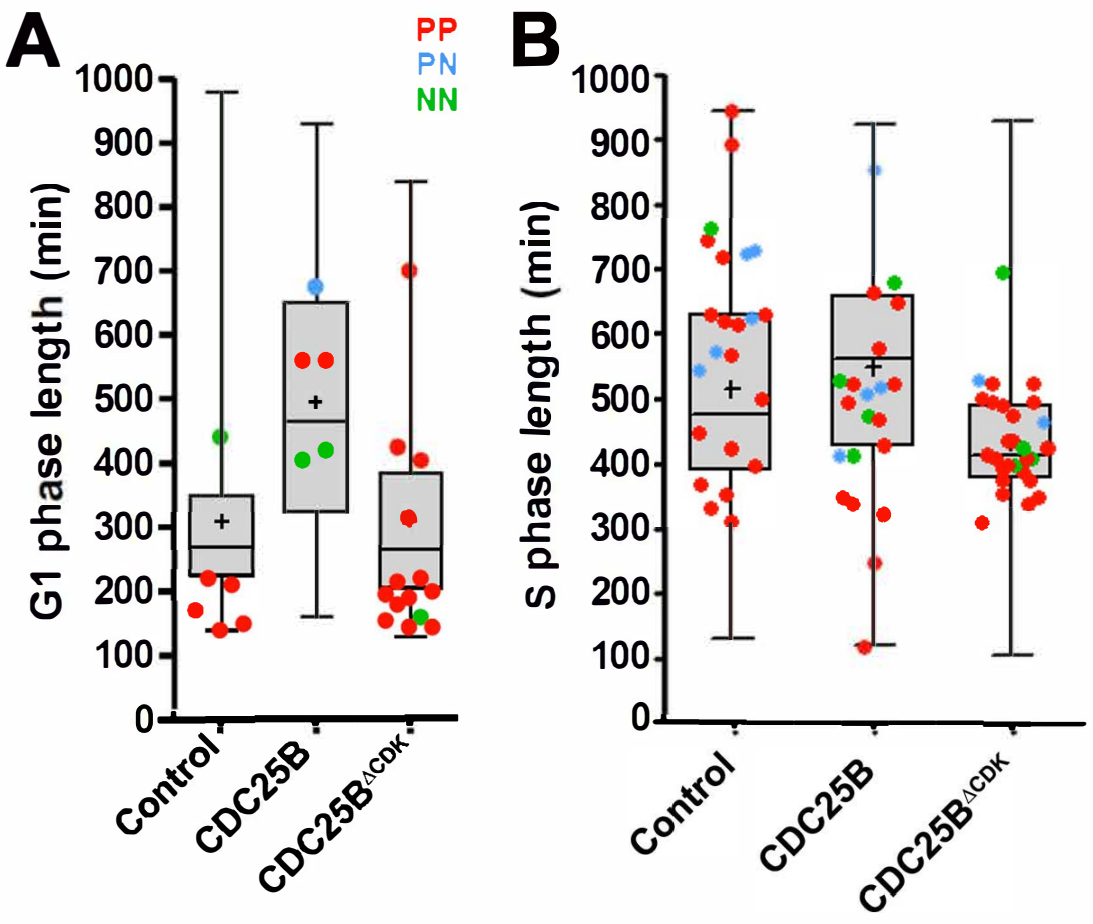

Fig. S8. Modes of division and G1 phase length. Box and whiskers plot representing the distribution of lengths of G1 phase (**A**) or S phase (**B**) in Control, CDC25B, CDC25B$^{\Delta CDK}$ associated with scatter dot-plot representing the G1 lengths of individual NPCs performing PP divisions in the following cell cycle (red dots), NPCs giving rise to a progenitor and a cell with a long G1 (asymmetric division, green dots) and NPCs generating 2 daughter cells with long G1s (blue dots).

Table S1. Column statistics of the cell cycle parameters.

		Tc (min)	G1 (min)	S (min)	G2 (min)	M (min)
Control	Mean	841	309	439	77	31
	Median	815	268	395	75	30
	Minimum	595	140	130	35	20
	Maximum	1485	980	945	175	55
	Minimal duration (Dm)	595	140	130	35	20
	Exit time (τ)	246	169	309	42	11
	Std. Deviation	205	148	149	30	7
	Number of values	33	50	41	54	50
Complete Cycles	Mean	841	307	423	80	30
	Median	815	265	395	80	30
	Minimum	595	140	315	35	20
	Maximum	1485	980	895	175	50
	Minimal duration (Dm)	584	139	311	33	20
	Exit time (τ)	247	166	110	45	12
	Std. Deviation	205	156	108	29	6
	Number of values	33	33	33	33	33
CDC25B	Mean	1099	494	488	67	33
	Median	1170	465	493	60	30
	Minimum	595	160	120	10	20
	Maximum	1585	930	855	170	45
	Minimal duration (Dm)	595	160	120	10	20
	Exit time (τ)	505	334	368	57	13
	Std. Deviation	266	202	147	34	6
	Number of values	23	35	38	61	76
CDC25B $^{\Delta CDK}$	Mean	809	310	416	79	31
	Median	775	265	415	70	30
	Minimum	515	130	105	30	20
	Maximum	1200	840	930	170	45
	Minimal duration (Dm)	509	130	105	30	20
	Exit time (τ)	294	180	311	49	11
	Std. Deviation	170	144	116	33	5
	Number of values	45	71	66	86	98

Table S2. percentage of the mode of divisions observed during time lapse under various conditions.

Mode of division	Control (32)	CDC25B (27)	CDC25B$^{\Delta CDK}$ (48)
PP	59,4%	40,7%	58,3%
PN	3,1%	14,8%	2,1%
NN	3,1%	14,8%	8,3%
P?	34,4%	25,9%	25,0%
N?	0%	3,7%	6,3%

P? and N? correspond to cells for which only one daughter cell could be identified

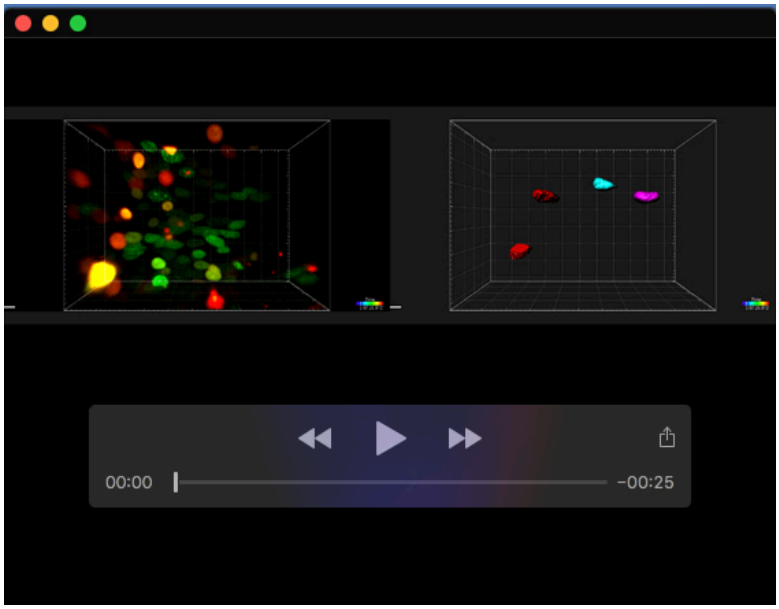

Movie 1. Expression of the cell cycle biosensor within the nucleus of NPCs allows the identification of the four cell cycle phases. Left panel- Live imaging movie. The four cell cycle phases are discriminated by the differential expression of the sensor, as well as the movements of nuclei inside the neural tube (Interkinetic Nuclear Movement, INM). Right panel - Segmentation of some analyzed nuclei. Time interval between frames = 5 min. Scale bar = 10 μm.

Contents

1 Data Descriptions **2**
- 1.1 Data summaries . . . 2
  - 1.1.1 CONTROL . . . 2
  - 1.1.2 CDC25B . . . 2
  - 1.1.3 CDC25B$^{\Delta CDK}$ . . . 2
- 1.2 Statistics of durations . . . 3
  - 1.2.1 Minimal durations . . . 3
  - 1.2.2 Standard deviation of phase durations . . . 3
  - 1.2.3 Mean exit times . . . 3
- 1.3 Survival curves for each condition. . . . 4
  - 1.3.1 CONTROL . . . 4
  - 1.3.2 CDC25B . . . 5
  - 1.3.3 CDC25B$^{\Delta CDK}$ . . . 6

2 Subset with complete tracking of phases within the same cycle **7**
- 2.1 Graphical summaries . . . 7
- 2.2 Variation Partitionning (Venn Diagrams) . . . 8
- 2.3 Tests of correlation among phases . . . 9
  - 2.3.1 Statistical results . . . 9
  - 2.3.2 Graphics for CONTROL . . . 10
  - 2.3.3 Graphics for CDC25B . . . 17
  - 2.3.4 Graphics for CDC25B$^{\Delta CDK}$ . . . 24
- 2.4 Predicted survival curves for total duration under independence hypothesis. . . . 31
  - 2.4.1 Theoretical *null* model for total duration . . . 31
  - 2.4.2 Null model by Monte Carlo permutation . . . 31
  - 2.4.3 Ordered permutations with full anti-correlation between G1 and S+G2+M . . . 31
- 2.5 Survival curves for phase exit time in each condition. . . . 32
  - 2.5.1 CONTROL . . . 32
  - 2.5.2 CDC25B . . . 33
  - 2.5.3 CDC25B$^{\Delta CDK}$ . . . 34
- 2.6 Survival curves for Tc. . . . 35
  - 2.6.1 CONTROL . . . 35
  - 2.6.2 CDC25B . . . 36
  - 2.6.3 CDC25B$^{\Delta CDK}$ . . . 37

3 Survival Analysis for the experimental treatment **38**
- 3.1 Tc . . . 39
- 3.2 G1 . . . 40
- 3.3 S . . . 41
- 3.4 G2 . . . 42
- 3.5 M . . . 43

1 Data Descriptions

We read durations data from 00-AllPhasesData.csv.

For complete cycles, we can compute Tc.

Note : in R outputs all along below, the condition is encoded as factor according to :

Condition	Code
CONTROL	CTL
CDC25B	CDC25B
CDC25B$^{\Delta CDK}$	DeltaCDK

1.1 Data summaries

1.1.1 CONTROL

```
   Condition        G1              S              G2              M              Tc
CTL     :54   Min.   :140.0   Min.   :130.0   Min.   : 35.00   Min.   :20.00   Min.   : 595.0
CDC25B  : 0   1st Qu.:227.5   1st Qu.:365.0   1st Qu.: 52.50   1st Qu.:25.00   1st Qu.: 690.0
DeltaCDK: 0   Median :270.0   Median :397.5   Median : 75.00   Median :30.00   Median : 815.0
              Mean   :308.7   Mean   :438.6   Mean   : 76.57   Mean   :31.27   Mean   : 840.9
              3rd Qu.:347.5   3rd Qu.:465.0   3rd Qu.: 85.00   3rd Qu.:35.00   3rd Qu.: 915.0
              Max.   :980.0   Max.   :945.0   Max.   :175.00   Max.   :55.00   Max.   :1485.0
              NA's   :3       NA's   :12                       NA's   :3       NA's   :21
```

1.1.2 CDC25B

```
   Condition        G1              S              G2              M              Tc
CTL     : 0   Min.   :160.0   Min.   :120.0   Min.   : 10.00   Min.   :20.00   Min.   : 595.0
CDC25B  :76   1st Qu.:327.5   1st Qu.:401.2   1st Qu.: 40.00   1st Qu.:30.00   1st Qu.: 906.2
DeltaCDK: 0   Median :465.0   Median :492.5   Median : 60.00   Median :30.00   Median :1130.0
              Mean   :494.4   Mean   :487.5   Mean   : 66.89   Mean   :32.76   Mean   :1099.8
              3rd Qu.:625.0   3rd Qu.:587.5   3rd Qu.: 80.00   3rd Qu.:35.00   3rd Qu.:1255.0
              Max.   :930.0   Max.   :855.0   Max.   :170.00   Max.   :45.00   Max.   :1585.0
              NA's   :41      NA's   :38      NA's   :15                       NA's   :54
```

1.1.3 CDC25B$^{\Delta CDK}$

```
   Condition        G1              S              G2              M              Tc
CTL     : 0   Min.   :130.0   Min.   :105.0   Min.   : 30.00   Min.   :20.00   Min.   : 515.0
CDC25B  : 0   1st Qu.:207.5   1st Qu.:376.2   1st Qu.: 56.25   1st Qu.:30.00   1st Qu.: 680.0
DeltaCDK:98   Median :265.0   Median :415.0   Median : 70.00   Median :30.00   Median : 775.0
              Mean   :309.6   Mean   :416.4   Mean   : 79.13   Mean   :31.48   Mean   : 809.3
              3rd Qu.:377.5   3rd Qu.:455.0   3rd Qu.: 93.75   3rd Qu.:35.00   3rd Qu.: 910.0
              Max.   :840.0   Max.   :930.0   Max.   :170.00   Max.   :45.00   Max.   :1200.0
              NA's   :27      NA's   :32      NA's   :12                       NA's   :53
```

1.2 Statistics of durations

For each phase: minimal duration, standard deviations of phases duration and mean latency before exiting the phase starting from this minimum (hereafter denoted *Exit times*).

1.2.1 Minimal durations

Condition	G1	S	G2	M	Tc
CONTROL	140	130	35	20	595
CDC25B	160	120	10	20	595
CDC25B$^{\Delta CDK}$	130	105	30	20	515

1.2.2 Standard deviation of phase durations

Condition	G1	S	G2	M	Tc
CONTROL	148	149	30	7	205
CDC25B	202	147	34	6	266
CDC25B$^{\Delta CDK}$	144	116	33	5	170

1.2.3 Mean exit times

Condition	G1	S	G2	M	Tc
CONTROL	169	309	42	11	246
CDC25B	334	368	57	13	505
CDC25B$^{\Delta CDK}$	180	311	49	11	294

1.3 Survival curves for each condition.

We add noise to avoid ties. Actually, snaps were made every 5 min, so the event has occured within the last 5 minutes. Hence we distribube its date randomly within those last 5 minutes.

1.3.1 CONTROL

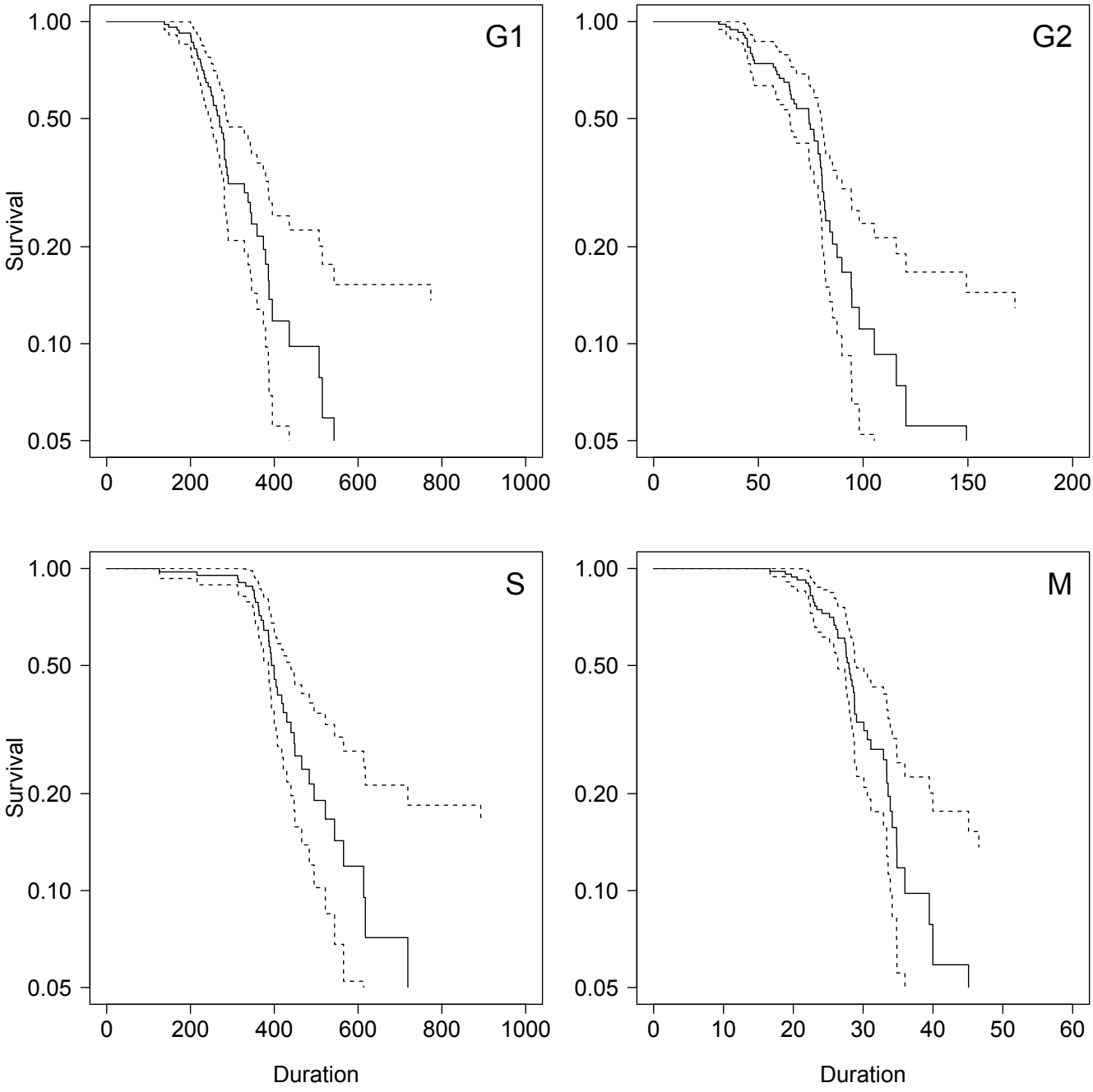

Fig. S1. Phases Survival curves

1.3.2 CDC25B

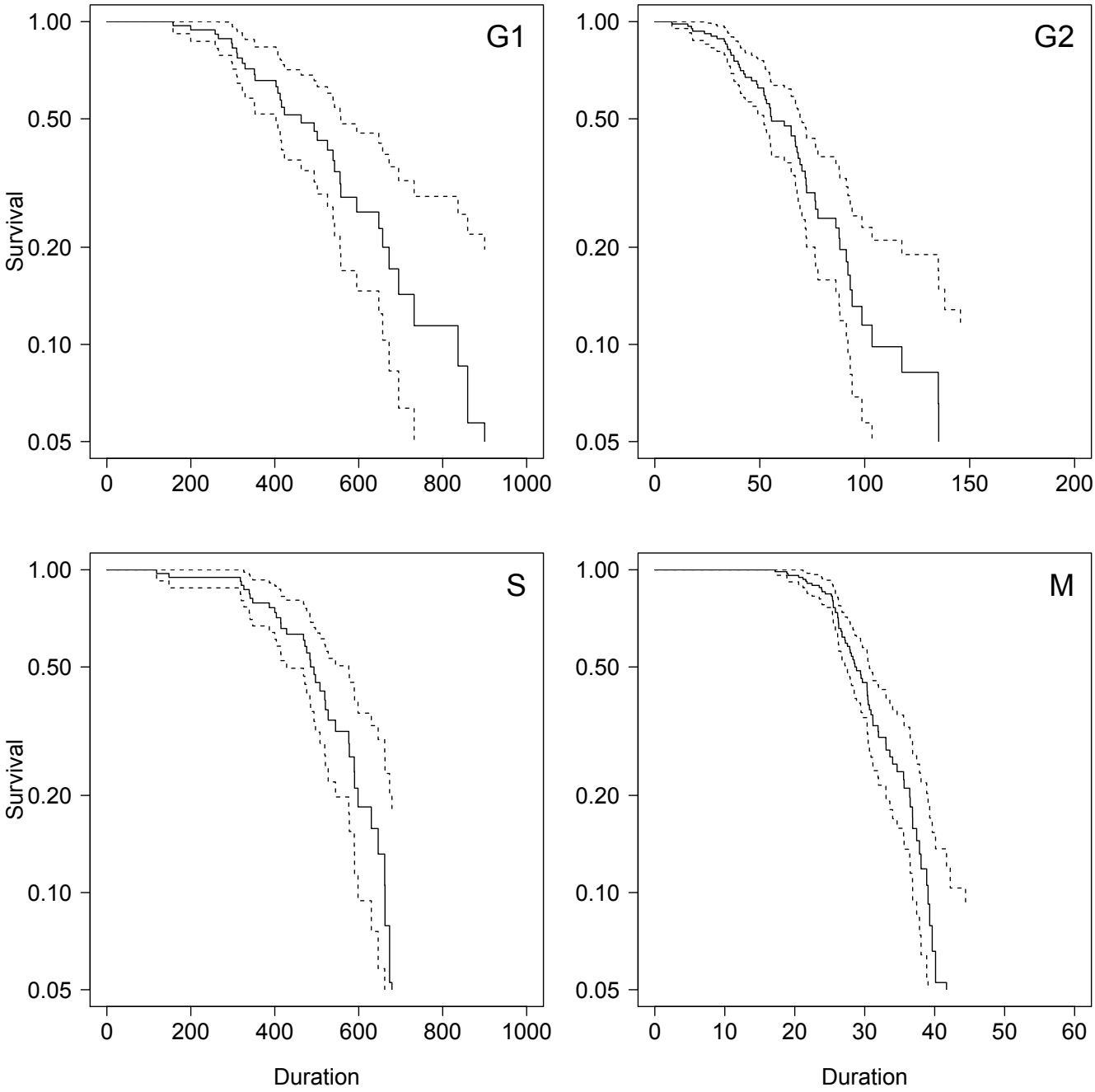

Fig. S2. Phases Survival curves

1.3.3 CDC25B$^{\Delta CDK}$

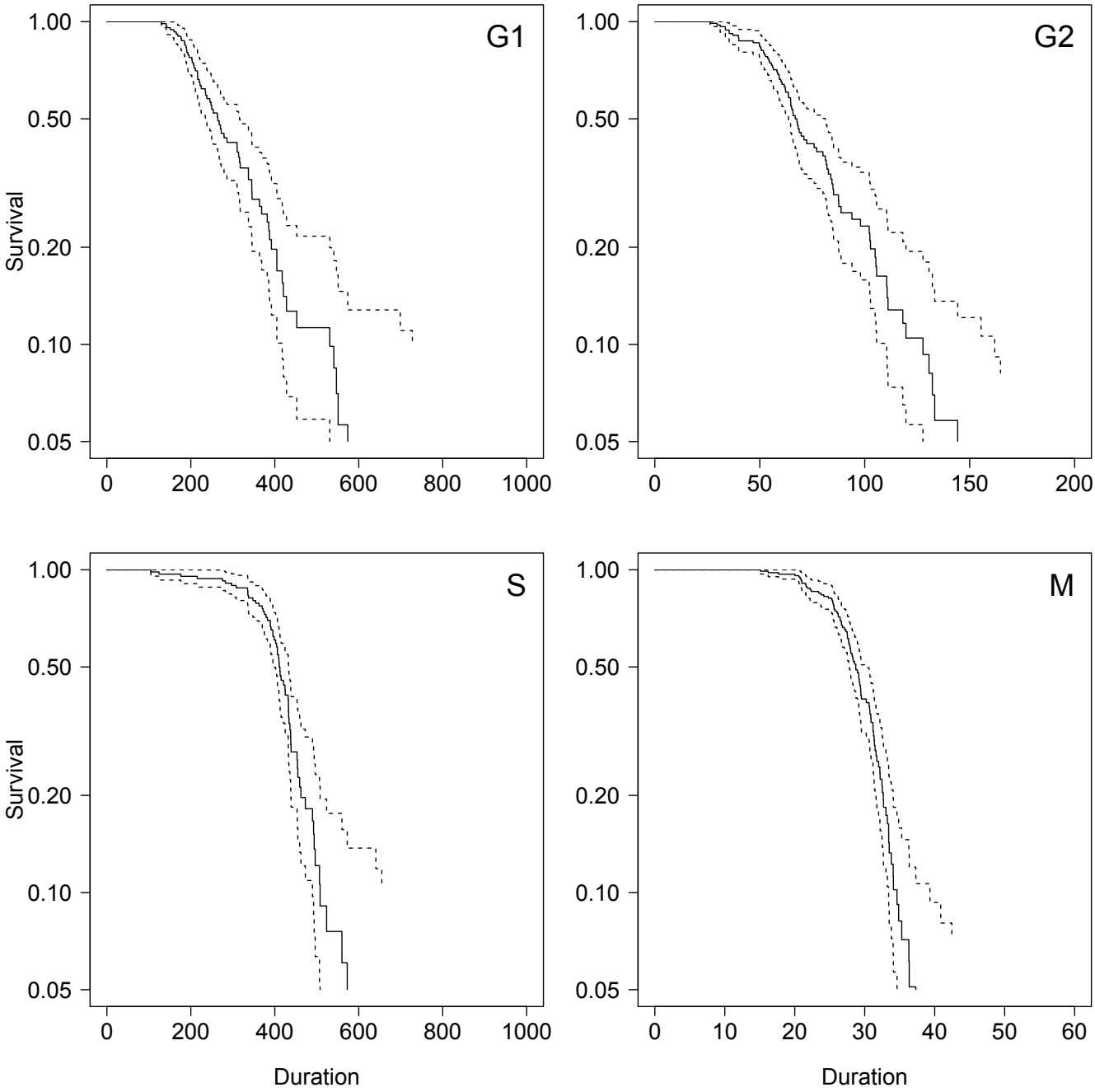

Fig. S3. Phases Survival curves

2 Subset with complete tracking of phases within the same cycle

In this section, we only use the subset of data with complete cell cycle measures.

2.1 Graphical summaries

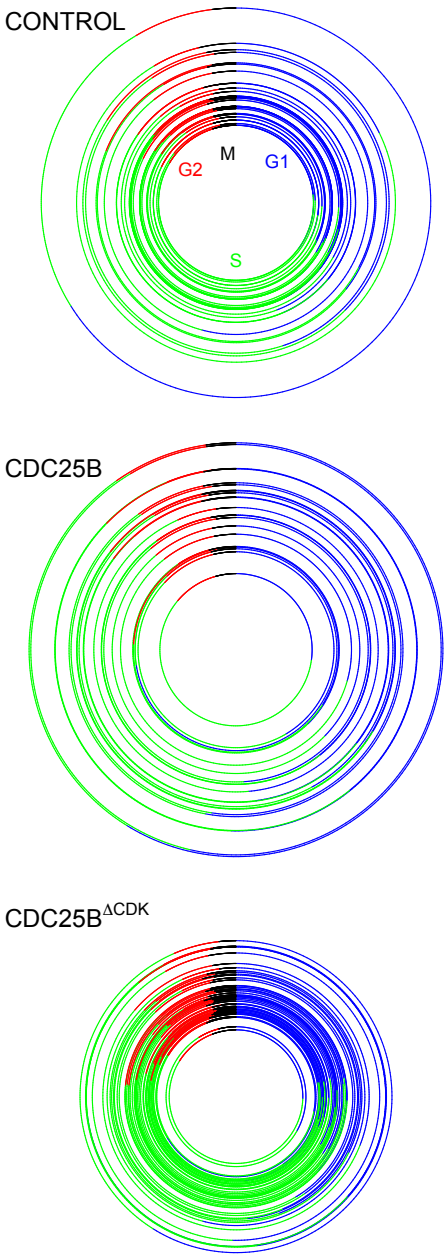

Fig. S4. Graphical summary of data

2.2 Variation Partitionning (Venn Diagrams)

The variation of cycle length is partionned in regards to phases to examine how much variation is explained by each phase.

See : Jari Oksanen, F. Guillaume Blanchet, Michael Friendly, Roeland Kindt, Pierre Legendre, Dan McGlinn, Peter R. Minchin, R. B. O'Hara, Gavin L. Simpson, Peter Solymos, M. Henry H. Stevens, Eduard Szoecs and Helene Wagner (2019). vegan: Community Ecology Package. R package version 2.5-6. https://CRAN.R-project.org/package=vegan

In Venn Diagrams, the number represent adjusted-Rsquare. For the sake of clarity, values below 0.05 are not reported.

In the three conditions, G1 phase duration explains the largest part of total length variations.

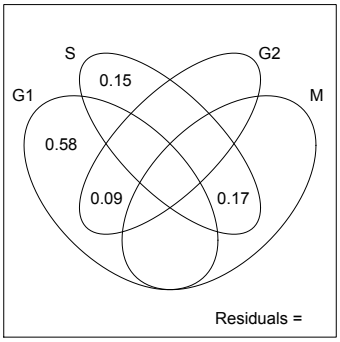

Fig. S5. Venn Diagrams for CONTROL condition.

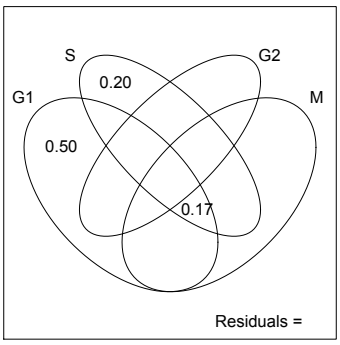

Fig. S6. Venn Diagrams for CDC25B gain of fonction

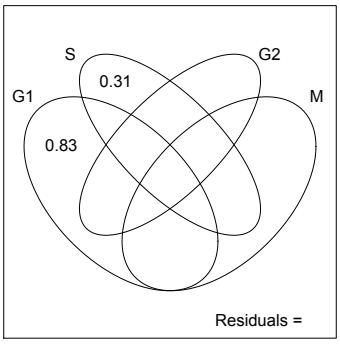

Fig. S7. Venn Diagrams for DeltaCDK condition.

2.3 Tests of correlation among phases

2.3.1 Statistical results

We test every pair of phases for linear regression. Tables below report R^2 values with their p-value, as well as correlation values with their associated p-value.

The symbol *SG2M* stands for S+G2+M

2.3.1.1 CONTROL

Phase	Phase	R^2	p-val	Pearson	p-val	Kendall	p-val	Spearman	p-val	Signif
G1	S	0.00	0.90	0.02	0.90	0.17	0.18	0.23	0.20	—
G1	G2	0.09	0.08	0.30	0.08	0.22	0.07	0.33	0.06	—
G1	M	0.01	0.57	0.10	0.57	0.09	0.45	0.17	0.35	—
S	G2	0.00	0.80	0.05	0.80	-0.00	0.99	-0.01	0.94	—
S	M	0.49	0.00	0.70	0.00	0.33	0.01	0.47	0.01	yes
G2	M	0.04	0.26	0.20	0.26	0.15	0.22	0.24	0.17	—
G1	SG2M	0.01	0.58	0.10	0.58	0.25	0.04	0.35	0.05	—

2.3.1.2 CDC25B

Phase	Phase	R^2	p-val	Pearson	p-val	Kendall	p-val	Spearman	p-val	Signif
G1	S	0.05	0.30	0.23	0.30	0.17	0.29	0.24	0.29	—
G1	G2	0.02	0.53	0.14	0.53	0.16	0.31	0.21	0.36	—
G1	M	0.16	0.07	0.40	0.07	0.31	0.05	0.43	0.05	—
S	G2	0.04	0.39	0.19	0.39	0.11	0.50	0.18	0.41	—
S	M	0.26	0.01	0.51	0.01	0.38	0.01	0.50	0.02	yes
G2	M	0.05	0.31	0.23	0.31	0.19	0.22	0.26	0.23	—
G1	SG2M	0.07	0.24	0.26	0.24	0.21	0.18	0.31	0.16	—

2.3.1.3 CDC25B$^{\Delta CDK}$

Phase	Phase	R^2	p-val	Pearson	p-val	Kendall	p-val	Spearman	p-val	Signif
G1	S	0.01	0.56	-0.09	0.56	0.13	0.22	0.18	0.24	—
G1	G2	0.03	0.28	-0.17	0.28	-0.10	0.33	-0.19	0.21	—
G1	M	0.01	0.48	-0.11	0.48	-0.05	0.65	-0.09	0.58	—
S	G2	0.00	0.98	-0.00	0.98	-0.00	0.98	0.01	0.97	—
S	M	0.03	0.27	0.17	0.27	0.18	0.09	0.26	0.09	—
G2	M	0.01	0.59	0.08	0.59	0.01	0.93	0.03	0.84	—
G1	SG2M	0.02	0.34	-0.14	0.34	0.02	0.85	0.02	0.92	—

2.3.2 Graphics for CONTROL

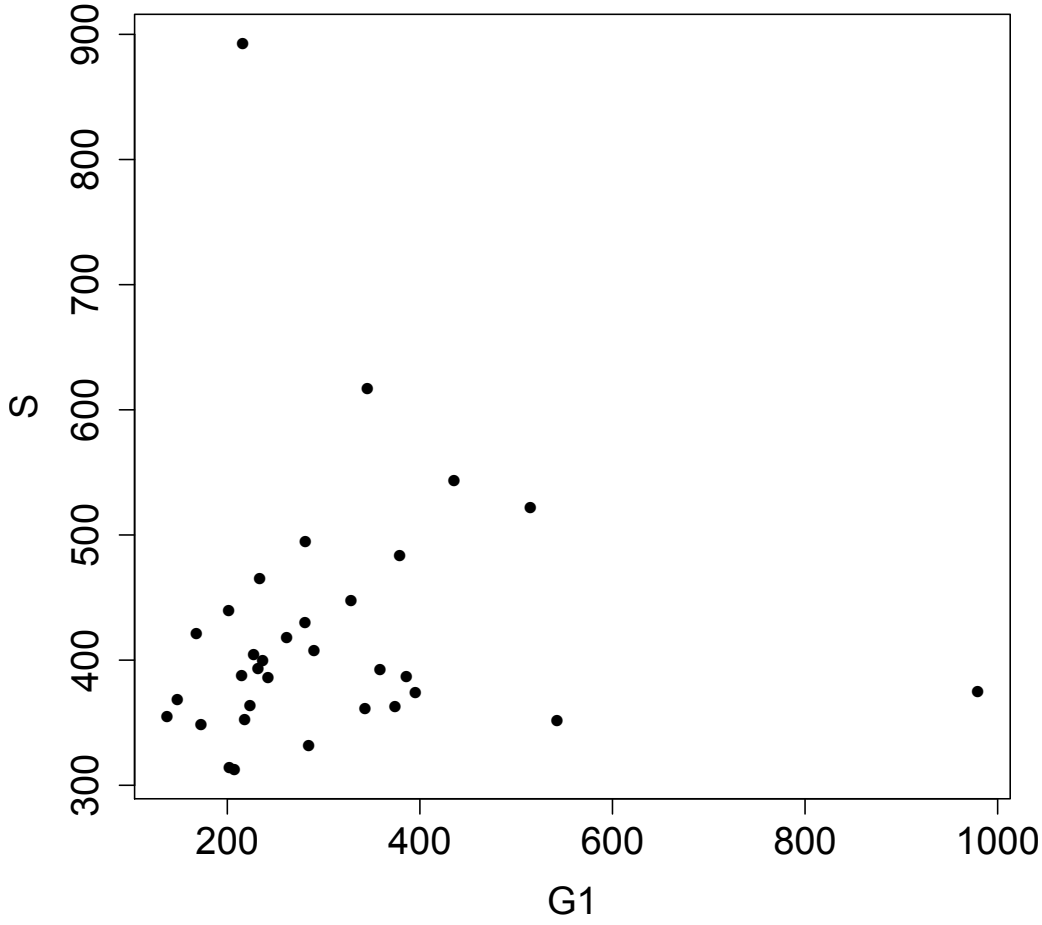

Fig. S8. CTL : S duration vs. G1 duration

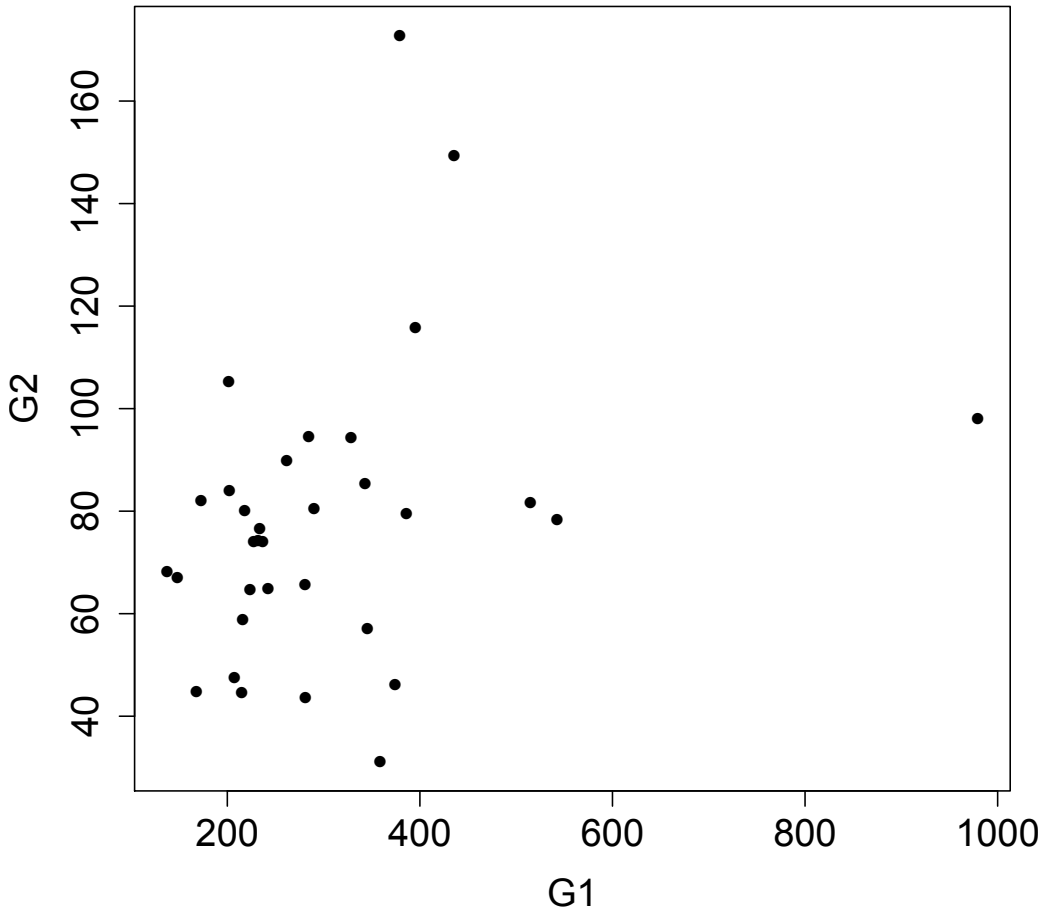

Fig. S9. CTL : G2 duration vs. G1 duration

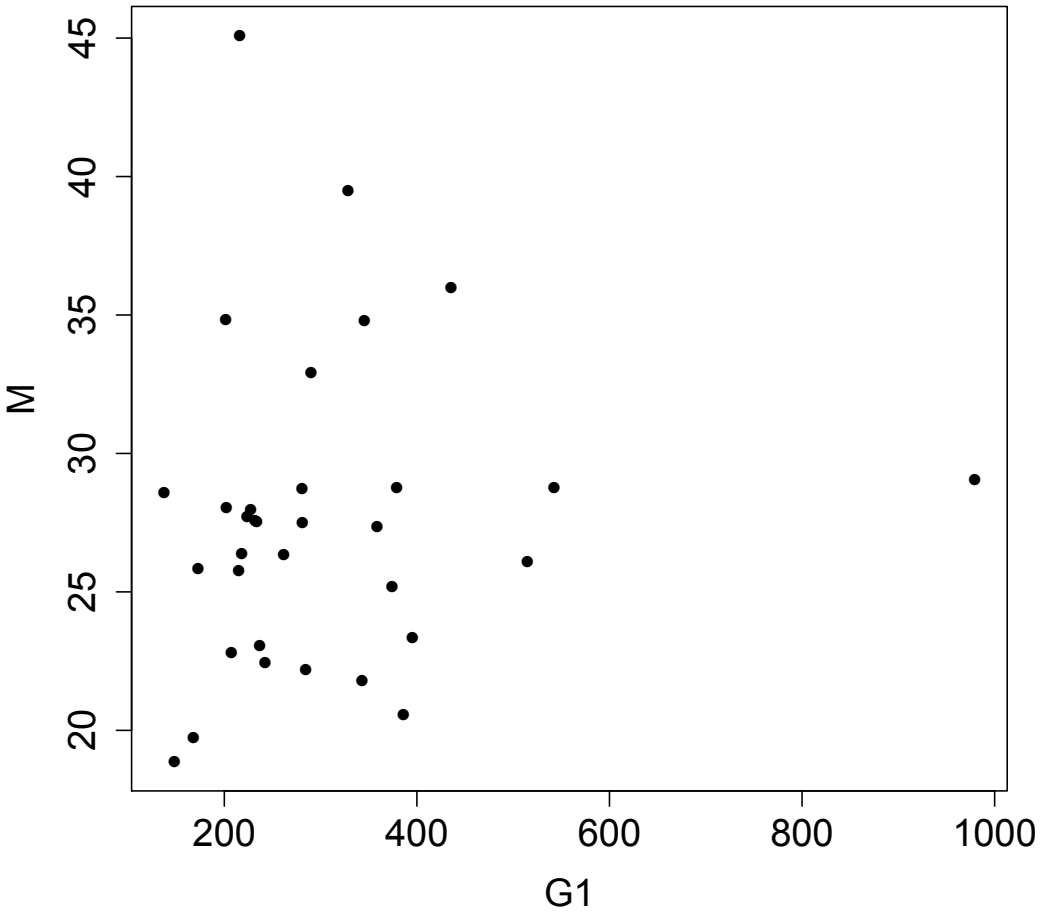

Fig. S10. CTL : M duration vs. G1 duration

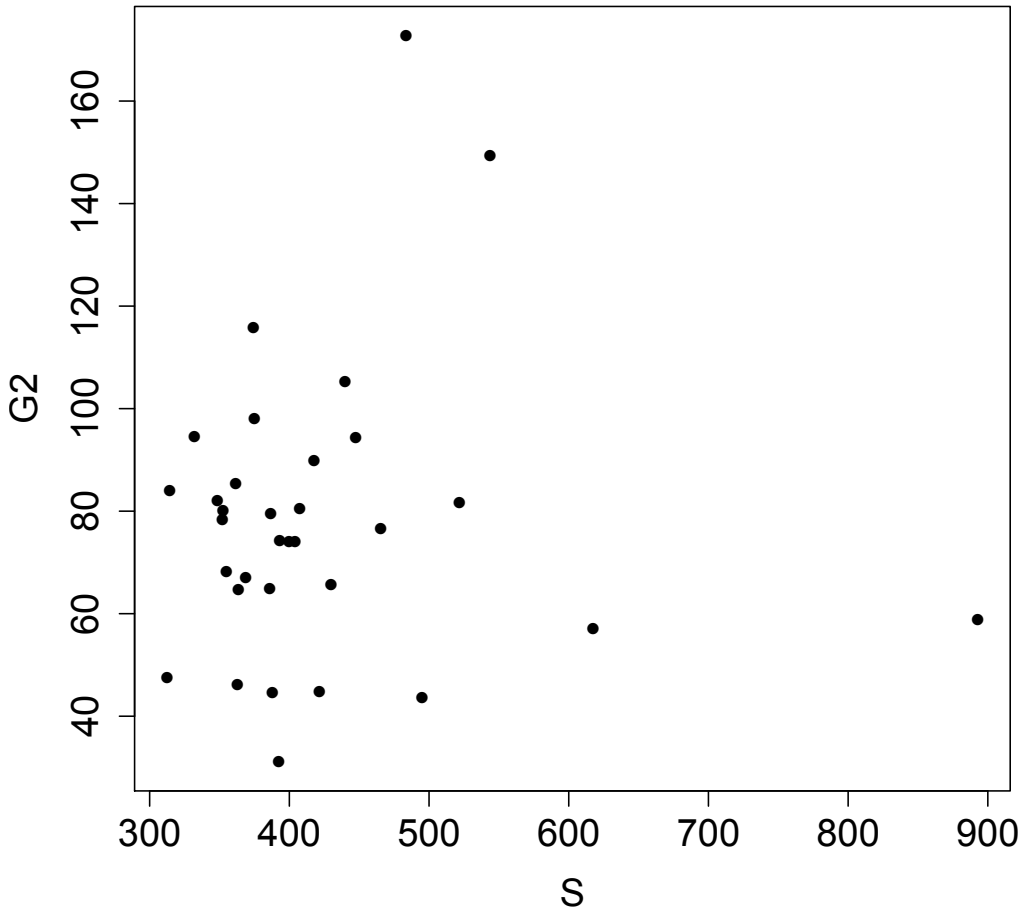

Fig. S11. CTL : G2 duration vs. S duration

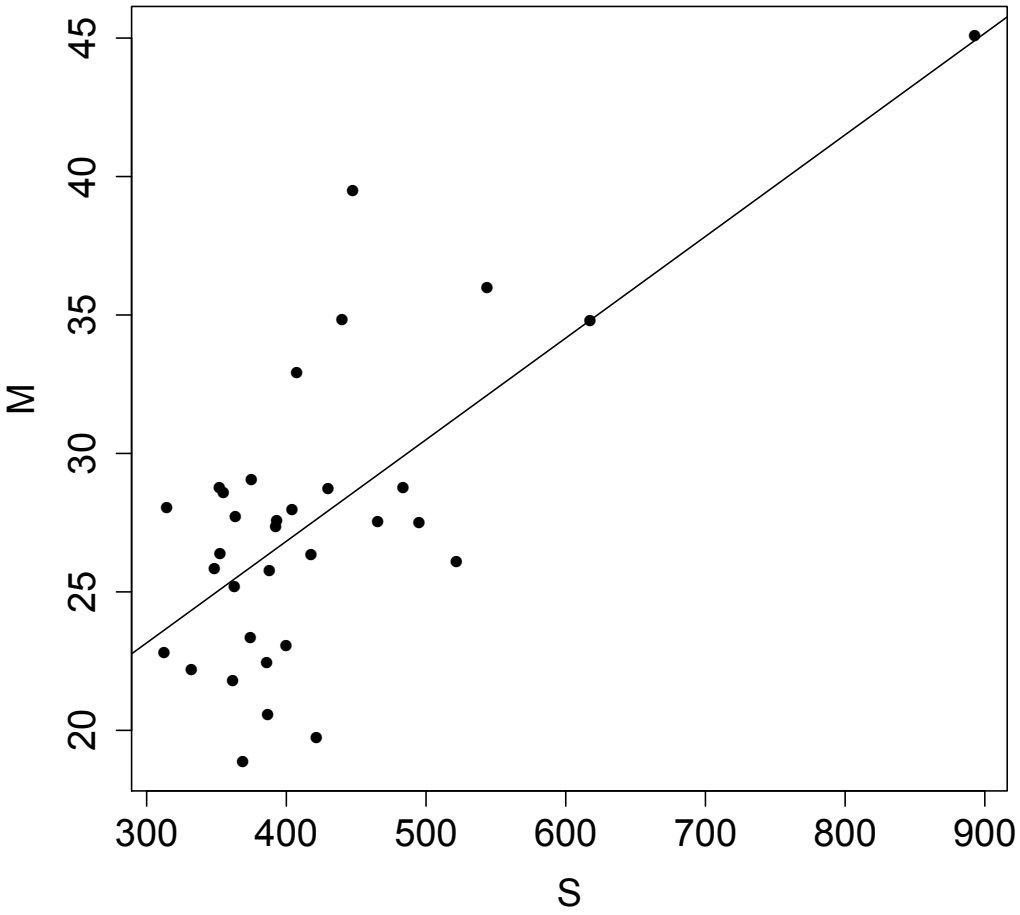

Fig. S12. CTL : M duration vs. S duration

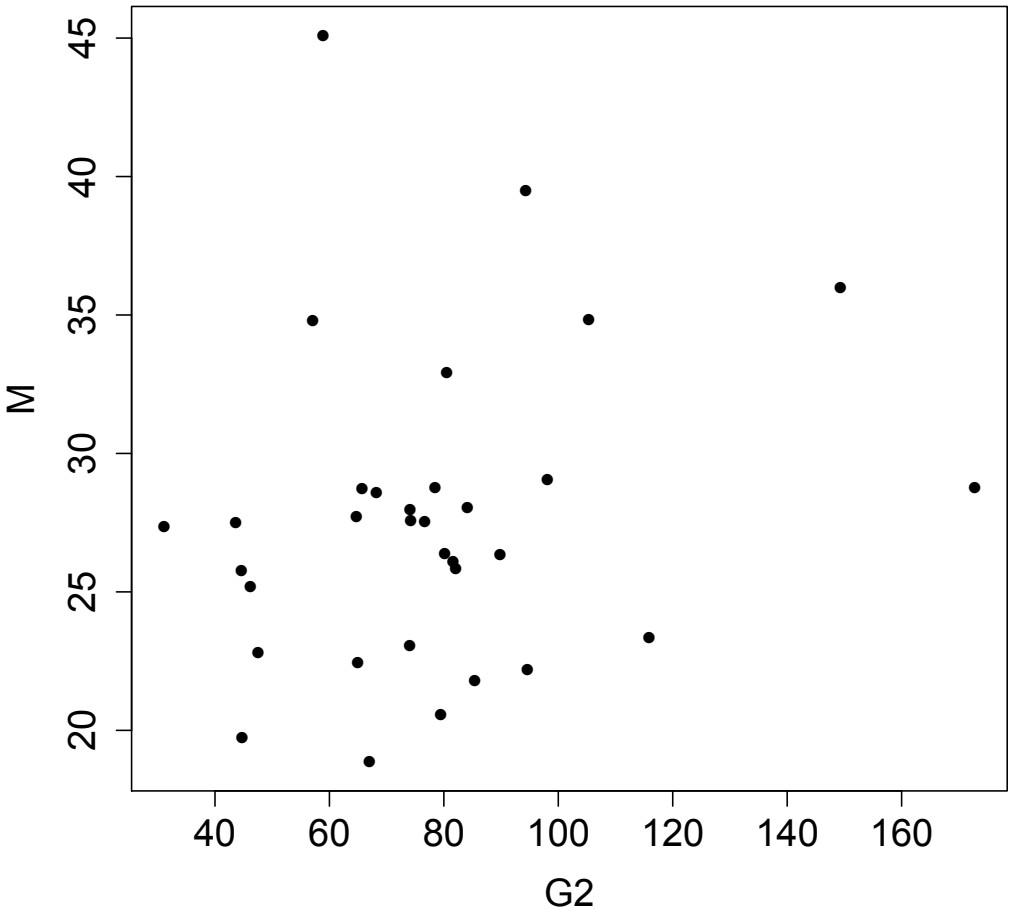

Fig. S13. CTL : M duration vs. G2 duration

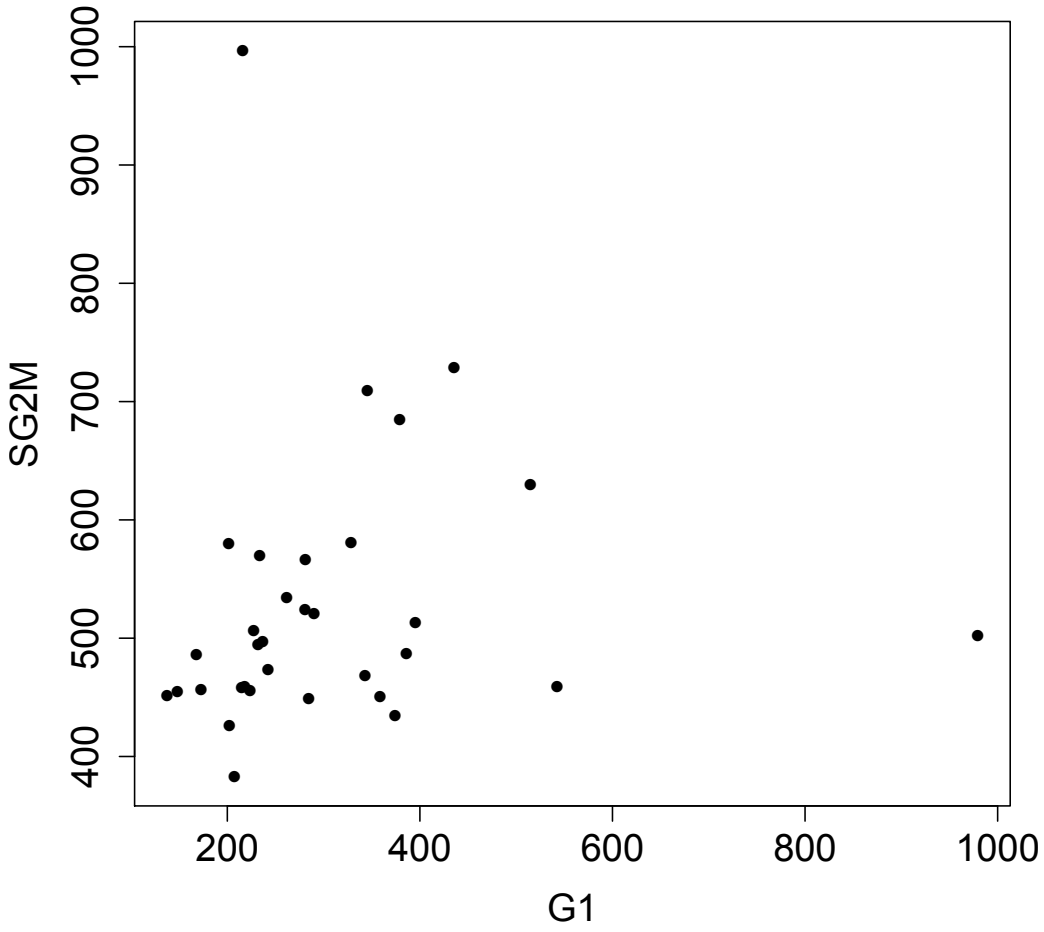

Fig. S14. CTL : S+G2+M duration vs. G1 duration

2.3.3 Graphics for CDC25B

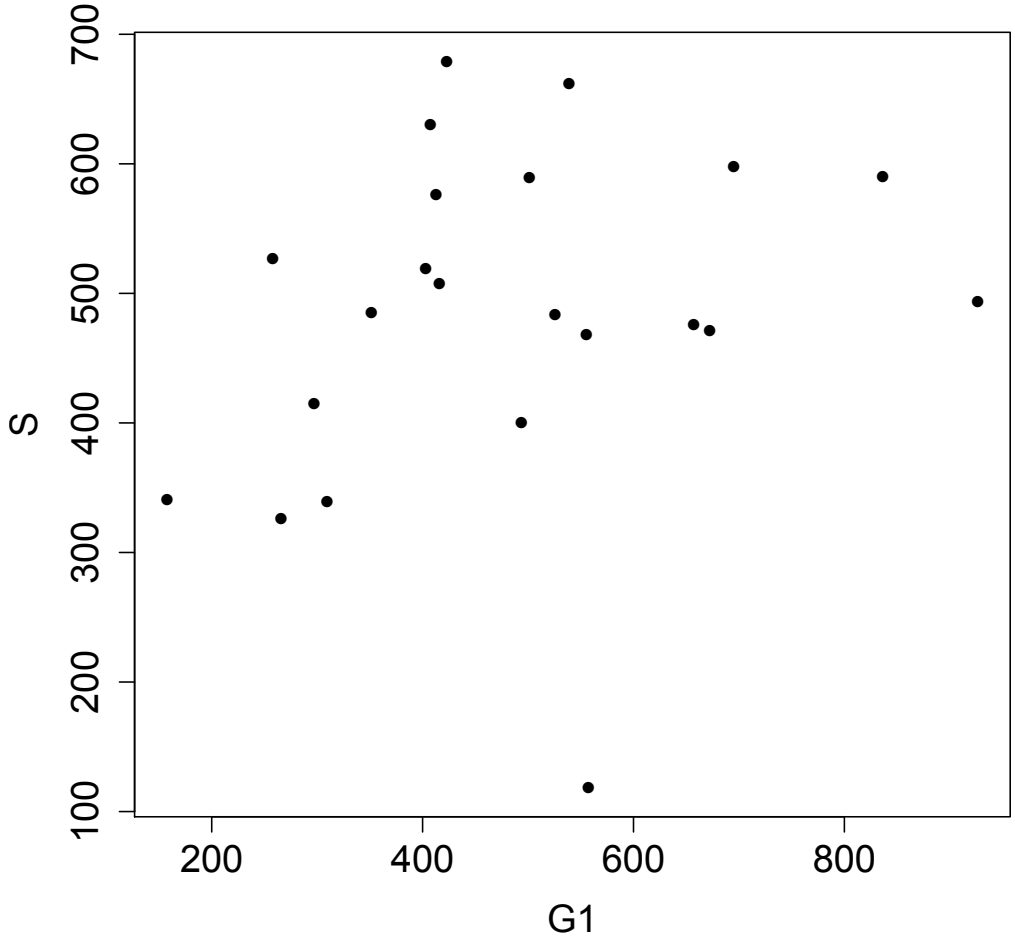

Fig. S15. CDC25B : S duration vs. G1 duration

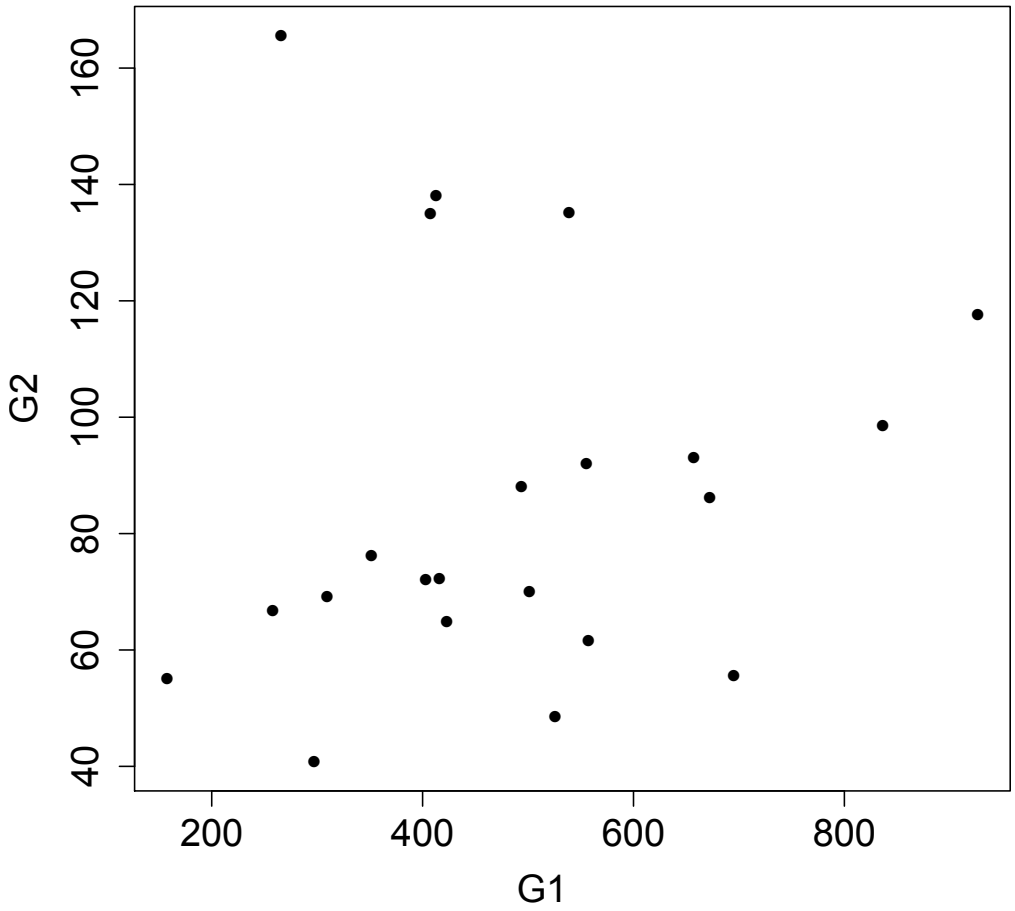

Fig. S16. CDC25B : G2 duration vs. G1 duration

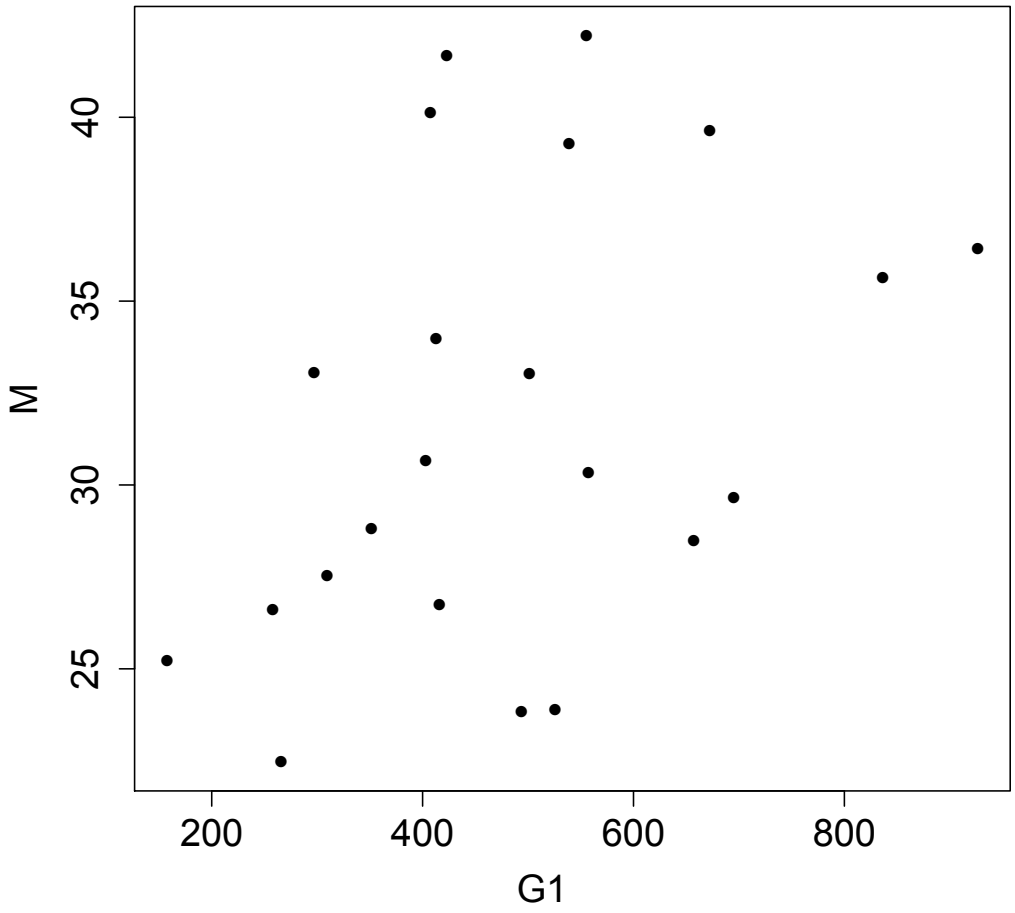

Fig. S17. CDC25B : M duration vs. G1 duration

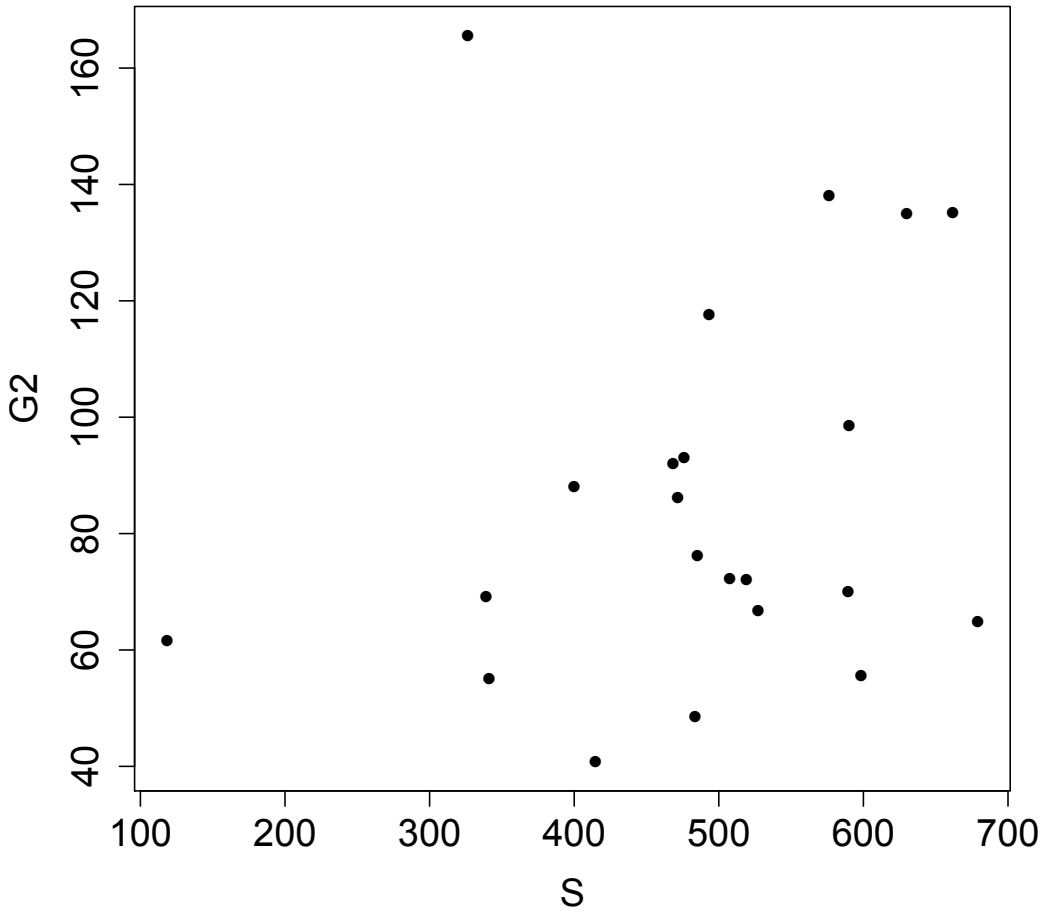

Fig. S18. CDC25B : G2 duration vs. S duration

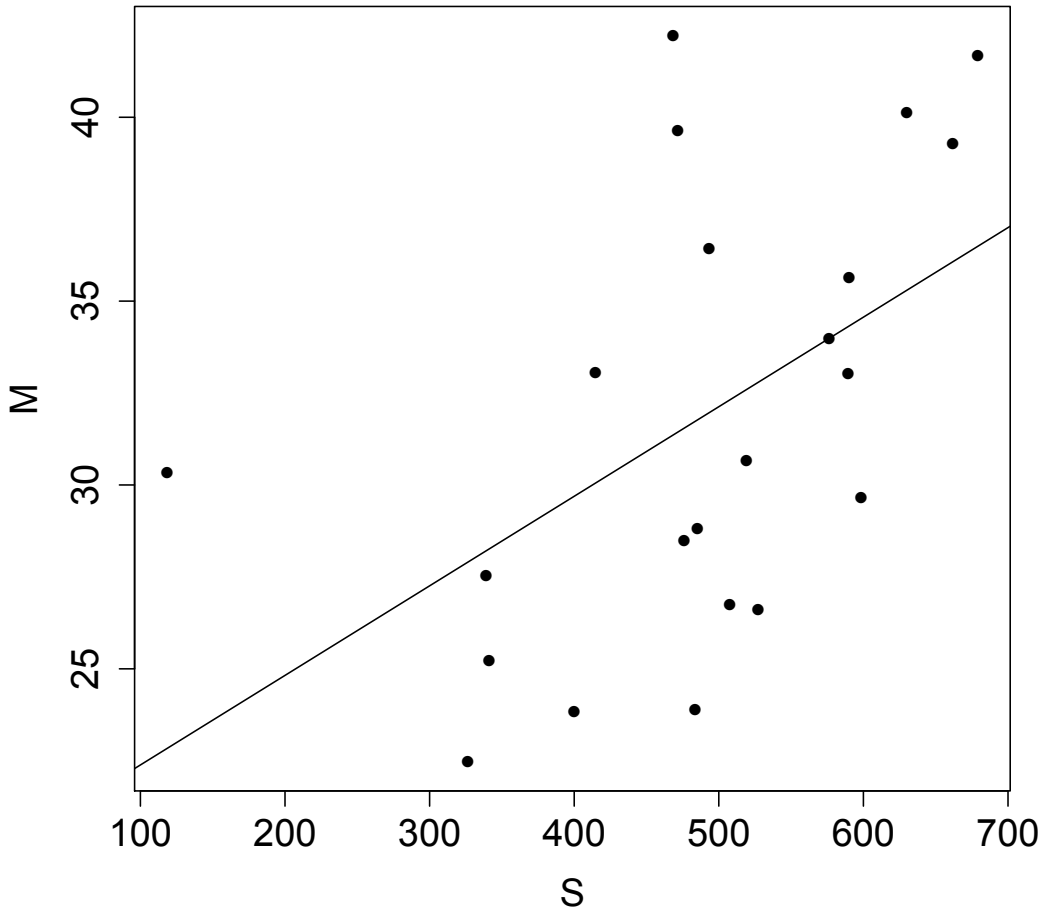

Fig. S19. CDC25B : M duration vs. S duration

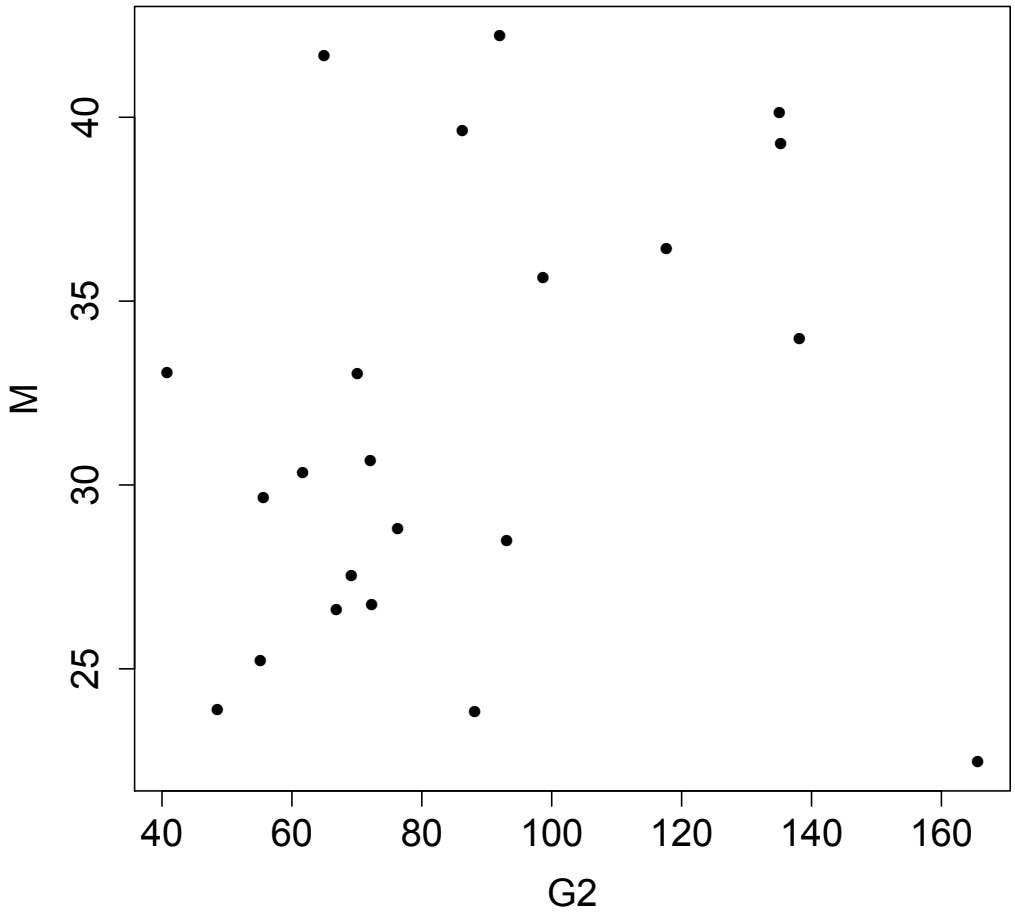

Fig. S20. CDC25B : M duration vs. G2 duration

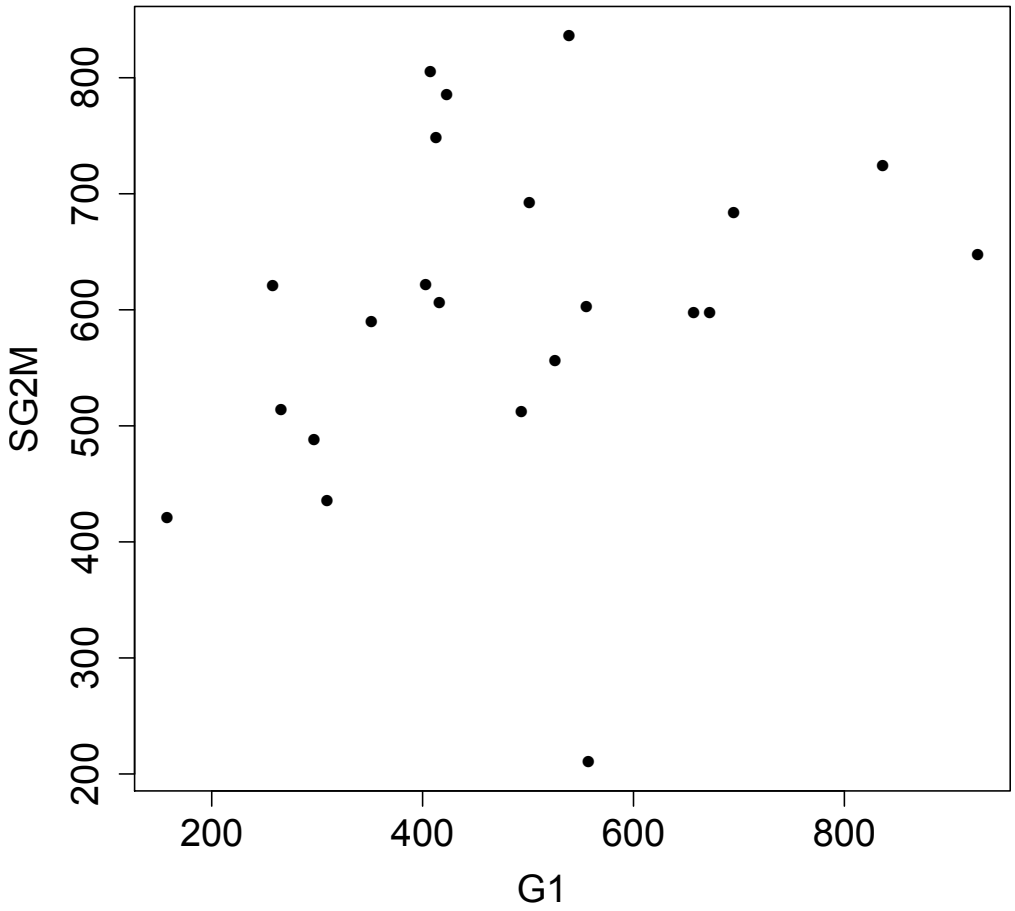

Fig. S21. CDC25B : S+G2+M duration vs. G1 duration

2.3.4 Graphics for CDC25B$^{\Delta CDK}$

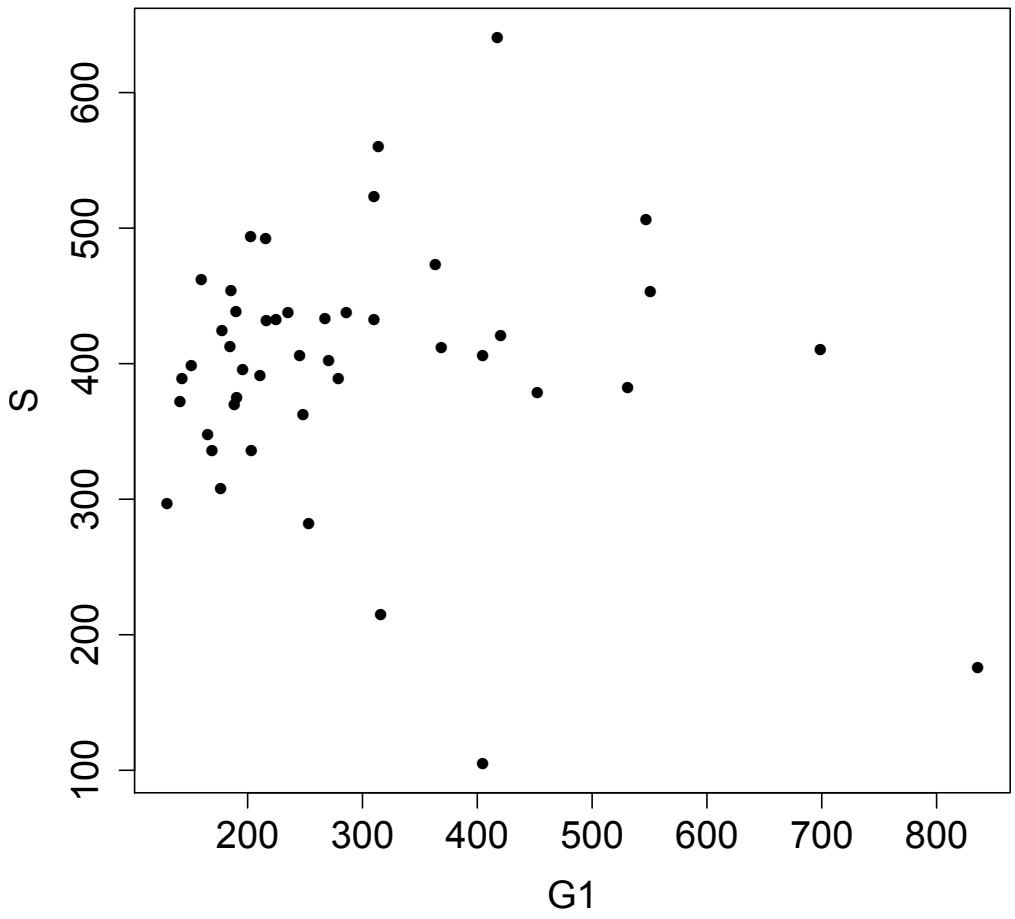

Fig. S22. DeltaCDK : S duration vs. G1 duration

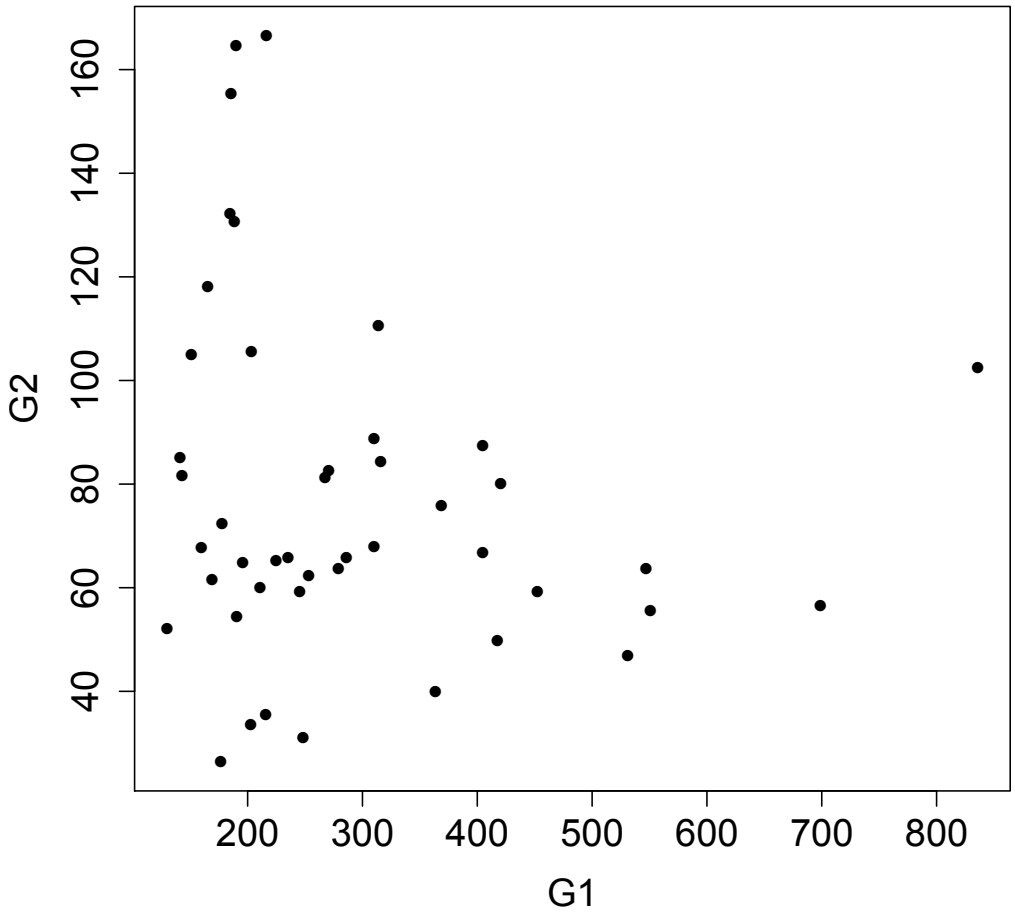

Fig. S23. DeltaCDK : G2 duration vs. G1 duration

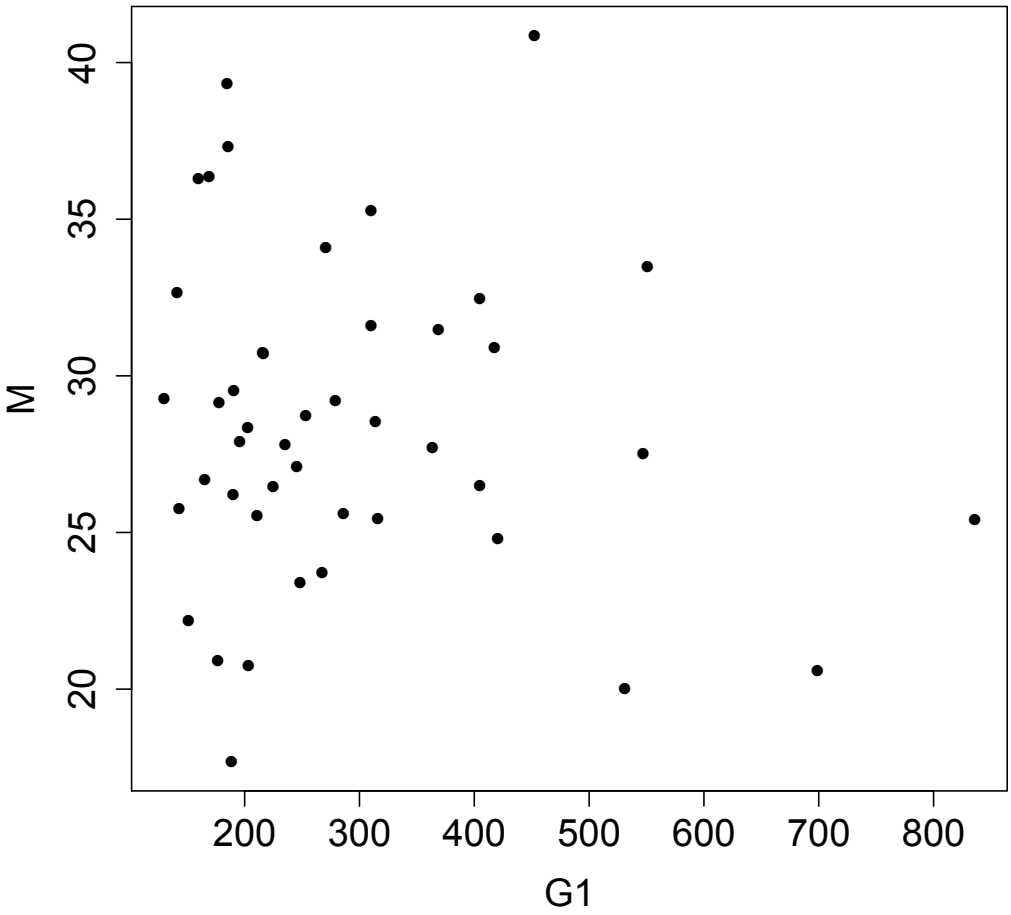

Fig. S24. DeltaCDK : M duration vs. G1 duration

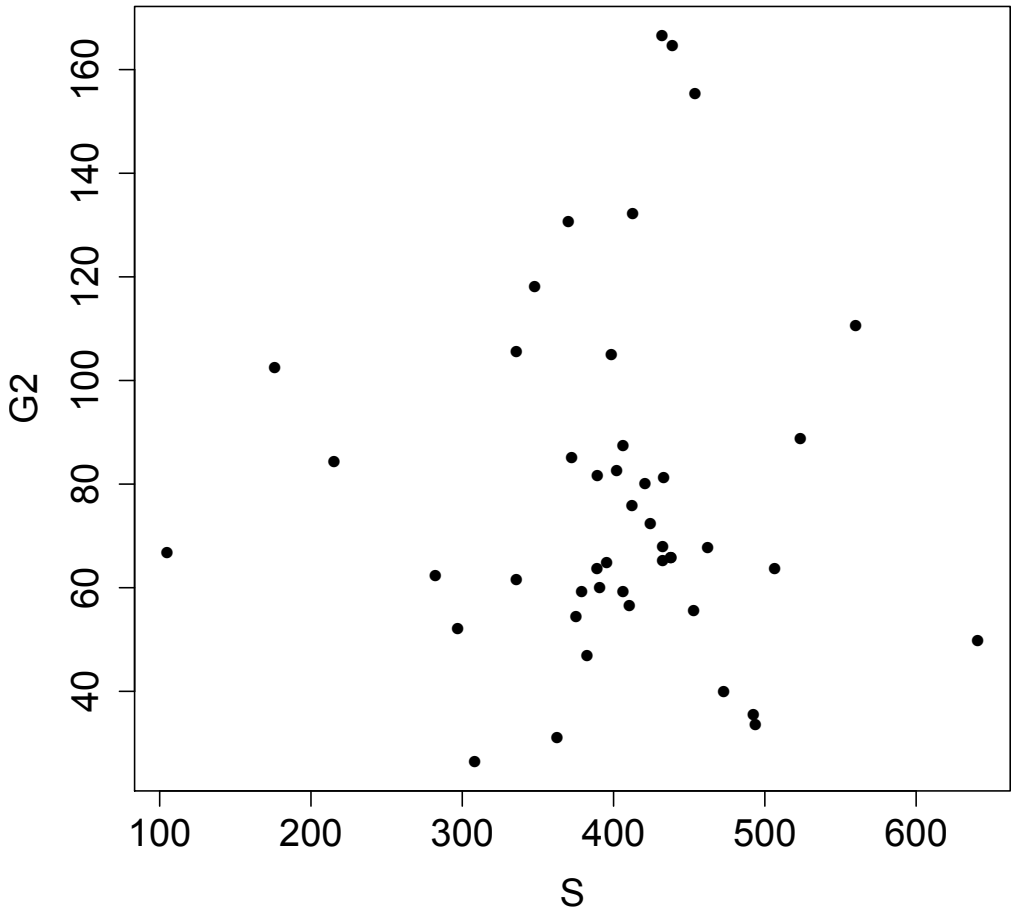

Fig. S25. DeltaCDK : G2 duration vs. S duration

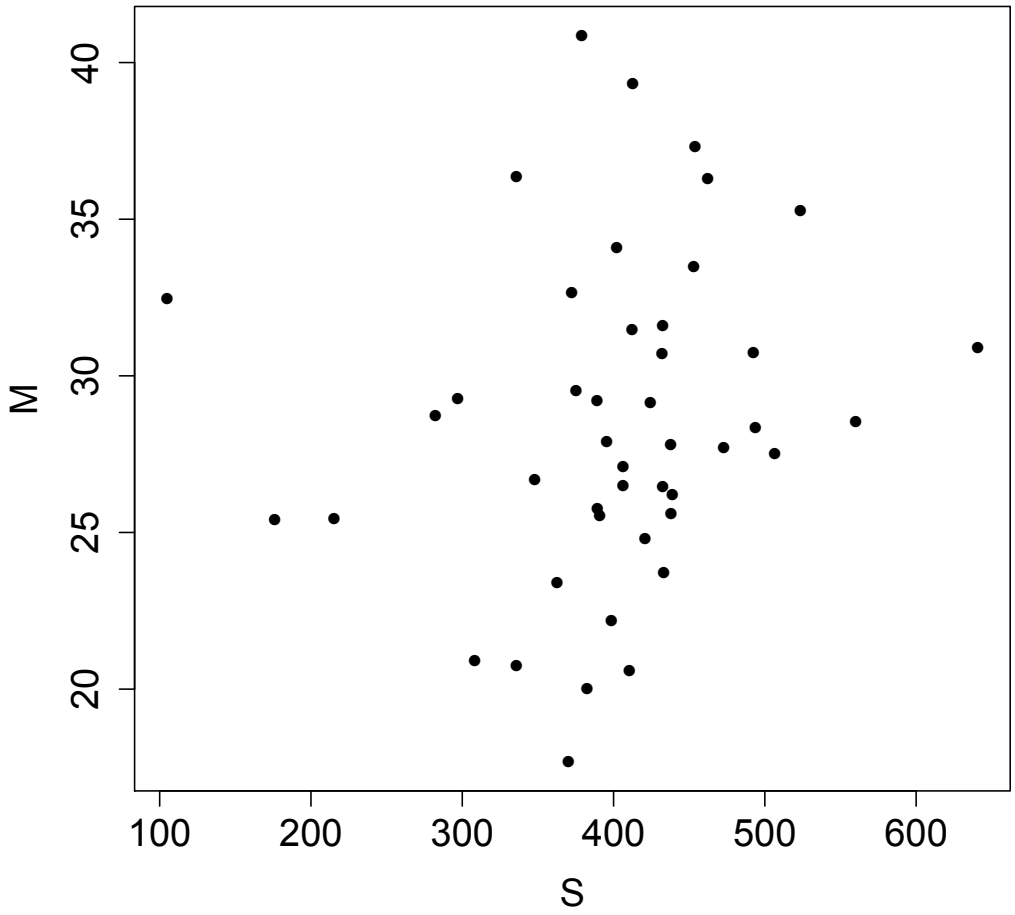

Fig. S26. DeltaCDK : M duration vs. S duration

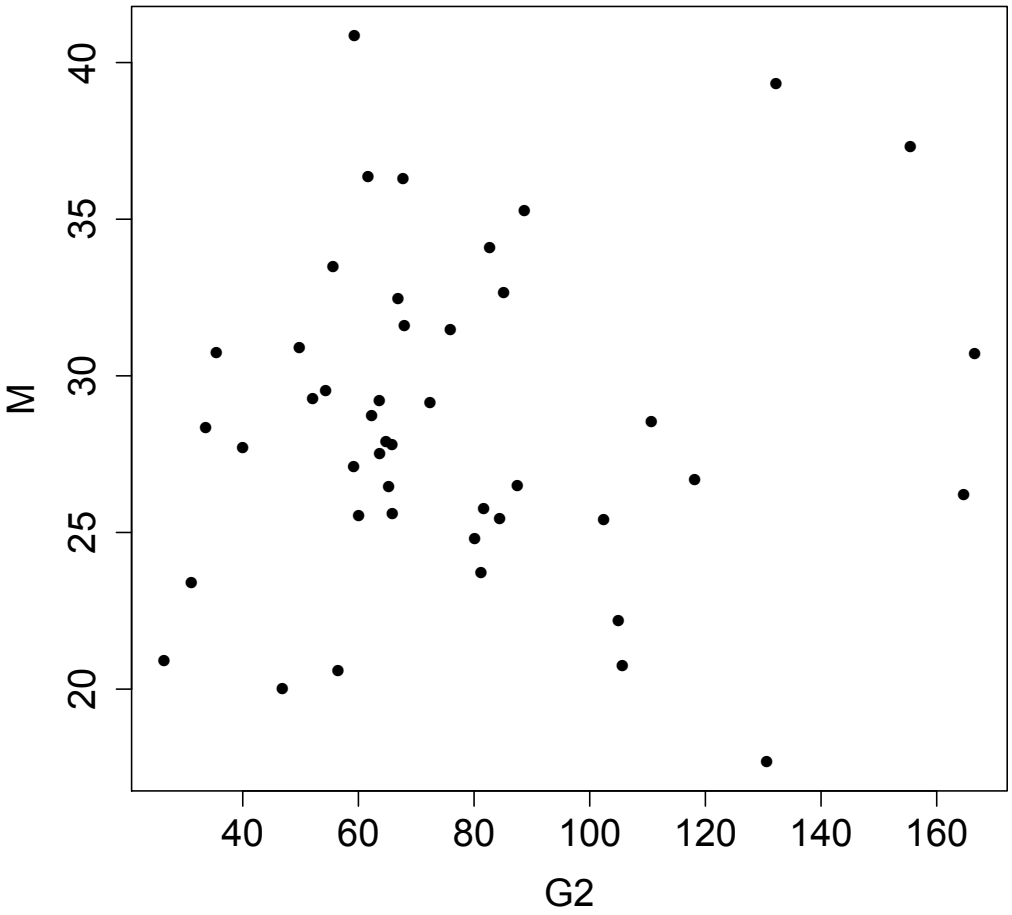

Fig. S27. DeltaCDK : M duration vs. G2 duration

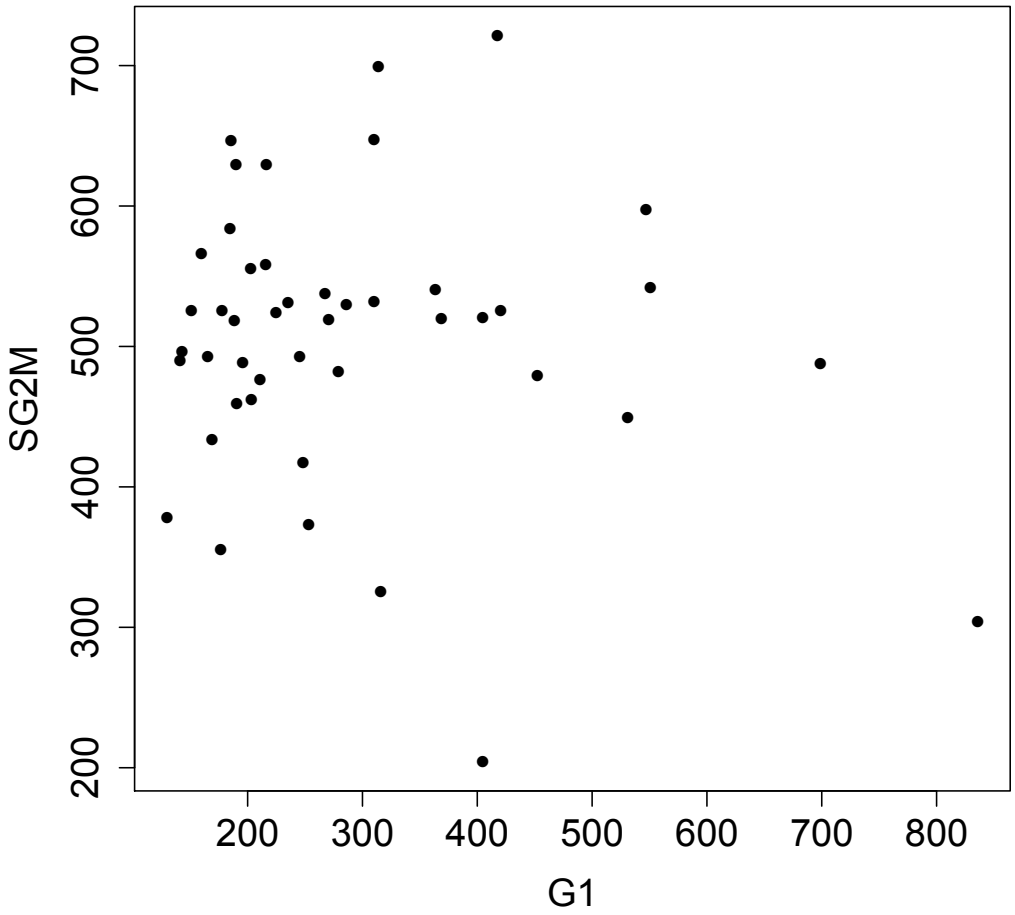

Fig. S28. DeltaCDK : S+G2+M duration vs. G1 duration

2.4 Predicted survival curves for total duration under independence hypothesis.

Survival curves for total duration Tc will be used to comfort the observation that phase durations are not correlated.

For this, we can compare the observed distribution of total durations to a theoretical model established under the null hypothesis of no correlation among phases duration.

However, such a theoretical model can be obtained only for restrictive condition and is used here only for CTL condition.

An alternative is to build a theoretical distribution using the data (Monte Carlo permutations).

2.4.1 Theoretical *null* model for total duration

Under the hypotheses that phase durations are independent from each other, and that exit time from each phase is a pure memoryless random process, we have a theoretical model for the statistical distribution of the total duration as a sum of four exponential distributions, each with its own parameter. Let denote R_i the *exit rates* (the inverse of the average exit time), then the survival function of total exit rate would follow:

$$S(t) = 1 - \left[\prod_{i=1}^{4} R_i\right] \sum_{i=1}^{4} \frac{e^{-R_i t}}{\prod_{k=1,\neq i}^{n} (R_k - R_i)}$$

See : Bibinger, M. (2013). Notes on the sum and maximum of independent exponentially distributed random variables with different scale parameters. https://arxiv.org/abs/1307.3945)

The expected distribution of Tc is obtained by adding the sum of the four minimal durations to this.

2.4.2 Null model by Monte Carlo permutation

Inspired from Monte Carlo permutation tests, the expected distribution of Tc under phase duration independence hypothesis can be built from data by random picking among observed values (mixing among the observed cycles). If there were some kind of compensation between phases within cycles to ensure some regulation of Tc, then the distribution of total duration would be more homogeneous that the one obtained by such random permutation : the slope of survival curve for observed data would be steeper than survival curve of random sampling.

2.4.3 Ordered permutations with full anti-correlation between G1 and S+G2+M

To illustrate how compensation of duration between G1 phase and the other phases would affect the survival curve and a more homogeneous series, we build the extreme case where the durations would be perfectly anti-correlated. To do this, we pair the G1 series sorted in ascending order with the S+G2+M series sorted in descending order.

2.5 Survival curves for phase exit time in each condition.

Here we check whether exponential decay could apply.

2.5.1 CONTROL

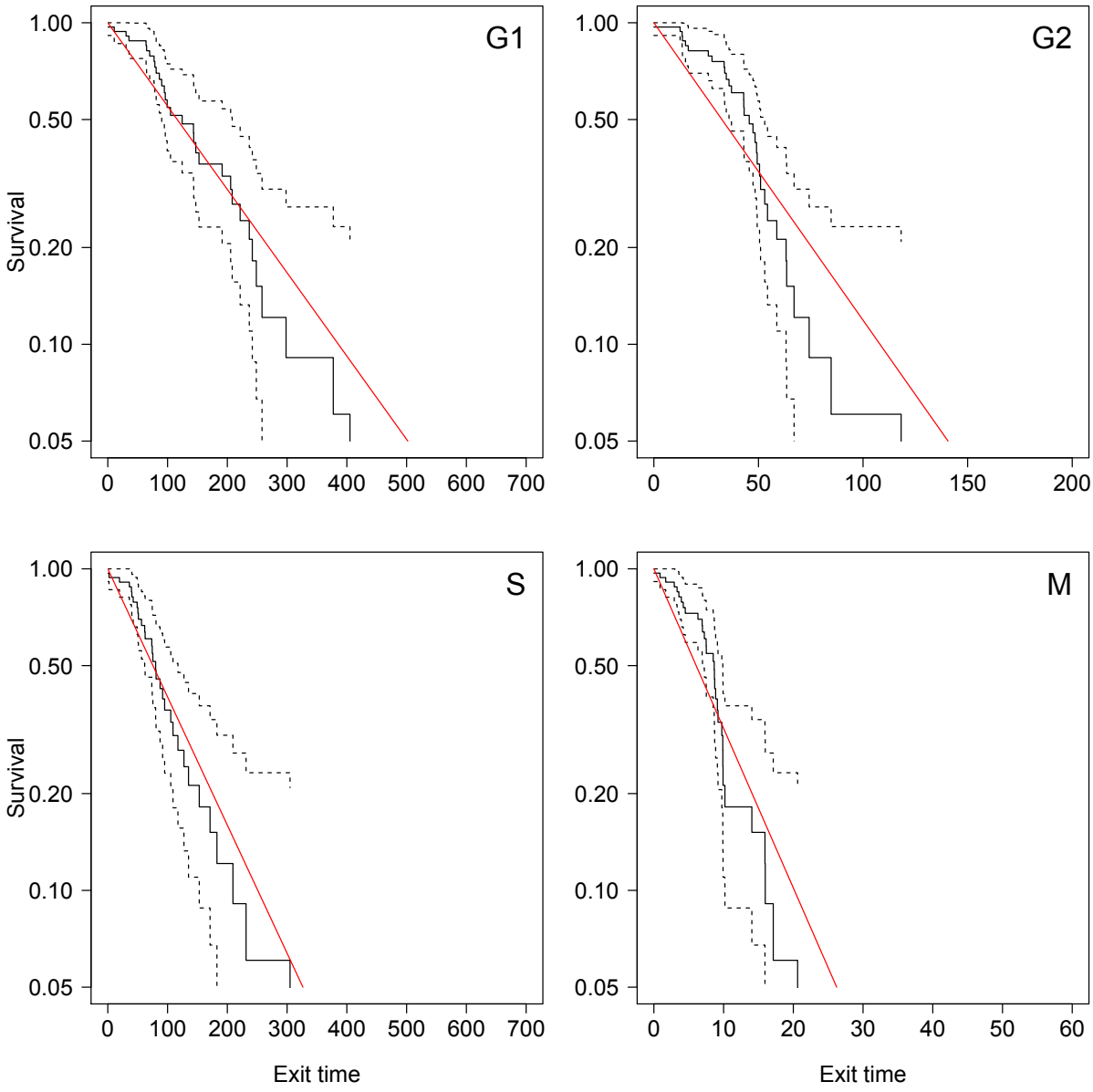

Fig. S29. Phases Survival curves for exit time. If we substract the minimal duration, the exit time process seems compatible with an exponential decay (pure random memoryless process)

2.5.2 CDC25B

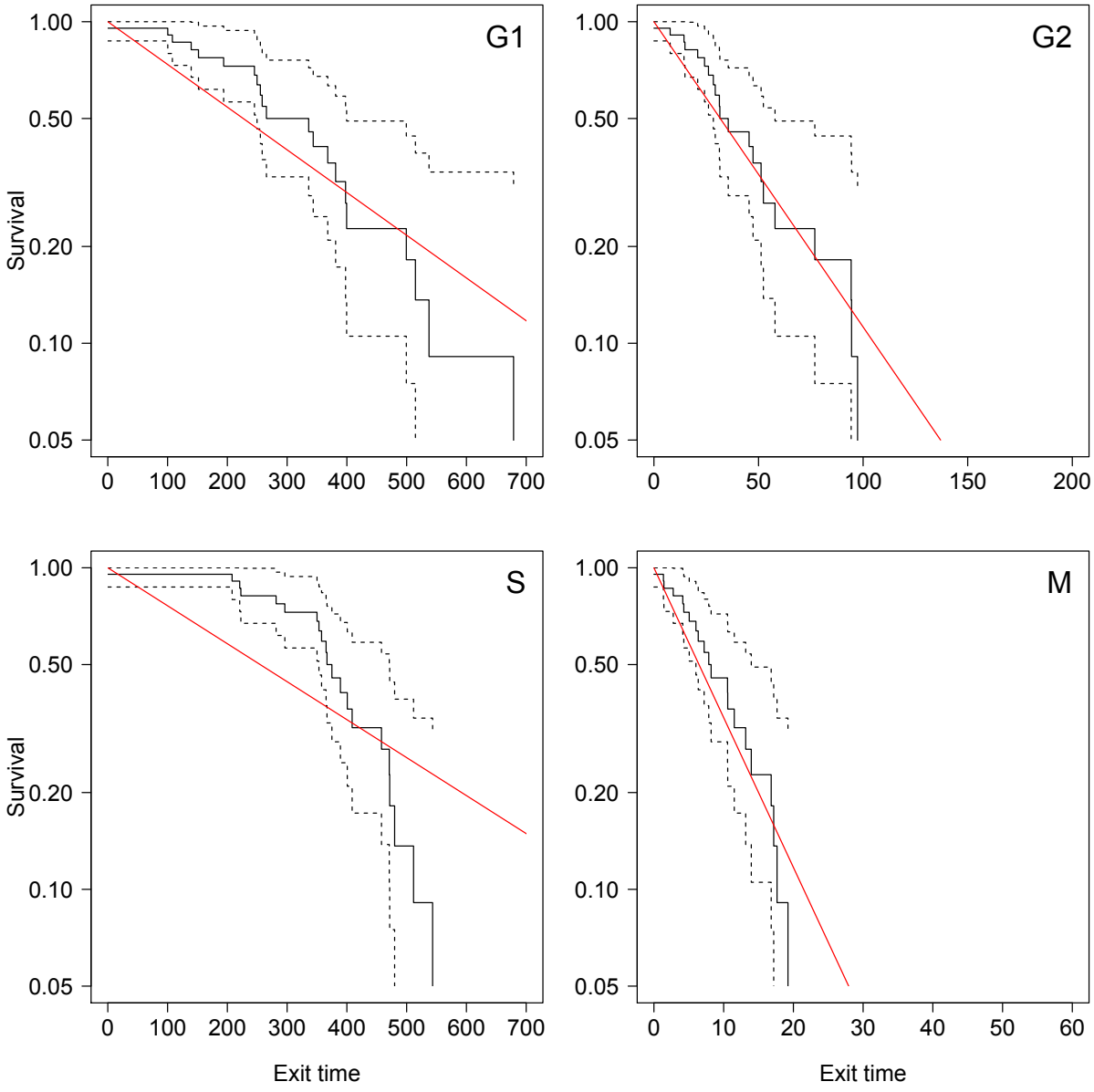

Fig. S30. Phases Survival curves. The exit time process for S phase does not fit an exponential decay (accelerated process)

2.5.3 CDC25B$^{\Delta CDK}$

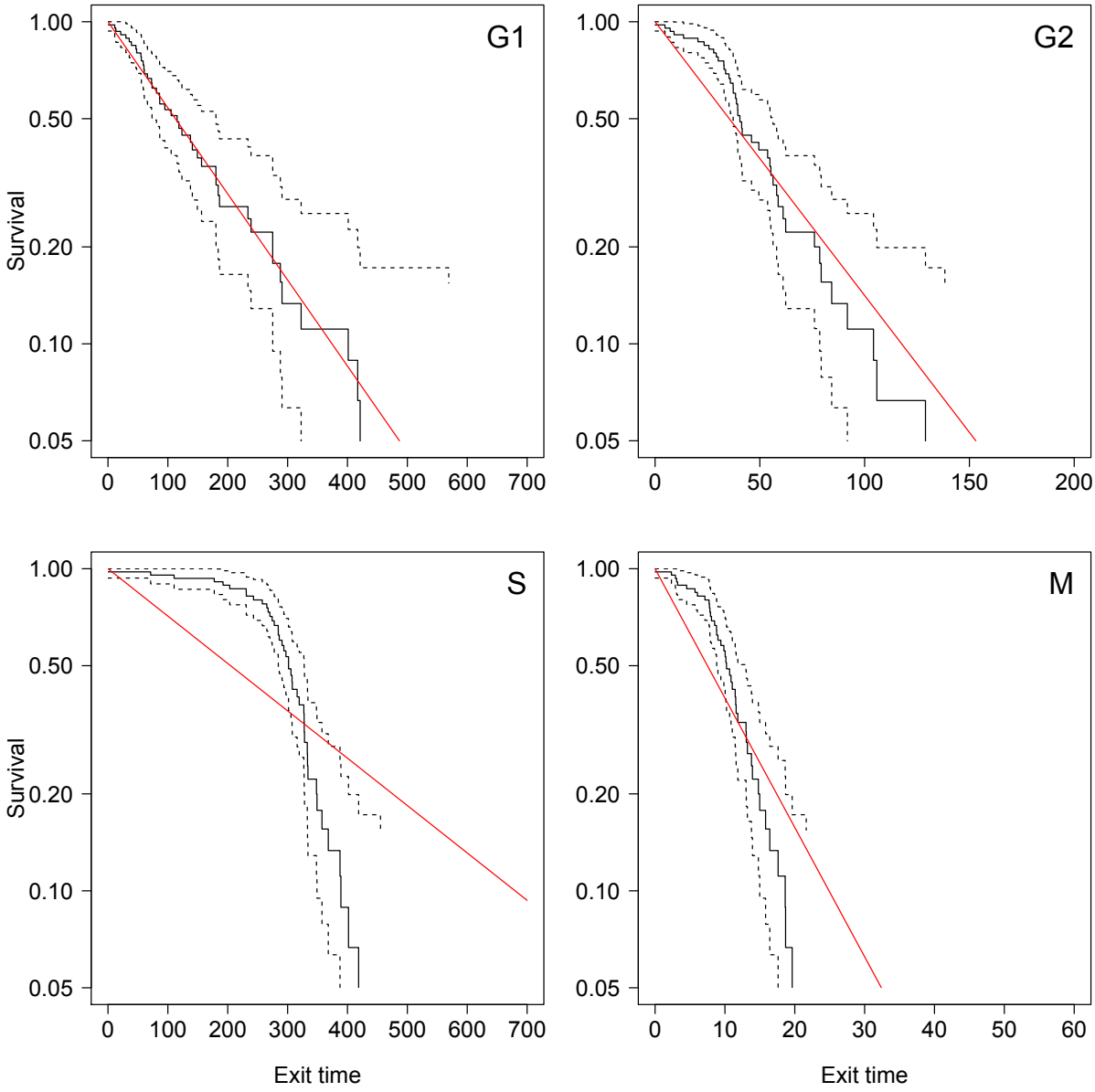

Fig. S31. Phases Survival curves. The exit time process for S phase does not fit an exponential decay (accelerated process)

2.6 Survival curves for Tc.

2.6.1 CONTROL

Data vs. Random sampling of phases

```
    Two-sample Kolmogorov-Smirnov test

data:  data and random
D = 0.10717, p-value = 0.8444
alternative hypothesis: two-sided
```

Data vs. anti-correlated

```
    Two-sample Kolmogorov-Smirnov test

data:  data and anticor
D = 0.42424, p-value = 0.004793
alternative hypothesis: two-sided
```

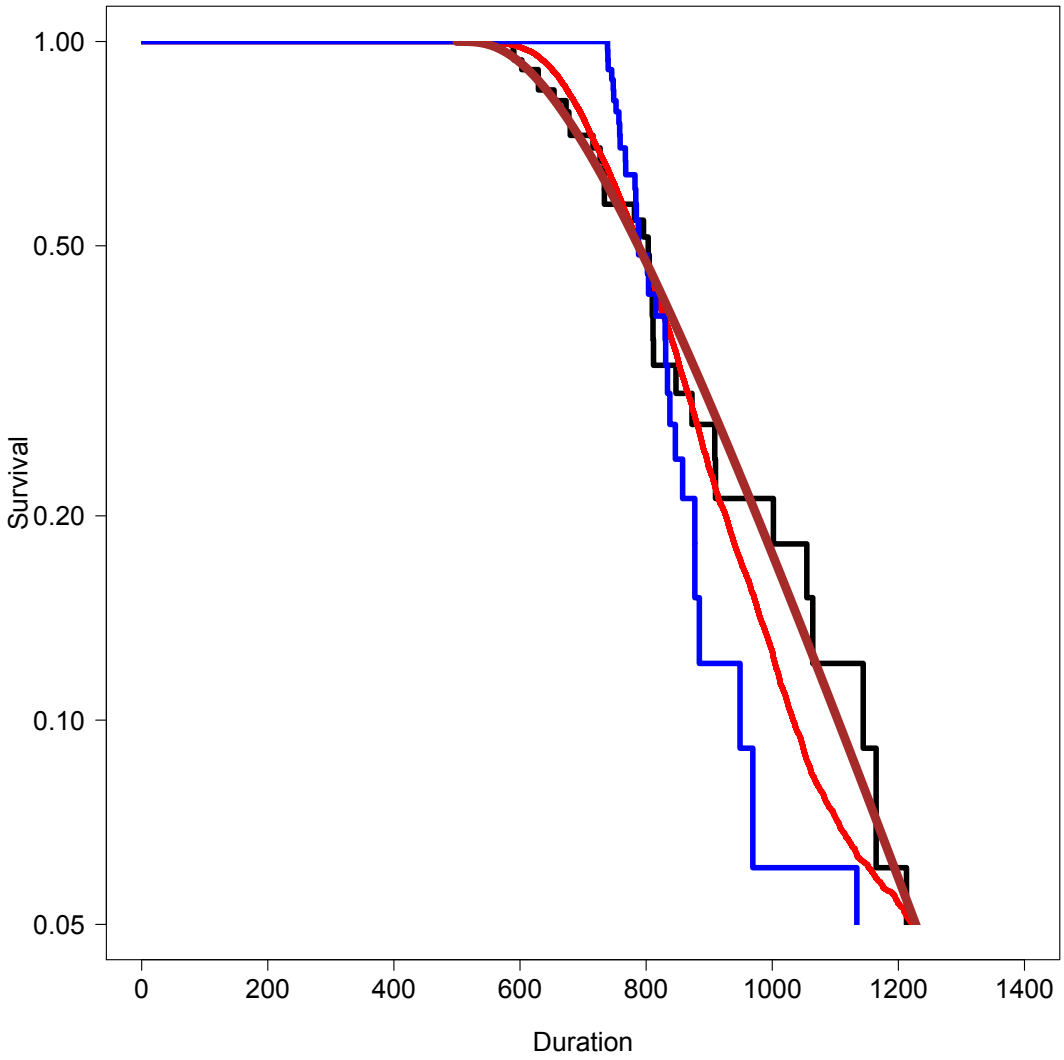

Supplemental Figure S32: Tc Survival curve. Brown curve indicates the theoretical prediction of the null model of phase duration independence. Red curve indicates the survival obtained by Monte Carlo permutations of phase durations from the data set (10^4 samples). Blue curve indicates the survival for the anti-correlated pairing.

2.6.2 CDC25B

Data vs. Random sampling of phases

```
    Two-sample Kolmogorov-Smirnov test

data:  data and random
D = 0.10717, p-value = 0.8444
alternative hypothesis: two-sided
```

Data vs. anti-correlated

```
    Two-sample Kolmogorov-Smirnov test

data:  data and anticor
D = 0.42424, p-value = 0.004793
alternative hypothesis: two-sided
```

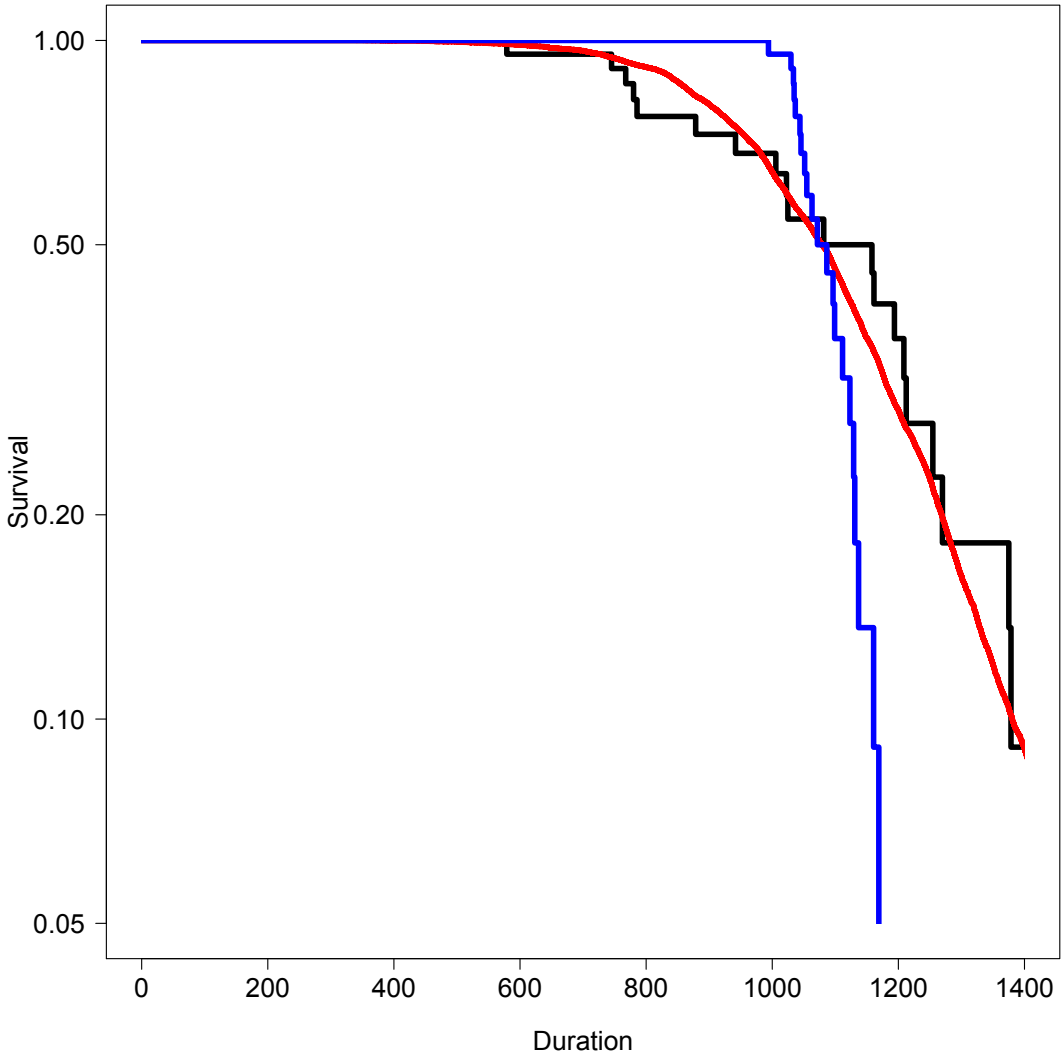

Supplemental Figure S33: Tc Survival curve. Since the survival curves for phase durations do not match exponential decay, the theoretical null model does not apply and is not shown. Red curve indicates the survival of total lengths obtained by Monte Carlo permutations of phase durations from the data set. Blue curve indicates the survival for the anti-correlated pairing.

2.6.3 CDC25B$^{\Delta CDK}$

Data vs. Random sampling of phases

```
    Two-sample Kolmogorov-Smirnov test

data:  data and random
D = 0.10717, p-value = 0.8444
alternative hypothesis: two-sided
```

Data vs. anti-correlated

```
    Two-sample Kolmogorov-Smirnov test

data:  data and anticor
D = 0.42424, p-value = 0.004793
alternative hypothesis: two-sided
```

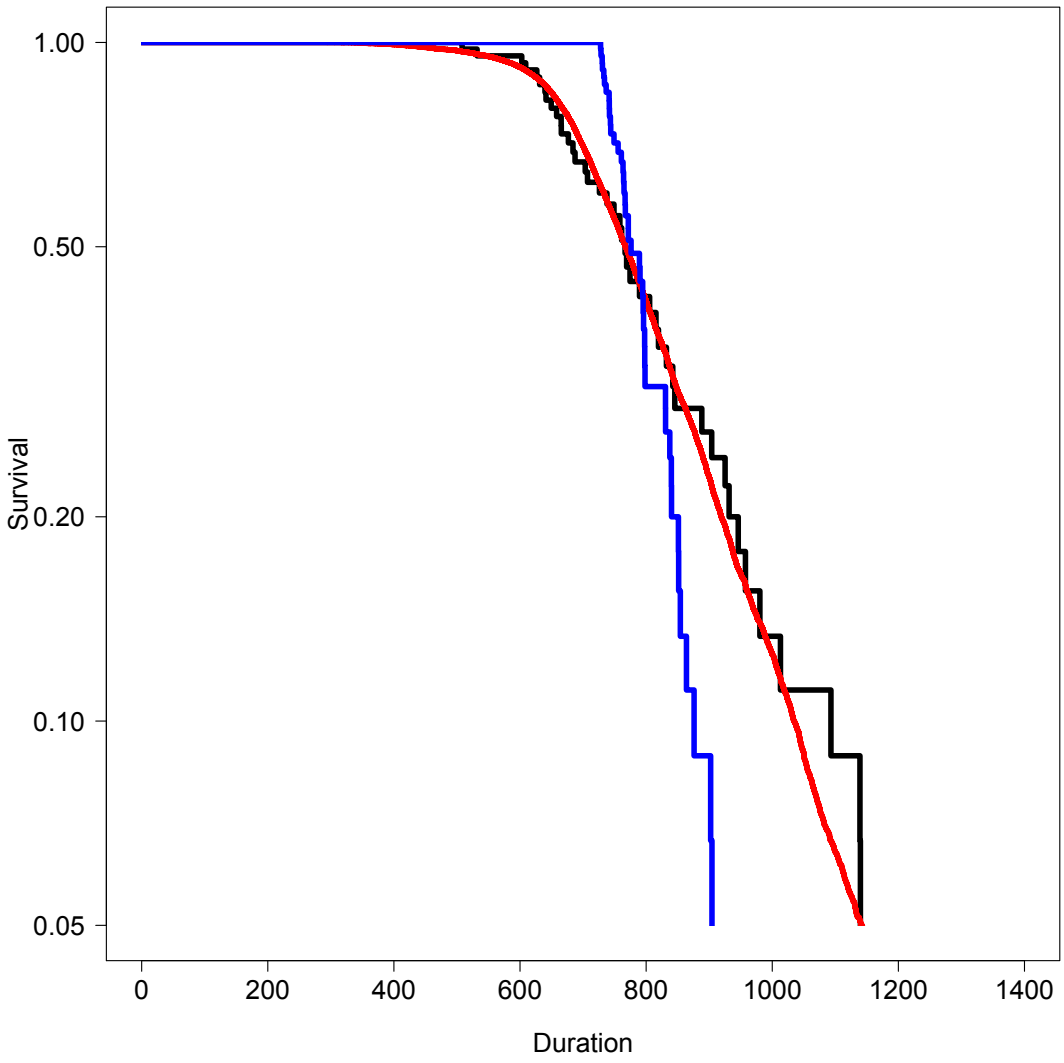

Supplemental Figure S34: Tc Survival curve. Since the survival curves for phase durations do not match exponential decay, the theoretical null model does not apply and is not shown. Red curve indicates the survival of total lengths obtained by Monte Carlo permutations of phase durations from the data set. Blue curve indicates the survival for the anti-correlated pairing.

3 Survival Analysis for the experimental treatment

For each condition, we report two graphical representations : a histogram representation (vertical dotted line reports the average of the distribution) and the corresponding survival curves.

The p-value of the survival test is given by the Score (logrank) test.

The output of Cox Proportional Hazard test is given for information to indicate the order of ratio between rates (e.g. exp(coef)=0.5 for CDC25B factor indicates that the exit rate is twice as slow as the baserate (CONTROL)).

For the sake of graphical clarity, confidence intervals are not reported.

For survival analysis of Tc, only cells with fully tracked cycles are used.

3.1 Tc

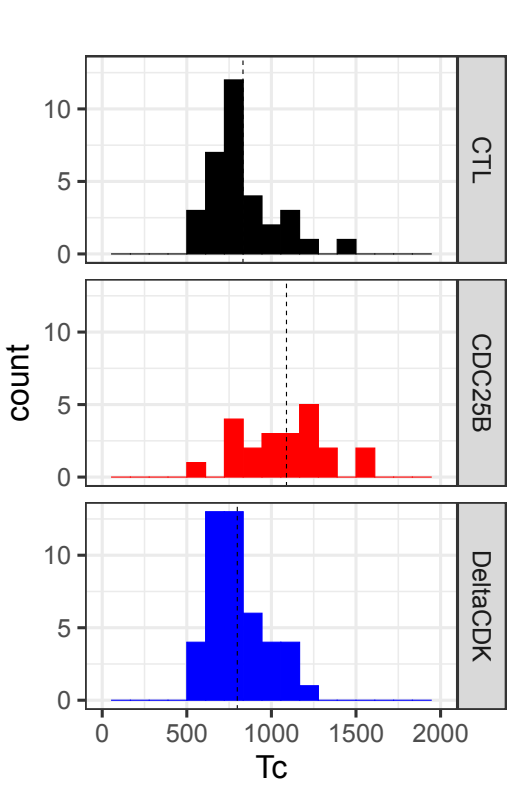

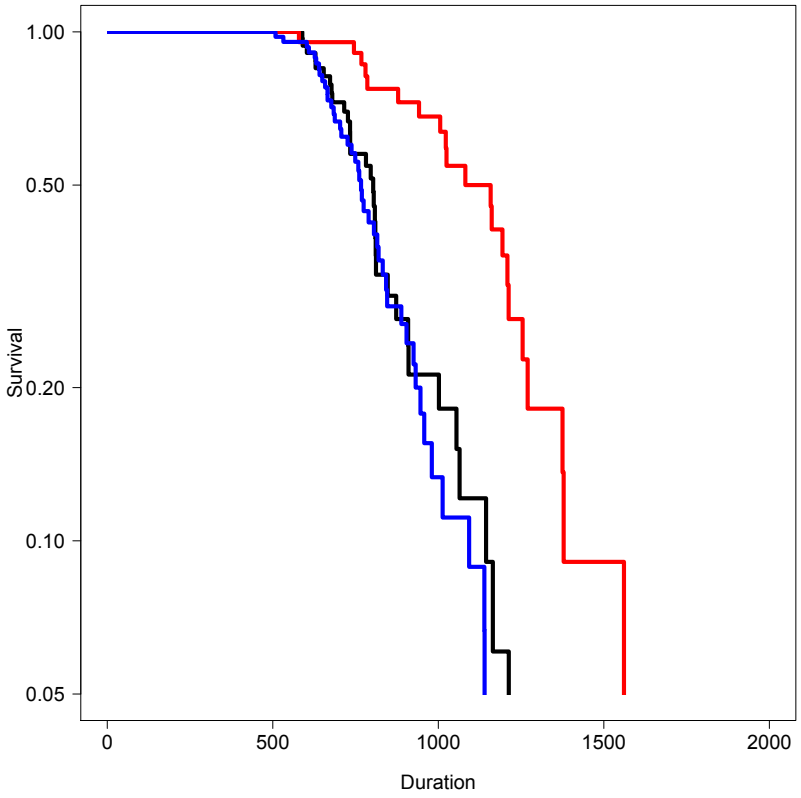


```
Call:
coxph(formula = Surv(dt$Tc, dt$sta) ~ dt$Condition)

  n= 100, number of events= 100
   (128 observations deleted due to missingness)

                        coef exp(coef) se(coef)      z Pr(>|z|)
dt$ConditionCDC25B   -1.0393    0.3537   0.2932 -3.544 0.000394 ***
dt$ConditionDeltaCDK  0.2690    1.3086   0.2352  1.144 0.252695
---
Signif. codes:  0 ‘***’ 0.001 ‘**’ 0.01 ‘*’ 0.05 ‘.’ 0.1 ‘ ’ 1

                     exp(coef) exp(-coef) lower .95 upper .95
dt$ConditionCDC25B      0.3537     2.8273    0.1991    0.6284
dt$ConditionDeltaCDK    1.3086     0.7641    0.8254    2.0749

Concordance= 0.615  (se = 0.031 )
Likelihood ratio test= 23.66  on 2 df,   p=7e-06
Wald test            = 20.13  on 2 df,   p=4e-05
Score (logrank) test = 21.74  on 2 df,   p=2e-05
```

3.2 G1

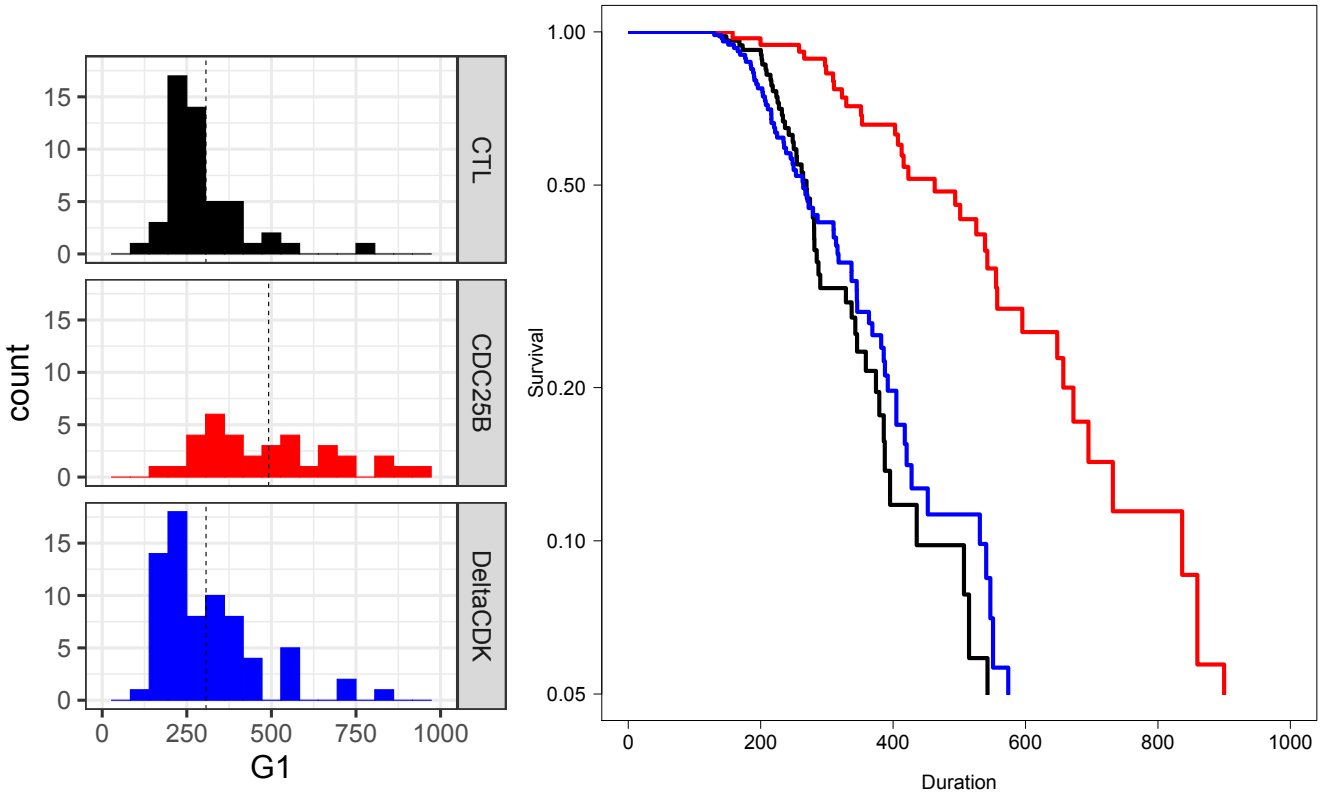


```
Call:
coxph(formula = Surv(dt$G1, dt$sta) ~ dt$Condition)

  n= 157, number of events= 157
   (71 observations deleted due to missingness)

                          coef exp(coef) se(coef)      z Pr(>|z|)
dt$ConditionCDC25B   -0.88337   0.41339  0.22647 -3.901  9.6e-05 ***
dt$ConditionDeltaCDK  0.01138   1.01145  0.18672  0.061    0.951
---
Signif. codes:  0 ‘***’ 0.001 ‘**’ 0.01 ‘*’ 0.05 ‘.’ 0.1 ‘ ’ 1

                     exp(coef) exp(-coef) lower .95 upper .95
dt$ConditionCDC25B      0.4134     2.4190    0.2652    0.6444
dt$ConditionDeltaCDK    1.0114     0.9887    0.7015    1.4584

Concordance= 0.608  (se = 0.025 )
Likelihood ratio test= 22.92  on 2 df,   p=1e-05
Wald test            = 20.17  on 2 df,   p=4e-05
Score (logrank) test = 21.29  on 2 df,   p=2e-05
```

3.3 S

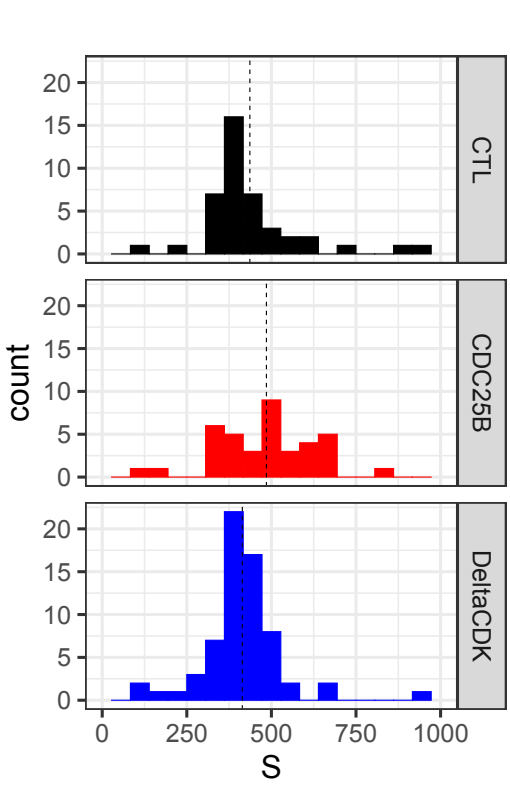

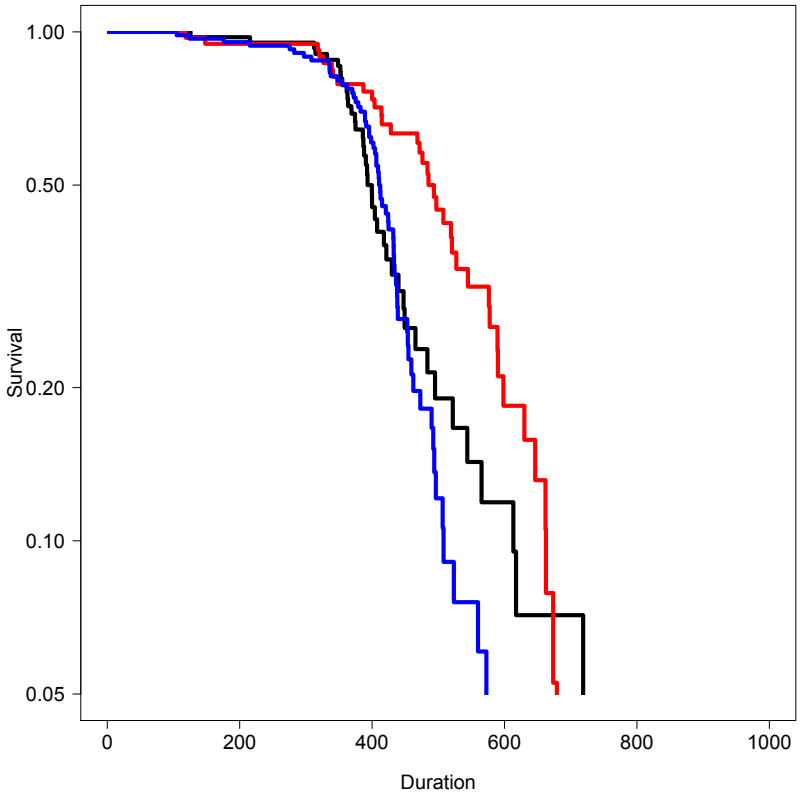


```
Call:
coxph(formula = Surv(dt$S, dt$sta) ~ dt$Condition)

  n= 146, number of events= 146
   (82 observations deleted due to missingness)

                        coef exp(coef) se(coef)      z Pr(>|z|)
dt$ConditionCDC25B   -0.4198    0.6572   0.2284 -1.838   0.0661 .
dt$ConditionDeltaCDK  0.1809    1.1983   0.2021  0.895   0.3706
---
Signif. codes:  0 ‘***’ 0.001 ‘**’ 0.01 ‘*’ 0.05 ‘.’ 0.1 ‘ ’ 1

                     exp(coef) exp(-coef) lower .95 upper .95
dt$ConditionCDC25B      0.6572     1.5217    0.4200     1.028
dt$ConditionDeltaCDK    1.1983     0.8345    0.8065     1.781

Concordance= 0.559  (se = 0.027 )
Likelihood ratio test= 8.69  on 2 df,   p=0.01
Wald test            = 8.25  on 2 df,   p=0.02
Score (logrank) test = 8.43  on 2 df,   p=0.01
```

3.4 G2

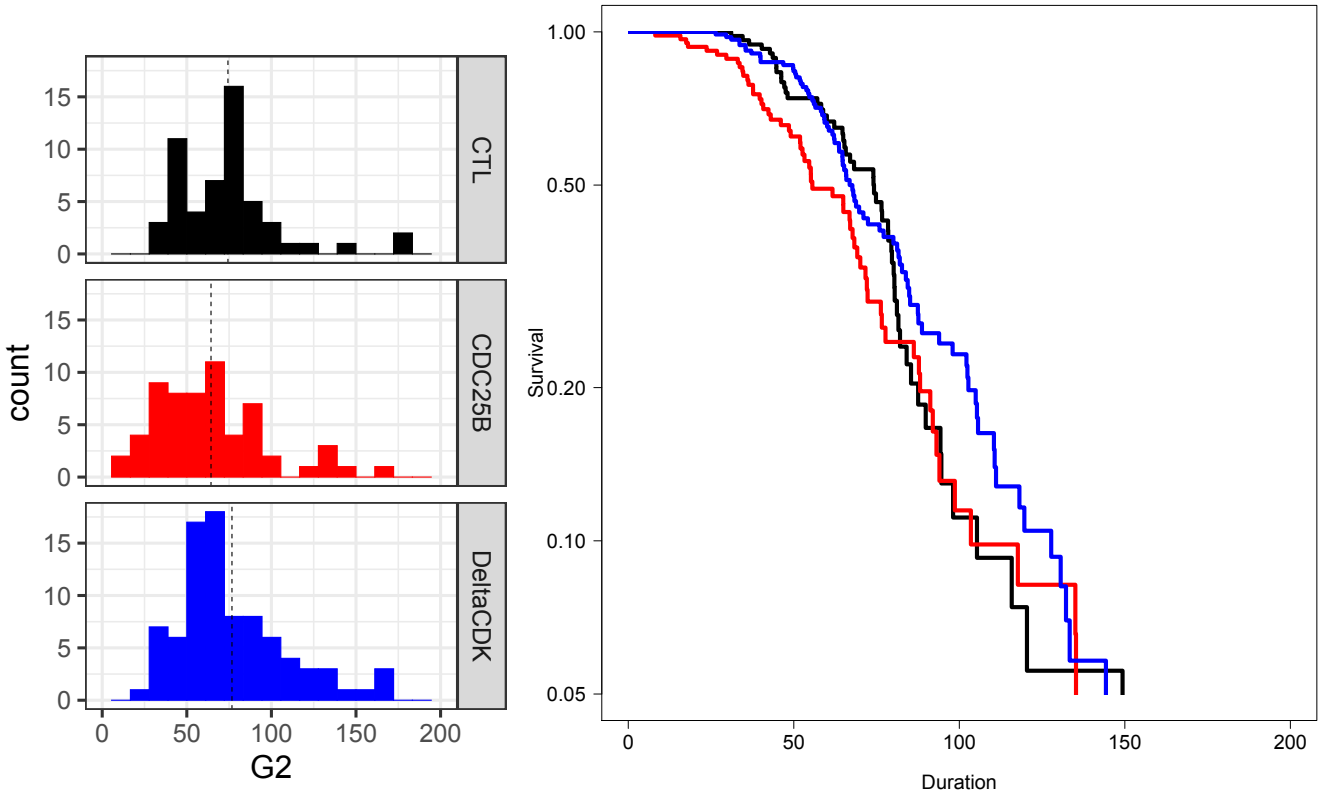


```
Call:
coxph(formula = Surv(dt$G2, dt$sta) ~ dt$Condition)

  n= 201, number of events= 201
   (27 observations deleted due to missingness)

                          coef exp(coef) se(coef)      z Pr(>|z|)
dt$ConditionCDC25B     0.26603   1.30478  0.18989  1.401    0.161
dt$ConditionDeltaCDK -0.02233   0.97792  0.17675 -0.126    0.899

                       exp(coef) exp(-coef) lower .95 upper .95
dt$ConditionCDC25B        1.3048     0.7664    0.8993     1.893
dt$ConditionDeltaCDK      0.9779     1.0226    0.6916     1.383

Concordance= 0.55  (se = 0.023 )
Likelihood ratio test= 3.19  on 2 df,   p=0.2
Wald test            = 3.31  on 2 df,   p=0.2
Score (logrank) test = 3.33  on 2 df,   p=0.2
```

3.5 M

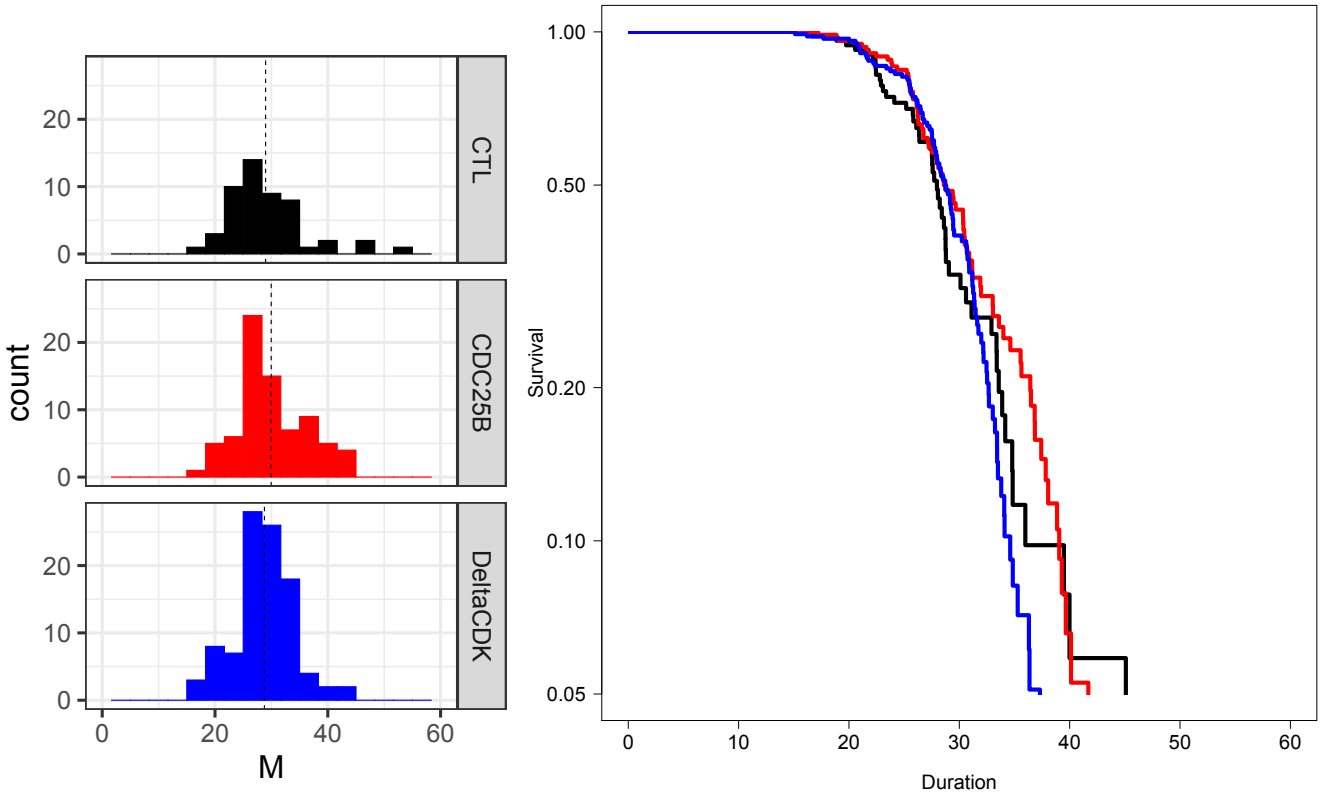


```
Call:
coxph(formula = Surv(dt$M, dt$sta) ~ dt$Condition)

  n= 225, number of events= 225
   (3 observations deleted due to missingness)

                         coef exp(coef) se(coef)      z Pr(>|z|)
dt$ConditionCDC25B   -0.07976   0.92334  0.18570 -0.430    0.668
dt$ConditionDeltaCDK  0.13998   1.15025  0.17888  0.783    0.434

                     exp(coef) exp(-coef) lower .95 upper .95
dt$ConditionCDC25B      0.9233     1.0830    0.6416     1.329
dt$ConditionDeltaCDK    1.1502     0.8694    0.8101     1.633

Concordance= 0.513  (se = 0.021 )
Likelihood ratio test= 2.07  on 2 df,   p=0.4
Wald test            = 2.07  on 2 df,   p=0.4
Score (logrank) test = 2.08  on 2 df,   p=0.4
```